

ISSN: 0128-7680

Pertanika Journal of

SCIENCE & TECHNOLOGY

VOLUME 13 NO.1
JANUARY 2005



A scientific journal published by Universiti Putra Malaysia Press

Pertanika Journal of Science & Technology

■ About the Journal

Pertanika, the pioneer journal of UPM, began publication in 1978. Since then, it has established itself as one of the leading multidisciplinary journals in the tropics. In 1992, a decision was made to streamline Pertanika into three journals to meet the need for specialised journals in areas of study aligned with the strengths of the university. These are (i) **Pertanika Journal of Tropical Agricultural Science** (ii) **Pertanika Journal of Science & Technology** (iii) **Pertanika Journal of Social Science & Humanities**.

■ Aims and Scope

Pertanika Journal of Science & Technology welcomes full papers and short communications in English or Bahasa Melayu in the fields of chemistry, physics, mathematics, and statistics, engineering, environmental control and management, ecology and computer science. It is published twice a year in January and July.

Articles must be reports of research not previously or simultaneously published in other scientific or technical journals.

Communications are notes of a significant finding intended spaced typewritten pages and must be accompanied by a letter from the author justifying its publication as a communication.

Reviews are critical appraisals of literature in areas that are of interest to a broad spectrum of scientist and researchers. Review papers will be published upon invitation.

■ Submission of Manuscript

Three complete clear copies of the manuscript are to be submitted to

The Chief Editor
Pertanika Journal of Science & Technology
Universiti Putra Malaysia
43400 UPM, Serdang, Selangor Darul Ehsan
MALAYSIA
Tel: 03-89468854; Fax: 03-89416172

■ Proofs and Offprints

Page proofs, illustration proofs and the copy-edited manuscript will be sent to the author. Proofs must be checked very carefully within the specified time as they will not be proofread by the Press editors.

Authors will receive 20 offprints of each article and a copy of the journal. Additional copies can be ordered from the Secretary of the Editorial Board.

EDITORIAL BOARD

Prof. Ir. Abang Abdullah Abang Ali- *Chief Editor*
Faculty of Engineering

Assoc. Prof. Ir. Dr. Norman Mariun
Faculty of Engineering

Assoc. Prof. Ir. Dr. Mohd. Saleh Jaafar
Faculty of Engineering

Assoc. Prof. Dr. Gwendoline Ee Cheng Lian
Faculty of Science & Environmental Studies

Prof. Dr. Abu Bakar Salleh
Faculty of Science & Environmental Studies

Prof. Dr. W. Mahmood Mat Yunus
Faculty of Science & Environmental Studies

Assoc. Prof. Dr. Noor Akma Ibrahim
Faculty of Science & Environmental Studies

Assoc. Prof. Dr. Hamidah Ibrahim
Faculty of Information Technology & Science
Computer

Rosta Harun
Faculty of Science & Environmental Studies

Sumangala Pillai - *Secretary*
Universiti Putra Malaysia Press

Published by Universiti Putra Malaysia Press
ISSN No. 0128-7680

INTERNATIONAL PANEL MEMBERS

Prof. D.J Evans
Parallel Algorithms Research Centre

Prof. F. Halsall
University College of Swansea

Prof. S.B Palmer
University of Warrick

Prof. Dr. Jerry L. Mc Laughlin
Purdue University

Prof. Dr. John Loxton
MaxQuarie University

Prof. U.A Th. Brinkman
Vrije Universiteit

Prof. A.P. Cracknell
University of Dundee

Prof. A.J. Saul
University of Sheffield

Prof. Robert M. Peat
University of Florida

Prof. J.N Bell
Imperial College of Science, Technology and Medicine

Prof. Yadolah Dodge
University De Neuchatel

Prof. W.E Jones
University of Windsor

Prof. A.K. Kochar
UMIST

ARCHIVE COPY
(Please Do Not Remove)

Pertanika Journal of Science & Technology

Volume 13 No. 1, 2005

Contents

Developing Translation Rules for Converting Relational to Object Oriented Database Conceptual Schema – <i>Hamidah Ibrahim, Soon Lay Ki, Ali Mamat & Zaiton Muda</i>	1
Study of Photobleaching Mechanism in Methylene Blue Sensitized Gelatin Using a Single Beam UV-Vis. Fibre Optics Spectrophotometer – <i>Chan Kok Sheng & W. Mahmood Mat Yunus</i>	23
Static and Dynamic Analysis of Rockfill Dam Using Finite-infinite Element Method – <i>J. Noorzaei, M. Karami, Waleed A. Thanoon & M. S. Jaafar</i>	31
Studies of Equilibria Involving the Binary and Ternary Complexes of Aluminium with Eriochrome Cyanine R (ECR) and Cetylpyridinium Chloride (CP) – <i>Musa Ahmad & Ramaier Narayanaswamy</i>	43
A Cryptosystem Analogous to LUCELG and a Digital Signature Scheme – <i>Choo Mun Yoong & Mohamad Rushdan Md Said</i>	61
Kaedah Kolorimetri untuk Analisis Kuantitatif Kapsaisin Secara Pencaman Corak Menggunakan Jaringan Neural Tiruan – <i>Mohamad Nasir Mat Arip, Musa Ahmad, Ahmed Mahir Mokhtar, Mohd. Nasir Taib & Lee Yook Heng</i>	75
Effect of Specimen Size and Shape on the Compressive Strength of High Strength Concrete – <i>Alaa S. Malaikah</i>	87
In-time Rice Irrigation Water Management Under Limited Water Supply – <i>T. S. Lee, M. Aminul Haque & M.M.M. Najim</i>	97
Enhancing Design for Aesthetics Based on Product Platform Architecture – <i>Ahmad Baharuddin Abdullah & Zaidi Mohd Ripin</i>	113
Superconductivity in Layerd Cuprate $(\text{Ru}_{1-x}\text{Nb}_x)\text{Sr}_2\text{GdCu}_2\text{O}_8$ – <i>R. Abd-Shukor, C. A. Kek & W. K. Yeoh</i>	127

Developing Translation Rules for Converting Relational to Object Oriented Database Conceptual Schema

Hamidah Ibrahim, Soon Lay Ki, Ali Mamat & Zaiton Muda

Department of Computer Science

Faculty of Computer Science and Information Technology

Universiti Putra Malaysia

43400 UPM, Serdang, Selangor, Malaysia

E-mail: hamidah@fsktm.upm.edu.my

Received: 27 November 2001

ABSTRAK

Pangkalan data multi adalah satu persekutuan sistem pangkalan data teragih, heterogen dan berotonomi yang telah wujud. Kebiasaannya, proses integrasi adalah perlu dalam usaha membentuk satu sistem pangkalan data teragih yang heterogen. Proses ini secara amnya mengandungi dua fasa utama, iaitu fasa penterjemahan skema konseptual diikuti dengan fasa integrasi. Makalah ini mempersembahkan satu pendekatan penterjemahan untuk menukar skema pangkalan data hubungan kepada skema pangkalan data berorientasi objek. Pendekatan penterjemahan tersebut mengandungi satu set peraturan penterjemahan, yang berdasarkan kepada kebergantungan terangkum, atribut kunci dan jenis atribut. Satu prototaip alat penterjemahan skema pangkalan data, dipanggil RETOO dibangunkan berdasarkan kepada pendekatan penterjemahan yang dicadangkan. RETOO menerima skema pangkalan data hubungan sebagai data input dan menjana skema pangkalan data berorientasi objek sebagai output. Pendekatan penterjemahan bukan sahaja dapat memelihara semantik skema pangkalan data hubungan tersebut, tetapi juga meningkatkan semantik skema berorientasi objek yang diterjemahkan melalui konsep permodelan data berorientasi objek.

ABSTRACT

A multidatabase is a confederation of pre-existing distributed, heterogeneous, and autonomous database system. Obviously, the integration process is essential in the effort of forming a distributed, heterogeneous database system. This process generally consists of two main phases, which are conceptual schema translation phase followed by the integration phase. This paper presents a translation approach to convert relational database schema to object-oriented database schema. The translation approach consists of a set of translation rules, which is based on inclusion dependencies, key attributes and types of attributes. A database schema translation tool prototype, called RETOO (RElational-To-Object-Oriented) is then developed based on the proposed translation approach. RETOO receives a relational database schema as input data and generates an object-oriented database schema as the output. The translation approach is not only able to maintain the semantics of the relational database schema, but also enhance the semantics of the translated object-oriented schema via object-oriented data modeling concepts.

Keywords: Relational schema, object-oriented schema

INTRODUCTION

In today's information age, databases and database technology are having a major impact on the growing use of computers. The government, education, medicine, engineering, business and other areas have computerized all or part of their daily functions. Undoubtedly, these computerization processes often include database systems to model and store the information of the real-world entities involved in these functions. The computing environment in most of these contemporary organizations contains distributed, heterogeneous, and autonomous hardware and software systems. Therefore, there is an increasing need to support the co-operations of the services provided by these different software and hardware.

The existence of multiple, heterogeneous and autonomous databases within an organization means the globally important information exists in separate local database management systems (DBMSs), thus making the existing data inaccessible to remote users. One solution is to integrate these databases to form a single cohesive definition of a multi-database. Most of the integration is made possible with the support of database translation, which is the task of translation from one database conceptual schema into another.

Most works on schema translation deal with conversion from the entity-relationship (ER) model to the relational model or some extension of it (Castellanos *et al.* 1994; Castellanos and Saltor 1991). There are many works on translation from ER model into relational model or vice versa (Huang *et al.* 1997; Lukovic and Mogin 1996; Seol 1997). Besides, works on general frameworks for schema translation were also carried out (McBrien and Poulouvasilis 1998).

Nevertheless, only a few works have been done on translating relational schema into object-oriented (OO) schema (Castellanos *et al.* 1994; Castellanos and Saltor 1991; Fong 1997; Soon *et al.* 2001; Stanisic 1999). Stanisic (1999) focused his work not only on schema translation, but query translation as well. While Castellanos *et al.* (1994) proposed a methodology to translate the relational model into Barcelona Object-Oriented Model, namely BLOOM model. However, these works have their limitations respectively, especially in terms of translated OO model representation. The limitations in the BLOOM OO model include (i) the syntax of resulted BLOOM OO model is not easy to understand, such as the keywords *s_aggreg_of* and *compl_generaliz_of*; (ii) the model tends to create extra classes, which are sometimes not necessary; and (iii) the data types of attributes in BLOOM OO model are not specified.

In our work, a set of translation rules is proposed to translate relational database conceptual schema into OO database conceptual schema. This set of translation rules is applied in a database schema translation tool prototype, called RETOO (Relational-To-Object-Oriented), with the assumption that OO conceptual schema is used as the canonical conceptual schema (CCS). This canonical conceptual schema will then be integrated into the global conceptual schema (GCS) of the distributed, heterogeneous database system. *Fig. 1* briefly illustrates the system. InS_1, \dots, InS_n shown in *Fig. 1* are intermediate schemas or known as canonical conceptual schemas.

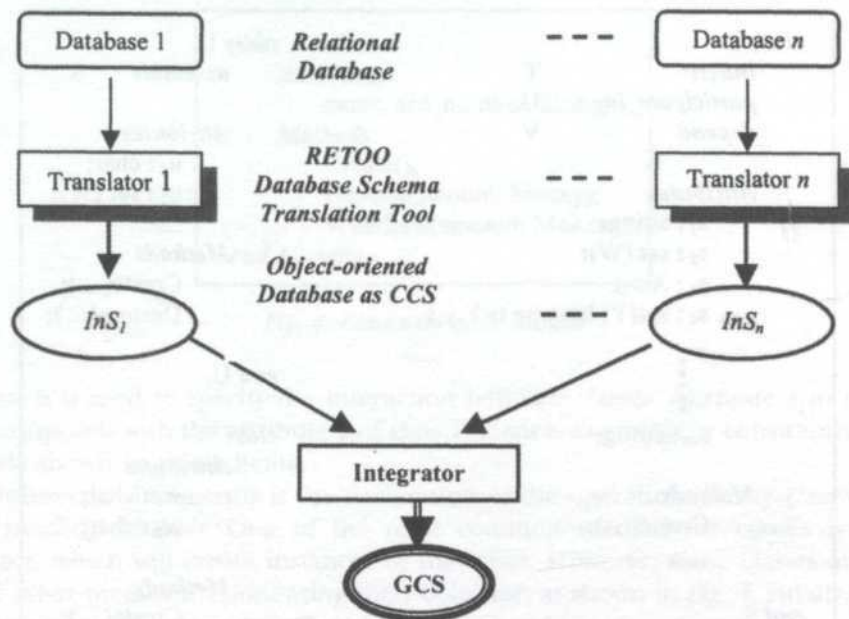


Fig. 1: Relational-to-object-oriented database schema translation tool

PRELIMINARIES

In our work, the relational conceptual schema and object-oriented conceptual schema are represented in the format as shown in Fig. 2 and Fig. 3, respectively.

S , T and U are the names of the relations while s_1 to s_n , t_1 to t_3 and u_1 to u_3 are the attributes of relations S , T and U respectively. Ds_1 to Ds_n , Dt_1 to Dt_3 and Du_1 to Du_3 are the data types (domain) associated with each attribute while the underlined attribute is the primary key. Note that relations S , T and U might have a primary key, k , which is defined over more than one attribute of these relations.

In Fig. 3, S , T , U , V , W , X and Y are the names of the classes. The interactions among classes are shown by keywords *inherit*, *inherited_by*, *assemble*, *participate_in*, *depend*, *has_dependent*, *set()* and *inverse is*. Every class has its attributes and methods or operations.

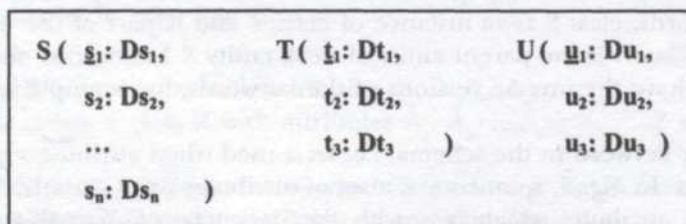


Fig. 2: Examples of the format of relational conceptual schema

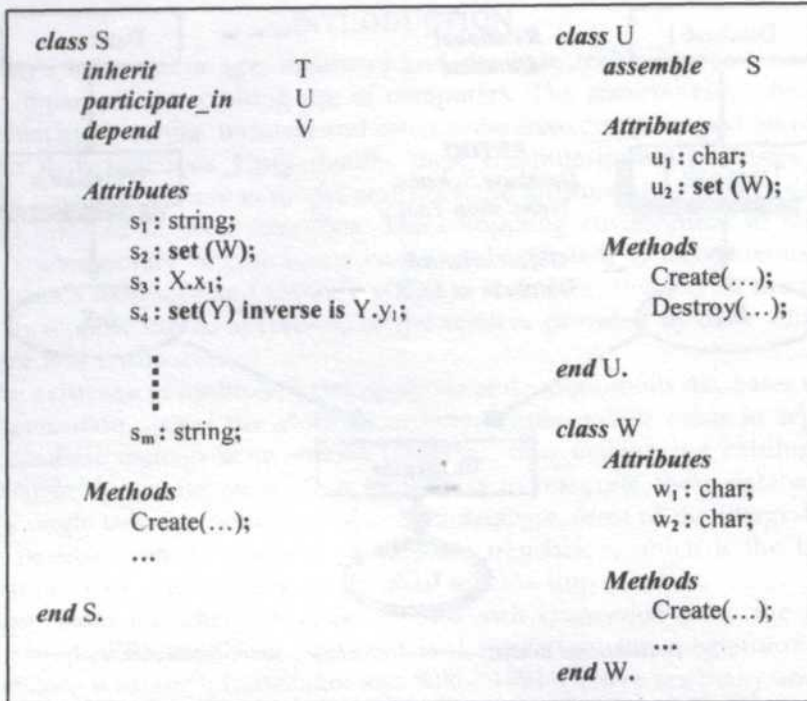


Fig. 3: Object-oriented conceptual schema

The format of the OO schema is modified from the standard object-oriented database schema to a more easy-to-understand format. As can be seen in Fig. 3, the first part of the schema is the declaration of the beginning of a class, which is *class S*. This is followed by the declaration part for the inheritance (*inherit*) and aggregation (*assemble* and *depend*) of the class. The word *depend* shows the way of presenting weak entity type in OO data modelling. Even though relationship between the weak entity and its parent entity is considered as a kind of aggregation, the keyword *depend* is used for the purpose of better understanding. All these three keywords have their own inverse versions, which are *inherited_by*, *participate_in* and *has_dependent*.

In this example, we have other six classes, namely *T*, *U*, *V*, *W*, *X* and *Y*. Class *S* inherits from class *T*, aggregated by class *U* and is the dependent of class *V*. In other words, class *S* is an instance of class *T* and is part of the aggregation of class *U*. Class *V* is the parent entity of weak entity *S*. In contrast, these inverse classes will have the inverse versions of the keywords, for example in class *U*, it has *assemble S*.

Another keyword in the schema, i.e. *set* is used when attribute's type is a set of attributes. In Fig. 3, *s₂* consists of a set of attributes from class *W*. Notice that there is an attribute, which is *s₃* with the data type of *X.x₁*, this means the attribute is 'mapped' from attribute *x₁* of class *X*. Besides these, the keyword

```

class Account
  Attributes
    name, acc_number: String;
  Methods
    Create();
    Deposit(amount: Money);
    Withdraw(amount: Money)
end Account.
    
```

Fig. 4: Class with extra methods

inverse is used to specify the interaction between classes. Attribute s_j in class S corresponds with the attribute y_i of class Y . Hence, the integrity constraints are clearly shown in this schema.

Followed subsequently is the declaration of the operations in the class with the heading *Methods*. One of the most common method for classes is the creator, which will create instances of that class. However, some classes might have other methods representing their behavior, as shown in Fig. 4. Finally, the closing of class is done by using the keyword *end*.

RELATIONAL TO OBJECT-ORIENTED DATABASE SCHEMA TRANSLATION APPROACH

The translation rules proposed by us are based on two characteristics of database schema, they are: (i) inclusion dependency and (ii) key attributes and types of attributes. Two phases are involved in translating relational to object-oriented database conceptual schema, which are: (i) identifying classes and (ii) identifying the operations. Both phases especially the second phase operate semi-automatically, since the information regarding the behavior of each class is not provided in the relational data model. To perform the translation process we have identified ten translation rules which are based on the mapping and normalization process in relational data modelling.

Identifying Classes

To identify objects or classes, there are four steps as presented below.

Step 1: Translating Relation into Class

The first rule is:

Rule 1: If R is a relation with attributes A_1, A_2, \dots, A_n ,
then create a class R with attributes A_1, A_2, \dots, A_n .

In this step all relations are formed into classes. Each class will have attributes and types of attributes. Below is an example:

```

Surgeon(  SName   : String,
          Street  : String,
          City    : String,
          Country : String,
          Phone-No : String )

```

After translation from Step 1, we have class *Surgeon* as shown below:

```

class Surgeon
  Attributes
    SName      : String;
    Street     : String;
    City       : String;
    Country    : String;
    Phone-No   : String;
end Surgeon.

```

Step 2: Identifying Composite Attributes

The general guideline to decide what an object is and what an attribute of an object is lies in the theory of data abstraction. This theory states that something should only be represented by a class if it represents a set of similar objects or concepts with meaningful properties and operations, which are required to be maintained by the system (Hughes 1991).

Composite attributes are attributes that can be divided into smaller subparts, which represent more basic attributes with independent meanings of their own (Elmasri 2003). Composite attributes represent a set of objects with meaningful simple attributes. There are three cases to be considered, namely: relation that consists of m composite attributes with (i) no overlapping attribute between the composite attributes; (ii) at least two of the composite attributes have a common attribute and (iii) at least one of the composite attribute consists of attributes which are common to another composite attribute. Each case is discussed below.

Case 1: No overlapping attribute between the composite attributes.

The second translation rule is stated as:

Rule 2: If relation R consists of m composite attributes CA_i , where $1 \leq i \leq m$ and $CA_i = \{A_{i1}, A_{i2}, \dots, A_{in}\}$ with no overlapping attributes between the CA_i , i.e. $\bigcap_{i=1}^m CA_i = \{ \}$,

then - the attributes forming the composite attribute CA_i are taken out from class R , and are formed as a newly defined class, say T_i ;

- in class R , attributes $A_{i1}, A_{i2}, \dots, A_{in}$ forming the composite attribute CA_i are replaced by statement $RCA_i: set(T_i)$, where RCA_i is an attribute in class R referring to class T_i .

Referring to the example in Step 1, there is a composite attribute *Address*, which consists of three attributes, namely: *Street*, *City*, and *Country*. As a result, these three attributes are taken out from the class *Surgeon* and formed as another class *Address*, as shown below:

```

class Address
    Attributes
        Street, City, Country    :    String;
end Address.
class Surgeon
    Attributes
        SName      :    String;
        SAddress   :    set(Address);
        Phone-No   :    String;
end Surgeon.
    
```

If there exists the same non-key composite attributes in another relation, redundancies can be solved by referring to the same new class formed.

To illustrate cases 2 and 3, let say we have a relation with attributes as follows:

```

Surgeon(    ID No      :    String,
           FName      :    String,
           MInit      :    String,
           LName      :    String,
           Phone-No   :    String
    
```

Case 2: At least two of the composite attributes have a common attribute.

The third translation rule is stated as:

Rule 3: If relation R consists of a composite attribute CA_i with attributes $\{A_{i1}, A_{i2}, \dots, A_{in}\}$ and another composite attribute CA_j with attributes $\{A_{j1}, A_{j2}, \dots, A_{jm}\}$, and there exists at least an attribute in CA_j , say A_{jk} , which exists in both CA_i and CA_j ¹

then

- the attributes forming CA_i are taken out from class R and formed as a newly defined class, say T_i ;
- the attributes forming CA_j are also taken out from class R and formed as another newly defined class, say T_j ;
- in class T_j , attribute A_{jk} is defined as $A_{jk}: T_i.A_{jk}$;
- in class R, attributes $A_{i1}, A_{i2}, \dots, A_{in}$ are replaced by statement $RCA_i: set(T_i)$, representing composite attribute CA_i ;
- similarly, statement $RCA_j: set(T_j)$ is used to replace attributes $A_{j1}, A_{j2}, \dots, A_{jm}$, representing composite attribute CA_j .

¹ And if there is an attribute in CA_j , say A_{jl} which is a simple attribute by itself, then in class T_j , attribute A_{jl} is defined as $A_{jl}:R.A_{jl}$; and attribute A_{jl} will remain in class R.

Let's assume that there are two composite attributes in this relation, which are:

- Name: FName, MInit, LName
- Staff_No: FName, Phone-No

In this case, we have an attribute *FName* that exists in both composite attributes *Name* and *Staff_No*. The attributes that form these composite attributes will be taken out from the original relation and formed as classes, same as the simpler case discussed earlier. Therefore, after the translation process, we will get the following three classes:

```

class Name
    Attributes
        FName, MInit, LName : String;
end Name.
class Staff_No
    Attributes
        FName : Name.FName;
        Phone-No : String;
end Staff_No.
class Surgeon
    Attributes
        ID_No : String;
        SName : set(Name);
        Staff_No : set(Staff_No);
end Surgeon.

```

Case 3: At least one of the composite attributes consists of attributes which are common to another composite attribute.

The fourth translation rule is stated as:

Rule 4: If relation *R* has a composite attribute $CA_1 = \{A_{11}, A_{12}, \dots, A_{1n}\}$ and another composite attribute $CA_j = \{A_{j1}, A_{j2}, \dots, A_{jm}\}$ where $CA_j \subset CA_1$ (CA_j is a subset of CA_1),

- then*
- the attributes $A_{11}, A_{12}, \dots, A_{1n}$ forming CA_1 are taken out from class *R* and formed as a newly defined class, say T_i ;
 - the attributes $A_{j1}, A_{j2}, \dots, A_{jm}$ forming CA_j are also taken out and formed as another newly defined class, say T_j ;
 - in class T_j , attribute A_{jk} where $1 \leq k \leq m$ is defined as $A_{jk} : T_i.A_{jk}$;
 - in class *R*, attributes $A_{11}, A_{12}, \dots, A_{1n}$ are replaced by statement $RCA_i : set(T_i)$ representing composite attribute CA_i ;
 - in class *R*, statement $RCA_j : set(T_j)$ is used to represent composite attribute CA_j .

In this case, let's assume that we have another two sets of composite attributes in the same relation *Surgeon*.

- Full_Name: FName, MInit, LName
- Name: FName, LName

Applying rule 4 will derive the following three classes:

```

class Full_Name
    Attributes
        FName, MInit, LName : String;
end Full_Name.
class Name
    Attributes
        FName : Full_Name.FName;
        LName : Full_Name.LName;
end Name.
class Surgeon
    Attributes
        ID_No : String;
        SFull_Name : set(Full_Name);
        SName : set(Name);
        Phone-No : String;
end Surgeon.
    
```

Step 3: Identifying Relations with Foreign Keys only

In this step, we identify relations, which have only foreign keys. According to the mapping process in relational data modelling, a relation will have only foreign key attributes when the relation is formed as a result of an interaction between or among other relations in M:N relationship. These foreign keys, which originated from the key attributes of the relations involved in that interaction will form the primary key of this newly formed relation.

Thus, when translating these relations, we will regard them as an object resulting from the interaction between or among the classes that the foreign key attributes refer to, as reflected in Rule 5:

Rule 5: If relation R consists of n attributes A_1, A_2, \dots, A_n where each A_i is the foreign key that refers to relations U_i , where $1 \leq i \leq n$,
then - class R is treated as interactions of all the classes $\{U_1, U_2, \dots, U_n\}$;
 - in class U_i , statements $\{R: set(U_i) \text{ inverse is } U_i.R, R: set(U_2) \text{ inverse is } U_2.R, \dots, R: set(U_n) \text{ inverse is } U_n.R\} - \{R: set(U_i) \text{ inverse is } U_i.R\}$ are stated;
 - class R is abolished.

The example below illustrates this translation step.

```

Paper( P#, Title, Issue# : String,
       Institute_Name, Vol# : String)
Author( AName, Nationality : String,
        Date_of_Birth : Date)
Writes( P#, AName : String)
ID: Writes.P#  $\subseteq$  Paper.P#
ID: Writes.AName  $\subseteq$  Author.AName
    
```

The *Writes* relation consists of two foreign key attributes where *P#* refers to the *P#* in relation *Paper* and *AName* refers to the *AName* in relation *Author*. Therefore, the relation *Writes* is representing the interaction between relations *Paper* and *Author*. Class *Writes*, which was formed in translation step 1 will be abolished.

class Paper

Attributes

P#, Title, Issue# : String;
 Institute_Name, Vol# : String;
 Written_by : set(Author)
 inverse is Author.write;

end Paper.

class Author

Attributes

AName, Nationality : String;
 Date_of_Birth : Date;
 Write : set(Paper)
 inverse is Paper.written_by;

end Author.

Step 4: Identifying Foreign Keys and Candidate Keys Being Referenced

In this step, we shall focus on the referential integrity, which includes identifying foreign keys and candidate keys being referenced. There are two possibilities identified regarding the referential integrity, as shown in Table 1.

TABLE 1
 Foreign key

Foreign Key	Candidate Key being Referenced
Key Attribute	Key Attribute
Non-key Attribute	Key Attribute

The first case (Case 1) occurs when both the foreign key and the candidate key being referenced are key attributes in both relations. The second case (Case 2) occurs when the foreign key is a non-key attribute whereas the attribute being referenced is a primary key attribute in the original relation.

Case 1: Both the foreign key and the candidate key being referenced are key attributes in both relations.

In this case, we can further divide it into four categories, as shown in Table 2.

Based on the definition of key constraint in relational modeling (Elmasri 2003), we know that when the key attribute of a relation R_1 is a foreign key, it implies that this relation refers to the whole relation R_2 that contains the key being referenced. Therefore, R_1 is an instance of R_2 whereby besides the

TABLE 2
Categories of case 1

Foreign Key	Candidate Key being Referenced
Simple primary key	Simple primary key
Composite primary key	Composite primary key
Composite primary key	Simple primary key
Part-of composite primary key	Simple/Composite primary key

attributes in R_2 , R_1 has its own attributes. In OO modelling, this situation is similar to one of the OO concepts, which is inheritance. A subclass is said to be inherited from a superclass if the subclass "is-an" instance of the superclass.

For category one, if both the foreign key and the candidate key being referenced are simple primary key attributes of the relations, our translation rule will consider the foreign key's relation inherits from another being referenced relation. This applies correctly even if both of the foreign key and the key being referenced are composite primary keys, which is the second category, as stated in Rule 6:

Rule 6: If both the foreign key in relation R and the candidate key being referenced in relation V are simple primary key attributes or composite primary keys,
then - class R is treated as an inheritance of class V;
 - statement *inherit V* is included in class R;
 - statement *inherited_by R* is included in class V.

For example, the *SName* attribute in *Consultant* is the foreign key, which refers to the primary key of *Surgeon*. In this case, we can say that the *Consultant* "is-a" *Surgeon*.

```
Surgeon(   SName, Street, City           :   String,
          Country, Phone_No           :   String)
Consultant( SName, Speciality :   String)
ID: Consultant.SName ⊆ Surgeon.SName
```

After translation, we shall get the following OO schema:

```
class Surgeon
    inherited_by      Consultant
    Attributes
        SName       :   String;
        SAddress    :   set(Address);
        Phone_No    :   String;
end Surgeon.
class Consultant
    inherit Surgeon
    Attributes
        Speciality  :   String;
end Consultant.
```

Category three indicates that there might exist a relation with more than one foreign key and all the foreign keys formed the primary key of the relation. Besides that, this relation also has its own attribute(s). If the subclass "is-an" instance of both the superclasses, we will treat the relationships among the relations as multiple inheritance. Based on this third category, we have the following rule:

Rule 7: If relation R has a set of foreign keys $\{fk_1, fk_2, \dots, fk_n\}$ where $n > 1$ and fk_i where $1 \leq i \leq n$ formed the primary key of R, and after being translated into class R, class R is an instance of the classes C_1, C_2, \dots, C_m where its foreign keys are referred to, i.e. $R.fk_i \subseteq C_i.pk^2$, where pk is the primary key of C_i ,

then

- class R is treated as an inheritance of classes C_1, C_2, \dots, C_m ;
- in class R, statements *inherit* C_i where $1 \leq i \leq m$ are included;
- statements *inherited_by* R are included in classes C_1, C_2, \dots, C_m .

For example, in a factory, it produces a *Toy*, which is a *CommercialProduct* and at the same time, it is also a *Gift* for customer:

```
CommercialProduct( CommercialID : String,
                   Packaging      : String,
                   Price          : Integer)
```

```
Gift( GiftID, Category : String,
      Coupon           : Integer)
```

```
Toy( CommercialID : String,
     GiftID        : String,
     Age           : Integer)
```

ID: Toy.CommercialID \subseteq CommercialProduct.CommercialID

ID: Toy.GiftID \subseteq Gift.GiftID

The *Toy* "is-a" *CommercialProduct* and also "is-a" *Gift* to the factory. As a result, the three classes will be formed as below:

```
class CommercialProduct
    inherited_by Toy
    Attributes
        CommercialID : String;
        Price         : Integer;
        Packaging      : String;
```

```
end CommercialProduct.
```

```
class Gift
    inherited_by Toy
    Attributes
        GiftID      : String;
        Category    : String;
        Coupon      : Integer;
```

```
end Gift.
```

² The symbol \subseteq shows the inclusion dependency.

```

class Toy
    inherit CommercialProduct
    inherit Gift
    Attributes
        Age          : Integer;
end Toy.
    
```

However, not all relations that have foreign keys as primary key will be considered as having multiple inheritance as presented in the following rule:

Rule 8: If relation R has a set of foreign keys {fk₁, fk₂, ..., fk_n} where n > 1 and fk_i where 1 ≤ i ≤ n formed the primary key of R, and after being translated into class R, class R is an aggregation of classes C₁, C₂, ..., C_m where its foreign keys are referred to, i.e. R.fk_i ⊆ C_i.pk, where pk is the primary key of C_i,

then - class R is treated as an aggregation of classes C₁, C₂, ..., C_m;

- statements *assemble* C_i where 1 ≤ i ≤ m are included in class R;

- statement *participate_in* R are included in classes C₁, C₂, ..., C_m.

Refer to the example below:

```

Programmer( SSN, Salary, Sex : String,
            BDate           : Date)
Project( P#, PName          : String,
        StartDate, DueDate  : Date)
Works_On( SSN, P#         : String,
          Hours             : Integer)
ID: Works_On.SSN ⊆ Programmer.SSN
ID: Works_On.P# ⊆ Project.P#
    
```

In this case, *Works_On* is neither "is-a" *Programmer* nor "is-a" *Project*. Rather, *Works_On* would be more suitable to be identified as an aggregation or assembler of the two classes. If we refer back to the mapping process in relational modeling, *Works_On* resulted from an interaction of M:N relationship of both *Programmer* and *Project*, in which the attribute *Hours* is an attribute obtained from the relationship between *Programmer* and *Project*.

In terms of aggregation, the important point is that, user of *Works_On* does not need to be concerned about the representation details of *Programmer* and *Project*. All the properties of the *Programmer* and *Project* associated with a particular *Works_On* are encapsulated by the class and may be accessed without explicit joins (Hughes 1991).

Therefore, the translation result would be:

```

class Programmer
    participate_in Works_On
    Attributes
        SSN, Salary, Sex : String;
        BDate           : Date;
end Programmer.
    
```

```

class Project
    participate_in Works_On
    Attributes
        P#, PName          : String;
        StartDate, DueDate : Date;
    end Project.
class Works_On
    assemble Programmer
    assemble Project
    Attributes
        Hours              : Integer;
    end Works_On.

```

Lastly, for the fourth category of this case, we identify another situation whereby the foreign key is a part of primary key. The candidate key(s) being referenced might be simple or composite primary key(s). According to the mapping and normalization process in relational data modelling, this situation happens when the relation that contains the foreign key(s) is a weak entity. The key attribute of the parent entity is included as a foreign key in the weak entity and will be part of the key attribute in the weak entity.

Thus, Rule 9 states that:

Rule 9. If part of the primary key of relation R is a foreign key attribute, which refers to a relation Q,

then - class R is treated as a weak entity, which depends on class Q;

- statement *depend Q* is included in class R;
- statement *has_dependent R* is included in class Q.

An example is shown below, the class *Children* is a weak entity that depends on its parent entity *Employee*.

```

Employee( SSN#, Name, Sex      : String)
Children( SSN#, Child Name, Sex : String,
          Age                : Integer)
ID: Children.SSN#  $\subseteq$  Employee.SSN#

```

As a result, we will get the following two classes:

```

class Employee
    has_dependent Children
    Attributes
        SSN#, Name, Sex      : String;
    end Employee.
class Children
    depend Employee
    Attributes
        Child_Name, Sex      : String;
        Age                  : Integer;
    end Children.

```

Case 2: The foreign key is a non-key attribute whereas the attribute being referenced is a primary key attribute in the original relation.

In the third and fourth step of the mapping process in relational modelling, for each regular binary 1:1 and 1:N relationship type R , identify the relation S that represents the participating entity type at the full participation or N-side of the relationship type. Include as foreign key in S the primary key of the relation T that represents the other entity type participating in R (Elmasri 2003).

Thus, the existence of the non-key attribute in relation S that refers to the key attribute of relation T means that the foreign key in S is merely referring to relation T and not an instance of relation T or even assembling relation T . Thus, the existence of this foreign key as non-key attribute will be treated as an interaction between S and T .

We shall conclude our translation approach with Rule 10:

Rule 10: If relation R has a foreign key fk which is not a key attribute, that refers to a relation P ,

then

- attribute fk shows the interaction between class R and class P ;
- in class R , statement $fk: set(P)$ inverse is $P.R$ replaces attribute fk ;
- in class P , statement $R: set(R)$ inverse is $R.fk$ is included.

Below is an example demonstrating our approach:

```
Employee( SSN, Sex      : String,
          Salary, DeptNo : String,
          BDate         : Date)
Department(DeptNo, DName, Location : String)
ID: Employee.DeptNo  $\subseteq$  Department.DeptNo
```

After being translated in this step:

```
class Employee
    Attributes
        SSN, Sex, Salary      : String;
        BDate                 : Date;
        Work_in               : set(Department)
        inverse is Department.
        Worked_by;
end Employee.
class Department
    Attributes
        DeptNo, Dname       : String;
        Location            : String;
        Worked_by           : set(Employee)
        inverse is E
        mployee.Work_in;
end Department.
```

Identifying the Operations

Operations that are applicable to a data abstraction are classified into three categories: (i) constructor/destructor functions; (ii) accessor/query functions and (iii) transformer/update functions. Since the information for the declaration of operations for each object or relation is not provided in the relational data model, user's information is very important in this phase. Initially, our approach will suggest two operations for each class, which are the constructor and destructor operations. Below is an example that shows these two basic operations applied to a class:

```
class Hotel
  Attributes
    name, owner    : String;
    location       : set(Address);
    manager        : String;
    ...
  Methods
    create(...);
    destroy(...);
end Hotel.
```

RESULTS AND DISCUSSION

In this section, we will compare the translation approaches proposed by Castellanos *et al.* (1994), Stanisic (1999) and Fong (1997) with our translation approach using two sets of relational database conceptual schema, as shown in Fig. 5.

Castellanos *et al.* (1994) worked on translation from relational to object-oriented model known as BLOOM OO model. Their approach creates extra

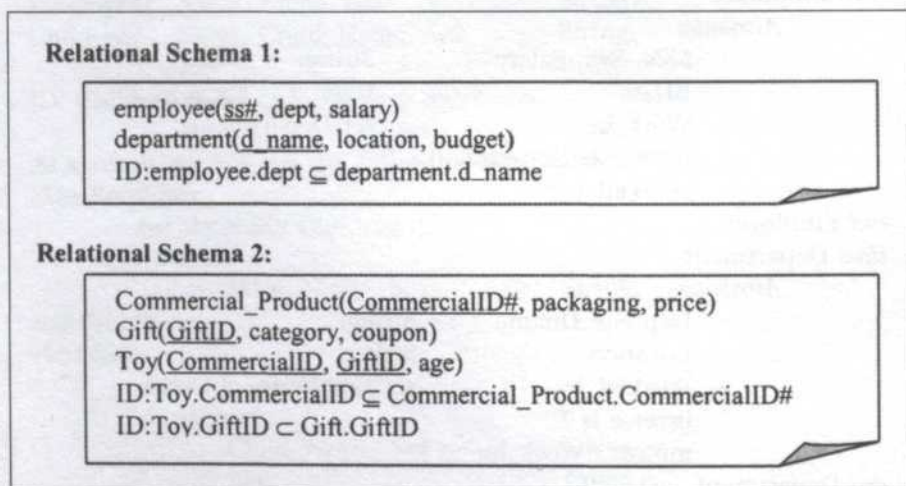


Fig. 5: Relational schemas used for comparisons

classes, which are sometimes not necessary. The translation of the first relational schema used for the comparison demonstrates this weakness.

The translated into BLOOM OO Model:

```

class employee          class privileged          class department
  subclass privileged    superclass employee    s_agg_of manager
  id ss#                exception_on dept    id d_name
  atrs dept             end_class            atrs budget
                        salary                end_class
end_class
    
```

In this example, one extra class *privileged* has been created. According to Castellanos *et al.* this class is created because *employee.dept* is not null-constrained. Therefore, it can exist as null value. For those employees whose *dept* attribute is null, they are considered as “privileged-employees”.

According to the definition of key constraint in relational database design, foreign key either exists as a value of the candidate key it refers to or is null. Therefore, the forming of class *privileged* is not necessary since the existence of null value for *dept* is perfectly fine. In our approach, the existence of *dept* in class *employee* will be indicated as *work_in:department.worked_by*, showing the interaction between these two classes. The translated OO conceptual schema from Relational Schema 1 using RETOO is shown in Fig. 6, while the comparison between Castellanos *et al.*'s and our approach on Relational Schema 2 is shown in Fig. 7.

We have also studied the translation approach proposed by Stanisic, which translates relational to object-oriented model. However, his translated OO schema is not semantically rich enough as he only considered inheritance and aggregation among the classes. Besides, the relationships among the classes are

```

class department
  Attributes
    d_name      : string;
    location    : string;
    budget      : string;
    worked_by   : set(employee) inverse is
                  employee.work_in;
end department.
class employee
  Attributes
    ss#         : string;
    work_in     : set(department) inverse is
                  department.worked_by;
    salary      : integer;
    
```

Fig. 6: Translated OO schema using RETOO approach

<i>By Castellanos</i>	<i>By RETOO</i>
<pre> class Commercial_Product partic_in Toy id CommercialID# atrs packaging, price end_class class Gift partic_in Toy id GiftID atrs category, coupon end_class class Toy cart_aggr_of Commercial_Product Gift atrs age end_class </pre>	<pre> class Commercial_Product inherited_by Toy Attributes CommercialID# : string; packaging : string; price : string; end Commercial_Product. class Gift inherited_by Toy Attributes GiftID : string; category : string; coupon : string; end Gift. class Toy inherit Commercial_Product inherit Gift Attributes age : integer; end Toy. </pre>

Fig. 7: Comparison of translation result on relational schema 2

not shown clearly in the translated OO schema. His translated OO schemas are shown in Figs. 8 and 9.

As shown in Fig. 9, class *Gift* and class *Commercial_Product* do not state their relationship with class *Toy*. However, with RETOO, the interactions among classes are specified clearly (refer to Fig. 7).

Fong (1997) also proposed an approach to translate relational to object-oriented model. Similarly, the translated OO schema is not semantically rich enough. For instance, his translation approach did not support multiple inheritance among classes. Fig. 10 illustrates Fong's approach in translating Relational Schema 1.

```

class department
  d_name      : string;
  location    : string;
  budget      : string;
end;
class employee
  ss#         : string;
  dept        : ref department;
  salary      : string;
end;

```

Fig. 8: Translated OO schema using Stanisis's approach on relational schema 1

```

class commercial_Product
  CommercialID#      : string;
  packaging          : string;
  price              : string;
end;
class gift
  GiftID            : string;
  category          : string;
  coupon            : string;
end;
class toy
  com_product       : ref commercial_product;
  gift              : ref gift;
  age               : number;
end;
    
```

Fig. 9: Translated OO schema using Stanisc's approach on relational schema 2

```

class department
  attr d_name      : string
  attr location    : string
  attr budget      : string
  association attr hire ref
                  set(Employee)
end
class employee
  attr ss#         : string
  attr salary      : string
  association attr hired_by ref
                  department
end
    
```

Fig. 10: Translated OO schema using Fong's approach on relational schema 1

Although there is not much difference shown in translating the first relational schema, according to his approach, the Relational Schema 2 will be translated into the OO schema, as shown below:

```

Class Commercial_Product
  attr CommercialID:string
  attr packaging:string
  attr price:integer
end
    
```

```

Class Gift
    attr GiftID:string
    attr category:String
    attr coupon:integer
end
Class Toy
    attr age:integer
    association attr CommercialID ref Commercial_Product
    association attr GiftID ref Gift
end
ID:CommercialID  $\subseteq$  Commercial_Product.OID
ID:GiftID  $\subseteq$  Gift.OID
    
```

From the above example, we can see clearly that class *Toy* is an instance of class *Commercial_Product* and also an instance of class *Gift*. Therefore, the relationship among these three classes would be more precisely labeled as multiple inheritance. If translated by RETOO, *Toy* will be considered as inheritance of both *Commercial_Product* and *Gift*, as clearly shown in Fig. 7.

SUMMARY

We have proposed a methodology to translate relational database conceptual schema into object-oriented database conceptual schema. The translation approach is developed based on the understanding of mapping and normalization processes in relational database modelling. Undoubtedly, the relational semantics are maintained perfectly when the relational model is translated into an object-oriented model. The determiners used in developing the translation rules are inclusion dependencies, key attributes and types of attributes. There are four main steps in the translation approach, which operate based on the ten translation rules.

Besides maintaining the relational semantics, the semantics of our translated object-oriented conceptual schema is also enhanced with richer object-oriented concepts such as aggregation and inheritance. Interaction between or among classes is shown clearly. We also reveal the behavior of every class by adding the methods in the OO conceptual schema. The translation rules differ from previous works in terms of simplified translation approach yet producing a complete and a better-understood object-oriented database conceptual schema.

REFERENCES

- CASTELLANOS, M., F. SALTOR and M. GARCÍA-SOLACO. 1994. Semantically enriching relational databases into an object oriented semantic model.
- CASTELLANOS, M. and F. SALTOR. 1991. Semantic enrichment of database schemas: an object-oriented approach. *Publication of IEEE*: 71-78.

- ELMASRI, NAVATHE. 2003. *Fundamentals of Database Systems*. 4th edition. The Benjamin/Cummings Publishing Company, Inc.
- FONG, J. 1997. Converting relational to object-oriented databases. *Publication of SIGMOID Record*, 26, No.1.
- HUANG, S.M., H.H. CHEN, C.H. LI and J. FONG. 1997. A data dictionary system approach for database schema translation. *Publication of IEEE*: 3966-3971.
- HUGHES, J.G. 1991. *Object-oriented Databases*. 1st edition. Prentice Hall.
- LUKOVIC, I. and P. MOGIN. 1996. An approach to relational database schema integration. *Publication of IEEE*: 3210-3215.
- MCBRIEN, P. and A. POULOVASSILIS. 1998. Automatic migration and wrapping of database applications – A schema transformation approach. Department of Computer Science Technical Report, King's College London.
- SEOL, Y.H. 1997. NAMCIC virtual repository schema translation. In *National Academic Medical Center Information Consortium*. <http://cat.cpmc.columbia.edu/namcic/trans.html>.
- SOON, L.K., H. IBRAHIM, A. MAMAT and C.S. PUA. 2001. Translating from relational model to object-oriented model. In the *International Conference on Information Technology and Multimedia (ICIMU 2001)*.
- STANISIC, P. 1999. Database transformation from relational to object-oriented database and corresponding query translation. In *Workshop on Computer Science and Information Technology CSIT*, p. 199-208.

Study of Photobleaching Mechanism in Methylene Blue Sensitized Gelatin Using a Single Beam UV-Vis. Fibre Optics Spectrophotometer

Chan Kok Sheng & *W. Mahmood Mat Yunus

Department of Physics,
Faculty of Science and Environmental Studies
Universiti Putra Malaysia
43400 UPM Serdang, Selangor, Malaysia

Received: 27 March 2002

ABSTRAK

Dalam penyelidikan ini, kami telah mengkaji kesan fotopelunturan metilin biru (MB) didopkan dalam gelatin matrik menggunakan spektrofotometer gantian optik uv-sinar nampak. Pemancaran sampel dengan cahaya uv-sinar nampak menyebabkan pengurangan puncak penyerapan dengan bertambahnya masa pemancaran. Ini menunjukkan dengan adanya pemancaran, pewarna molekul MB difotolunturkan kepada molekul MB tanpa warna. Keputusan hasil kajian ini menunjukkan proses fotopelunturan yang lambat berlaku pada kepekatan pewarna yang tinggi dalam matrik gelatin. Kajian ini menunjukkan metilin biru (MB) didopkan dalam matrik gelatin membuka kemungkinan yang baru dalam penggunaan bidang holografi.

ABSTRACT

In the present study, we have investigated the photobleaching of the methylene blue (MB) doped in Gelatin matrix using uv-visible fibre optic spectrophotometer. Illumination of the sample by uv-visible radiation resulted in a decrease of the absorption peak with the increasing of irradiation time. This indicates that upon irradiation MB dye molecule is photoreduced to its leuco form (colorless) of MB. The present experimental results indicate a slower photobleaching process occurring at higher concentration of dye doped in gelatin matrix. This study shows that the MB doped in gelatin solid matrix opens a new possibility in real-time holography applications.

Keywords: Photobleaching, methylene Blue gelatin, absorbance spectra photochemical reaction

INTRODUCTION

In recent years, holography finds very wide applications in the field of technology particularly in the usage of holograms memory elements. Holography memories could conceivably store huge amounts of digitized information conveniently and inexpensively. Holographic recording materials based on the dye-polymer system have contributed significantly to the recent growth of holographic applications (Pradeep *et al.* 2000).

* Corresponding author

It has been reported by Cristina *et al.* (1987) that certain dyes in the presence of electron donor became colorless when irradiated. This bleached dye is known to be the product of the light excited dye and an electron taken from the surrounding medium. The new molecule is known in chemistry as the leuco form of the dye (leuco dye). This leuco dye has been reported to be a strong reducing agent that is capable of reducing a variety of substances such as the dichromate ion into trivalent chromium.

Methylene Blue (MB) is the most used dye for formation of high spatial frequency amplitude and phase holograms with a conventional He-Ne laser as a light source. Photobleaching of MB is the principal mechanism of grating formation. It is known that MB cannot be bleached in a pure form. In order to bleach the MB molecules, they must be put into a suitable optical quality matrix. The matrices widely used for this purposes are: polyvinyl alcohol (PVA), poly(methylmethacrylate) (PMMA), dichromated gelatin and acrylamide base (Toshihiro *et al.* 1979; Sergio 1987; Cristina *et al.* 1987). In this study, the photobleaching mechanism of MB doped in gelatin matrix was investigated in details.

PHOTBLEACHING MECHANISM

The photochemical reactions that are believed to occur during the photobleaching of MB sensitized gelatin can be explained as follows (Cristina *et al.* 1987; Nadia 1991):

- (i) During illumination, the MB dye molecule absorbs a photon and is brought into the excited state (i.e. $^1\text{MB}^*$ is the first excited state and $^3\text{MB}^*$ is the transition of dye molecule to another state with a longer lifetime).



- (ii) The gelatin acts as an electron donor to bring MB to its leuco form (colorless):



- (iii) The excited MB dye molecules can return to the electronic ground state by a radiationless transition (Cristina *et al.* 1987), then:



or the dye-dye interactions produce the non-bleached molecules.



EXPERIMENTAL DETAIL

MB and gelatin supplied by BDH Chemicals Ltd. England were used as received. The molecular structure of the MB dye is shown in Fig.1. The

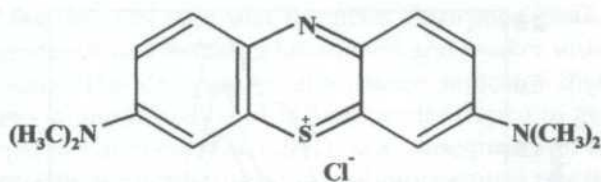


Fig. 1: The molecular structure of the methylene blue dye

preparation of MB doped Gelatin samples is similar to the one reported by Pradeep *et al.* (2000). The solution of gelatin was prepared by dissolving the required amount of gelatin in distilled water. A homogeneous solution with 8% (w/v) of gelatin was obtained after the solutions were heated at 80°C. The MB was then added to the gelatin solution and the mixture was heated for 5 min. Three solutions with different dye concentrations, namely 6.3×10^{-4} mol/l, 1.9×10^{-3} mol/l and 3.1×10^{-3} mol/l were prepared in the present study. The MB doped gelatin solid samples were obtained by keeping the solutions at room temperature in the dark for 48 hours. The solid gelatin sample was then kept in a dessicator under vacuum for another 24 hours. Finally, the samples were cut into were cut into circular shape with diameter 10 mm for the following investigation.

The optical absorbance and transmission spectra of the MB sensitized gelatin samples were recorded at room temperature using uv-visible fibre optics spectrophotometer (OCEAN Optics S2000, Inc), incorporated with a personal computer. The photochemical reaction in the samples were monitored by recording the absorbance and transmission curves for the exposure time 600 s with the intervals of 60 s.

RESULTS AND DISCUSSION

It is known that absorption is defined as the transfer of energy from an electromagnetic field to a molecular entity (Barakat *et al.* 2001). The optical absorption spectra of a pure gelatin sample and MB doped gelatin samples at three different dye concentrations are shown in Fig. 2. The pure gelatin matrix was transparent throughout the spectrum region 450 nm-800 nm with a very low absorbance level (i.e. ~ 0.06). For MB doped gelatin samples, we observed that a well-resolved characteristic absorption peak centered at 668 nm with a shoulder at 620 nm. The observed absorption peak at 668 nm is corresponding to the transitions between the ground state (S_0) and first excited singlet state (S_1) of the dye molecules when the sample irradiated with photon energy (Sergey *et al.* 1998). Nadia and Roger (1991) reported that the MB sensitized gelatin had an absorption band in the red part of the spectrum with the maximum absorption located around 670 nm. The main absorption peaks increases at higher concentration due to the increase in the number of dye molecules (Pradeep *et al.* 2000)

Fig. 3 shows that the absorption spectra for MB doped gelatin samples obtained for two dye concentrations (i.e 6.3×10^{-4} mol/l and 3.1×10^{-3} mol/l) at

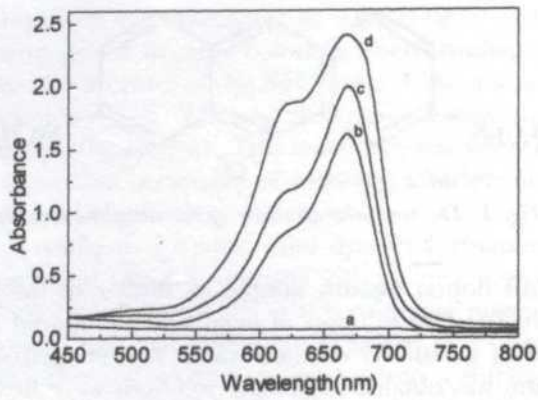


Fig. 2: The absorption spectra of (a) a typical pure gelatin sample and three different dye concentration of methylene blue with (b) 6.3×10^{-4} mol/l; (c) 1.9×10^{-3} mol/l and; (d) 3.1×10^{-3} mol/l

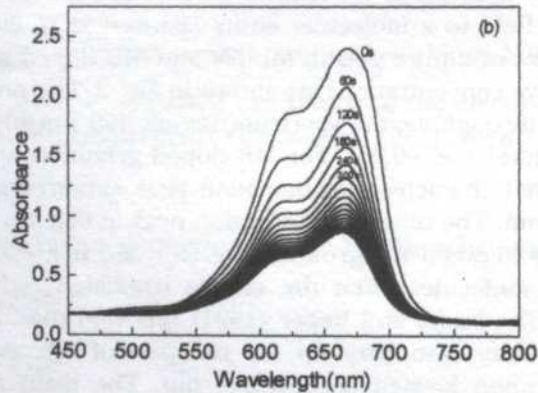
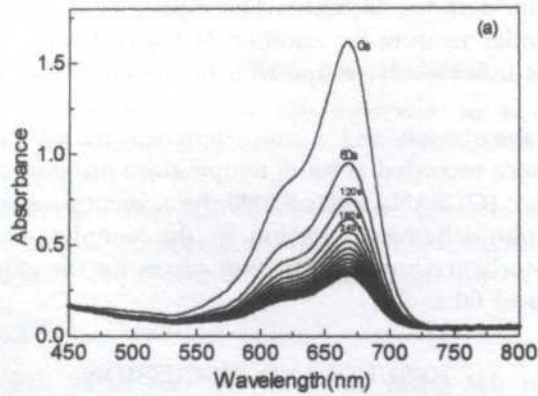


Fig. 3: Variation in the optical absorption spectra during uv-visible irradiation for 600 seconds at dye concentrations of : (a) 6.3×10^{-4} mol/l; (d) 3.1×10^{-3} mol/l

the interval of 60s. We observed that the main absorption peak located at 668 nm decreases gradually and becomes broadened and weaker with the increasing of irradiation time. The decrease in absorbance indicates that the uv-visible irradiation causes photobleaching of MB molecules doped in gelatin matrix. It has been reported by Carretero *et al.* (2001), as a consequence of light absorption, the MB dye molecule is photoreduced in a photochemical reaction resulting in a production of leuco form of dye molecules.

Kubota *et al.* (1976) had suggested that to favor the photoreduction of MB it is necessary to have an electron donor such as ethylene diamine tetraacetic acid (EDTA) in dichromated gelatin sensitized with MB. However, in the present study of MB sensitized gelatin, it is noticeable that the addition of EDTA is not necessary and that the reduction of the excited molecule is probably performed by the gelatin itself. This study shows that photobleaching of MB embedded in solid matrix is an appropriate medium for holographic elements, particularly for reflection grating (Nadia *et al.* 1988).

Effect of Dye Concentration on Photobleaching

Fig. 4 shows the decrease of absorbance peak (668 nm) with irradiation time for three different MB dye concentrations in gelatin matrix (i.e. 6.3×10^{-4} mol/l, 1.9×10^{-3} mol/l and 3.1×10^{-3} mol/l). Obviously, it could be observed from this figure that at lower concentration of MB (6.3×10^{-4} mol/l) the absorbance of the sample decreased much faster than that at a higher concentration of MB (3.1×10^{-3} mol/l). This indicates that the photoreduction of MB dye molecules to leuco MB appears much slower at higher concentration. These results were in a good agreement with those reported by Cristina *et al.* (1987) and Pradeep *et al.* (2000). They had reported that the sample with lower MB concentration shows faster rate of bleaching and for achieving faster bleaching at higher concentrations, higher exposure energy is needed. According to Cristina *et al.* (1987), the faster photobleaching process at lower concentration is due to the deexcitation process which is shown in Eqns. 4 and 5, where by increasing the concentration of the dye, one increases the possibility of an interaction between the two neighbored excited dye molecules ($^1\text{MB}^*$ and $^3\text{MB}^*$) and the nonexcited dye molecules (MB) resulting in the return of the excited molecule to the ground state.

Optical Transmission Spectra

The photobleaching phenomenon during uv-visible irradiation can also be observed by monitoring the changes in optical transmission spectra. Fig. 5 shows the recorded transmission spectra of the MB doped gelatin sample at a dye concentration of 3.1×10^{-3} mol/l. Before uv-visible irradiation, the colored transparent sample has a high optical transmission in the wavelength range of 450 nm-510 nm and 720 nm-800 nm with ~71% and ~80% of transmission, respectively. Obviously, the irradiation of the MB doped gelatin sample leads to an increase in overall transmission throughout the spectrum region with the increase of irradiation time. During irradiation, the lower optical transmission

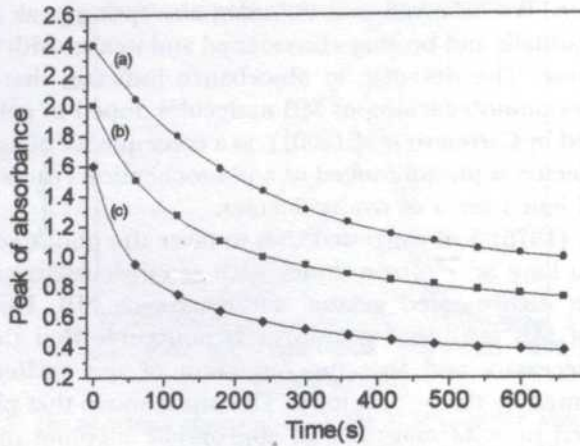


Fig. 4: Plot of absorption peak versus irradiation time at three different dye concentration with (a) 3.1×10^3 mol/l; (b) 1.9×10^3 mol/l and; (c) 6.3×10^4 mol/l

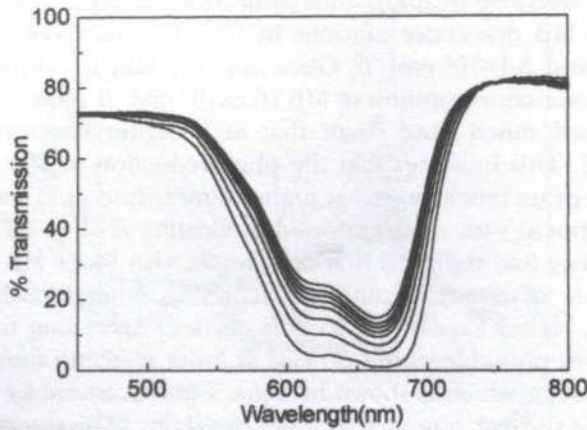


Fig. 5: Transmission spectra changes during uv-visible irradiation for methylene blue doped in gelatin sample at dye concentration of 3.1×10^3 mol/l

in the region of 600 nm-680 nm increases gradually which is purely due to the gradual photodegradation of MB dye molecule to leuco MB. After 600 s of irradiation, the bleached sample shows a higher transmission value of ~73% and ~83% in the wavelength range of 450 nm-510 nm and 720 nm-800 nm, respectively. This indicates that most of the MB is transformed into leuco MB upon uv-visible irradiation.

The Aging Effect

Another phenomenon showed that, after uv-visible irradiation, the absorbance peak of the sample (dye concentration 6.3×10^4 mol/l) was recovered after

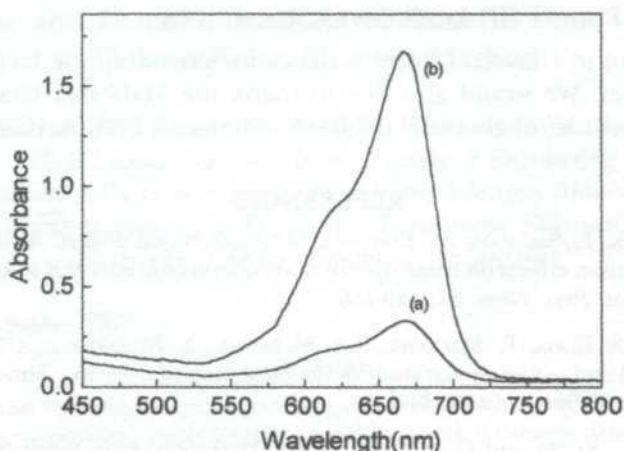


Fig. 6: Absorbance spectra for: (a) after uv-visible radiation and (b) after being exposed to atmospheric air for 12 hr

storage in the dark at room temperature for 12 hours (Fig. 6). It can be seen that the blue color of the MB doped gelatin matrix was restored after being exposed to atmospheric air. According to Nadia *et al.* (1988), this effect is due to the reoxidation of the leuco form of the dye molecules:



This means that the dye can return to its unexcited state when it is in contact with the molecular oxygen, which will remove the extra oxygen.

CONCLUSION

In this paper, the photochemical reactions of the MB doped in gelatin solid matrices have been studied by using uv-visible fibre optics spectrophotometer. The photobleaching of MB upon uv-visible irradiation was confirmed by a decrease of the absorption peak with the increasing of the exposure time. The colored MB dye molecule is photoreduced to its leuco form (colorless) of MB upon irradiation. The present experimental observation shows that a slower photobleaching process occurs at higher concentration of dye doped in gelatin matrix. This is mainly due to the dye-dye interaction between two neighbours excited dye molecule and nonexcited dye molecule resulting in the return to the ground state of the excited molecule. It is also observed that the bleached gelatin sample was recovered to its original color within 12 hours after uv-visible irradiation, because the leuco form of the dye can return to the nonexcited state when it is in contact with the molecular oxygen as reported by other researchers.

ACKNOWLEDGEMENTS

We are grateful to Universiti Putra Malaysia for providing the facilities to carry out this project. We would also like to thank the Malaysian Government for financial support through IRPA (02-04-09-0065) and PASCA (GS06618).

REFERENCES

- BARAKAT, M.F., K. EL-SALAMAVY, M. EL-BANNA, M. ABDEL-HAMID and A. ABDEL-REHIM TAHA. 2001. Radiation effects on some dyes in non-aqueous solvents and in some polymeric films. *Radiat. Phys. Chem.* **61**: 129-136.
- CARRETERO, L., S. BLAYA, R. MALLAVIA, R.A. MADRIGAL, A. BELENDEZ and A. FIMIA. 1998. Theoretical and experimental study of the bleaching of a dye in a film-polymerization process. *Appl. Opt.* **37**: 4496-4499.
- CRISTINA, S., A.L. ROGER and C. R. PIERRE. 1987. Methylene blue sensitized gelatin as a photosensitive medium for conventional and polarizing holography. *Appl. Opt.* **26**: 1989-1997.
- KUBOTA, T., T. OSE, M. SASAKI and K. HONDA. 1976. Hologram formation with red light in methylene blue sensitized dichromated gelatin. *Appl. Opt.* **15**: 556-558.
- NADIA, C. and A.L. ROGER. 1988. Processing of holograms recorded in methylene blue sensitized gelatin. *Appl. Opt.* **27**: 3008-3012.
- NADIA, C. and A.L. ROGER. 1991. Real time bleaching of methylene blue or thionine sensitized gelatin. *Appl. Opt.* **30**: 1196-1200.
- PRADEEP, G.M., S. CYRIAC, S. RAMKUMAR and C.S. KARTHA. 2000. Observation of retention of optical absorption change in methylene blue sensitized gelatin and poly(vinyl alcohol) plates on He-Ne laser irradiation. *Jpn. J. Appl. Phys.* **39**: 137-140.
- SERGEY, S., A. TAYLOR, P. VENKATESWARLU and A. WILKOSZ. 1998. Optical branching in dyedoped polymeric waveguide. *Opt. Commun.* **145**: 265-273.
- SERGIO, C. 1987. Dry polymer for holographic recording. *Appl. Opt.* **26**: 3904-3910.
- TOSHIHIRO, K. and T. OSE. 1979. Methods of increasing the sensitivity of methylene blue sensitized dichromated gelatin. *Appl. Opt.* **18**: 2538-2539.

Static and Dynamic Analysis of Rockfill Dam Using Finite-infinite Element Method

¹J. Noorzaei, ²M. Karami, ¹Waleed A. Thanoon & ¹M. S. Jaafar

¹Civil Engineering Department, Faculty of Engineering
Universiti Putra Malaysia, 43400 UPM, Selangor, Malaysia

²Post Graduate Student, Civil Engineering Department, Engineering College
University of Shahid Chamran, Ahwaz, Iran

Received: 5 May 2003

ABSTRAK

Dalam kertas ini, sebuah empangan dan tanah di bawahnya telah dimodelkan dengan menggunakan unsur tergabung terhingga-tak terhingga dalam keadaan terikan satah. Tegasan statik yang terjadi pada sistem empangan-asas disebabkan oleh beban-beban graviti dan hidrostatik telah dinilai. Analisis seismik kenyal-plastik sistem tersebut kemudiannya dilakukan dengan menggunakan kriteria Drucker-Prager untuk ketidakurusan bahan. Kesamaan gerakan diselesaikan melalui kaedah pengamiran tokokan masa Newmark. Kajian menekankan kelakuan struktur sistem empangan-asas yang dikenakan dengan gegaran gempa bumi. Kelakuan dalam bentuk kontur pesongan, agihan tegasan dan ragam kegagalan dibentangkan.

ABSTRACT

In this paper, the dam body and the underneath soil were modeled using coupled finite-infinite elements under plane strain conditions. Initially, static stresses developed in the dam-foundation system due to gravity and hydrostatic loads are evaluated. Elasto-plastic seismic analysis of the dam-foundation system is next carried out by adopting the Drucker-Prager criterion for the material nonlinearity. The equation of motion is solved by Newmark incremental time integration technique. The study focuses on the structural behaviour of the dam-foundation system under earthquake excitations. The behaviour in terms of displacement contours, stress distributions and the failure mode are presented.

Keywords: Finite-infinite elements, static, elasto-plastic seismic analysis

INTRODUCTION

The rockfill dam has been used in many parts of the world with increasing frequency in recent years. This type of the dam is one of the most attractive type for the consulting engineers because of its good adaptability, convenience of construction, good performance during the past earthquakes, safety and economy with the development of the technologies of construction and the application of new structural materials. Rock fill dams having different heights have been used in different parts of the world. As an example Kuzuryu dam which is 128 m high was constructed in Japan (Nose *et al.* 1980), Masjeid Soleyman dam which is 170 m high was built up in Iran (Jafarzadeh *et al.* 1998), and Messochara dam

which is 150 m high was completed in Greece (Thanopoulos *et al.* 1998). To study the variation of stresses in the body of the dams subjected to static and dynamic loading, the finite element technique has been widely used.

Skermer *et al.* (1973) analysed a rockfill dam with impervious core using a three-dimensional finite element model. A hyperbolic model was used to account for material nonlinearity. The comparisons between the results obtained from the finite element analysis with the results measured in the rockfill dam at site showed good agreement. Seed *et al.* (1985) reported a set of conventional finite element analyses aimed at estimating the magnitude of sliding deformations of typical concrete faced rockfill dams subjected to base accelerations with a peak acceleration amplitude (PGA) of 0.5 g. It is concluded that in high seismic active area, the geometry of the dam body and abutments should be 1.6H :1V or flatter. Bureau *et al.* (1985) presented a study dealing with the seismic performance of rockfill dams in general and the possible modes of failure of concrete faced rockfill dams in particular. The permanent deformation obtained directly using DSAGE software is based on finite difference method. Sayed Khaleed *et al.* (1990) used incremental and interface elements to discretise the Cethana concrete-faced rockfill dam assuming plain strain condition.

Gazetas *et al.* (1992, 1995) have studied the 3D seismic response of an actual 120 m tall concrete-faced rockfill dam, and concluded that tall concrete-faced rockfill dams in narrow canyons of solid rock may experience extremely intense shaking at mid crest during strong seismic motions. Roa *et al.* (1996) studied the Santa Juana dam under static and earthquake excitation having peak acceleration of 0.3 g. The deformation in the dam body and stresses in the concrete slab are obtained using the finite element method. Mircerska *et al.* (1998) analysed a rockfill dam for linear and nonlinear cases using Process Software under plane strain condition. The linear and nonlinear behaviour of the dam in terms of displacement, acceleration and stress histories were presented and discussed.

In the present study which is the continuation of the author's previous work (Noorzaei *et al.* 1999, 2000, 2002) the material nonlinearity of Kavar rockfill dam have been taken into consideration by employing the Drucker Prager yield criteria. The behaviour of the dam with respect to accelerations, displacements and stresses in the dam body has been discussed. Moreover, an attempt has been made to find out the mode of failure in the dam.

Static and Dynamic Analysis

Static stresses developed in the dam-foundation system due to gravity and hydrostatic loads are evaluated using usual finite element procedure available in many finite element textbooks. The nonlinear dynamic analysis of rockfill dams involves the solution of the well-known dynamic Equation of motion (Zeinkeiwicz *et al.* 1972; Owen and Hinton 1980):

$$[M]\{\ddot{u}\} + [c]\{\dot{u}\} + [k]\{u\} = -[M]\{\ddot{u}_{(g)}\} \quad (1)$$

Using the Newmark step-by-step integration method the solution of Eqn. (1) can be expressed by:

$$\dot{u}_{t+\Delta t} = \dot{u}_t + [(1-\gamma)\Delta t]\ddot{u}_t + (\gamma\Delta t)\ddot{u}_{t+\Delta t} \quad (2)$$

$$u_{t+\Delta t} = u_t + (\Delta t)\dot{u}_t + [(0.5-\beta)(\Delta t)^2]\ddot{u}_t + [\beta(\Delta t)^2]\ddot{u}_{t+\Delta t} \quad (3)$$

The record of the earthquake is divided into definite steps and in each step, the displacement vector determined from which the strains and stresses at each time step are calculated.

Drucker-Prager failure criteria was used to investigate the yielding of the materials in the dam-foundation system using:

$$f = \alpha J_1 + (J_2')^{0.5} - K \quad (4)$$

where, J_1 and J_2' are first and second stress invariants,

$$\alpha = \frac{2 \sin \phi}{\sqrt{3}(3 - \sin \phi)} \quad \text{and} \quad K = \frac{6C \cos \phi}{\sqrt{3}(3 - \sin \phi)}$$

At each time step, a check on material yielding is performed for all Gauss points using Eqn.(4). If the state of stress at a specific Gauss point exceeds the yielding stress, the effective stress and residual stress are calculated as:

$$\{\Delta f_r\} = \int_v [B]^T \{\sigma\} d_v - \{f_r\} \quad (5)$$

By comparing the effective stress with that obtained in the previous iteration, loading or unloading status at a specified Gauss point will be known. The portion of stress level that is greater than yield value must be brought back to the yield surface by iteration processes within each time step. This procedure is useful in earthquake analysis when accelerograms are used to characterise the ground motion when structural nonlinear effects are present.

ANALYSIS OF ROCKFILL DAM

Finite-Infinite Modeling

The numerical example selected to illustrate the structural behaviour of rockfill dam is the Kavar rockfill in southern part of Iran. The dam has been proposed and designed by the consulting engineers (Noorzai *et al.* 1999, 2000). The Finite element discretisation of the dam-foundation system is shown in Fig. 1. The total number of the nodal points is equal to 533. The number of finite and infinite elements are 160 and 8 respectively. The software used for the analysis of the dam is a multi-element and general purpose two-dimensional finite

element package developed by the author (Noorzai *et al.* 2002). Appendix A shows the different types of elements such as eight-noded finite and five-noded infinite isoparametric element along with their shape function used for the idealization of the dam section. The berm in the upstream (shown in Fig. 1) has been added to enhance the stability of the dam. Different materials have been used for the main body of the dam and the berm.

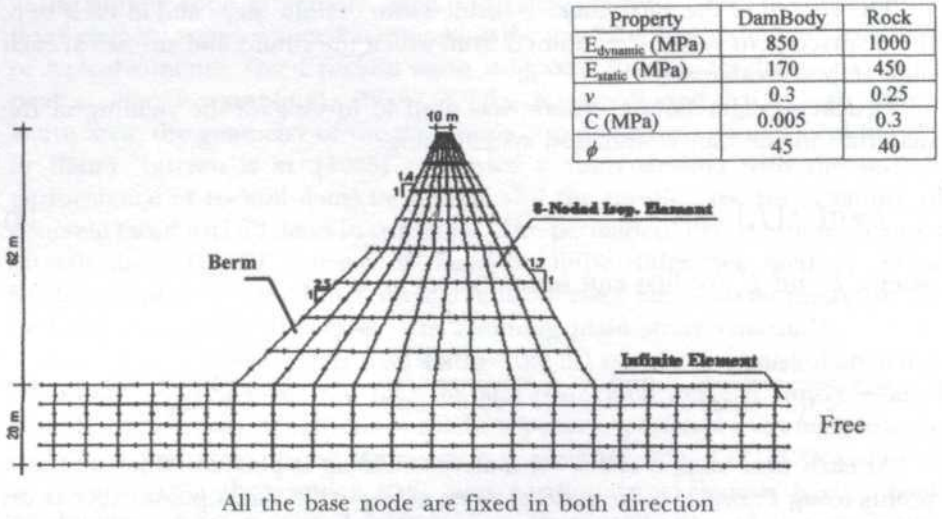


Fig. 1: Finite-infinite element discretisation of rockfill dam

Static Analysis

Initially static analysis of the dam for the dead weight has been performed. The corresponding static stress vector and load vector are stored for the earthquake analysis of the dam. Fig. 2 shows the contours of vertical and horizontal

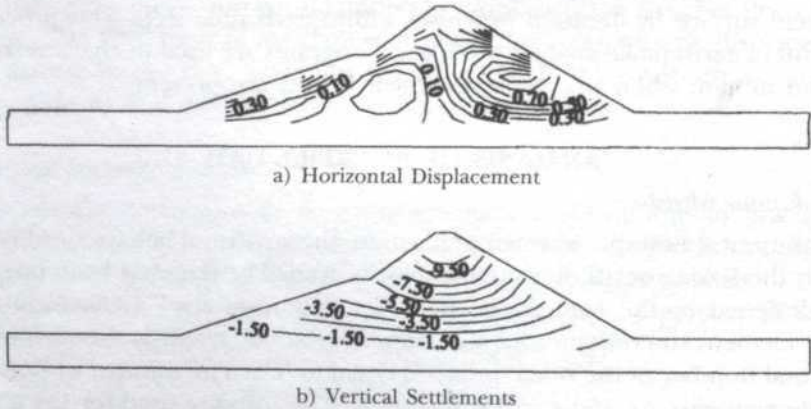


Fig. 2: Contour lines of maximum horizontal and vertical settlement due to static load

settlements obtained from static analysis. The contours indicate that there is an increase in the vertical displacement as the height of the dam is increased and has a maximum value of 9.5 cm at the crest level of the dam. On the other hand, there is negligible movement in the horizontal direction.

The distributions of the static stresses throughout the body of the dam in term and the contours of maximum and minimum principle stresses are shown in Fig. 3. It is clear from this plot that highest values of principal stresses are developed at the centre of the lower portion of the dam and their values are decreasing with the increase of the height of the dam. The contours also show that both maximum and minimum principle stresses are in compression.

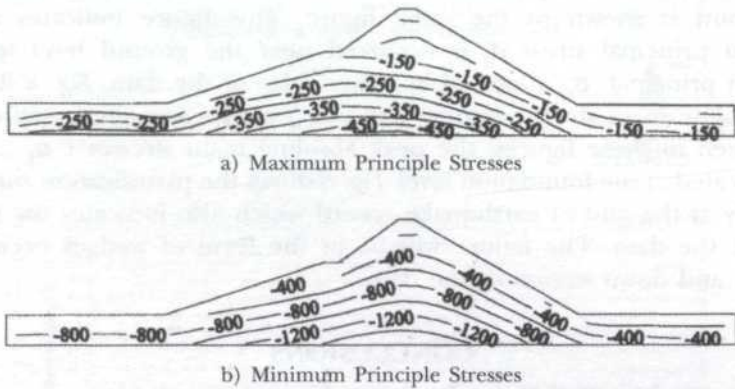


Fig. 3: Contour lines of maximum and minimum principle stresses due to static load

Dynamic Analysis

The dam-foundation system has been analysed for the earthquake excitation having $PGA=0.27g$ and duration time equal 6.1 seconds [DBL record] as shown in Fig. 4. By using the direct Newmark integration technique, the record of earthquake is divided into 1220 steps. Damping of 5% has been assumed for the analysis.

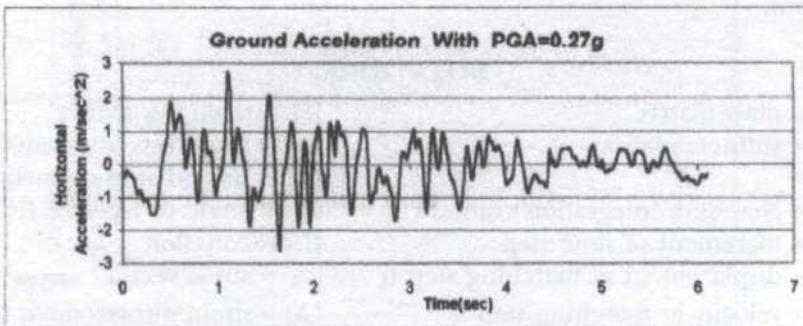


Fig. 4: Horizontal earthquake excitation record

The time history for the horizontal acceleration and displacement at three nodal points selected along the vertical central axis of the dam are shown in Figs. 5 and 6 respectively. Node 204 is selected at the ground level while nodes 326 and 439 are chosen to be at the berm and crest level of the dam respectively. Both acceleration and displacement increase with the increase of the height of the dam. The absolute horizontal acceleration at the top of the dam is found to be 10.7 m/s^2 , with an amplification factor (AF) of 3.96, while the peak absolute displacement at the top of the dam is found to be 3.03 centimeters.

Fig. 7 shows the time history of principle stresses and maximum shear stress at selected critical Gauss points in the dam section. The location of the selected Gauss point is shown in the same figure. This figure indicates that the maximum principal stress σ_1 is occurred near the ground level while the minimum principal, σ_3 is located at either sides of the dam. Fig. 8 shows the peak absolute main stress contours (σ_1, σ_3) in the dam cross-sections. As it can be seen in these figures, the peak absolute main stresses (σ_1, σ_3) are mostly located at the foundation level. Fig. 8 shows the plastification zone in the dam body at the end of earthquake record which also indicates the mode of failure of the dam. The failure will be in the form of wedges occurring at upstream and down stream of the dam.

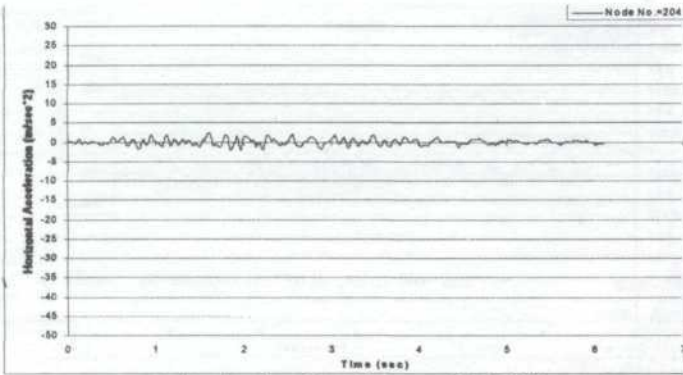
CONCLUSIONS

The main conclusions that can be drawn from this work are:

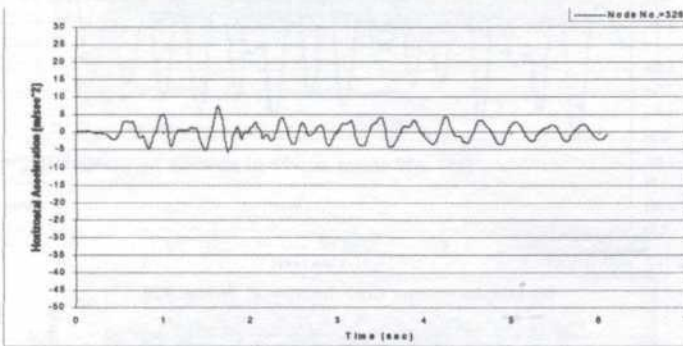
- (i) In static conditions, the maximum settlement occurred at the crest of the dam while the principal stresses reached their highest value in lower portions along the central core of the dam.
- (ii) The damage of rockfill dam, resulting from earthquake, is in the form of wedge failure occurring upstream and downstream of the dam.
- (iii) The maximum principal stress σ_1 occurred near the ground level while the minimum principal, σ_3 occurred at either sides of the dam.
- (iv) The maximum and minimum main stresses are much higher in the upstream side compared to those found in the downstream side of the dam.

NOTATIONS

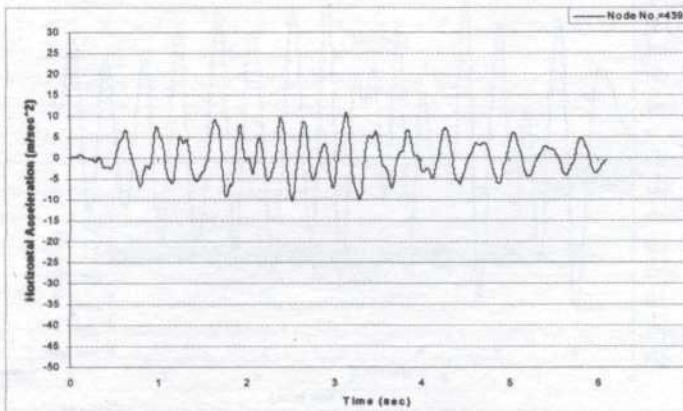
$[M]$ = mass matrix	$[c]$ = damping matrix
$[k]$ = stiffness matrix	J_1 = first stress invariants
α =	J_2' = second stress invariants
B = Newmark integration constant	ϕ = angle of internal friction
Δt = increment of time step	C = cohesion
U_n = displacement at marching step n	$\{\sigma\}$ = stress vector
\dot{u}_n = velocity at marching step n	$[B]$ = strain displacement matrix
\ddot{u}_n = acceleration at marching step n	$\{f\}$ = external load vector
$\{\dot{u}\}_{t+\Delta t}$ = velocity at time $t+\Delta t$	$\{\Delta f\}$ = residual force vector



a) Acceleration time history at Node 204

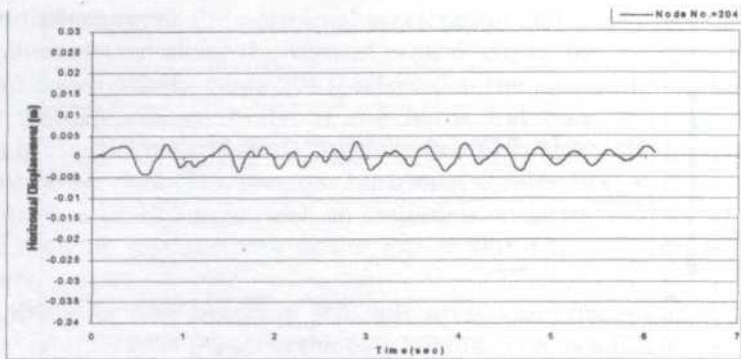


b) Acceleration time history at Node 326

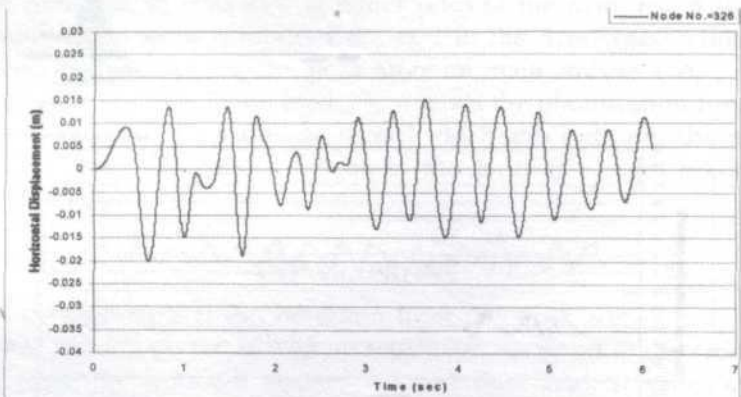


c) Acceleration time history at Node 439

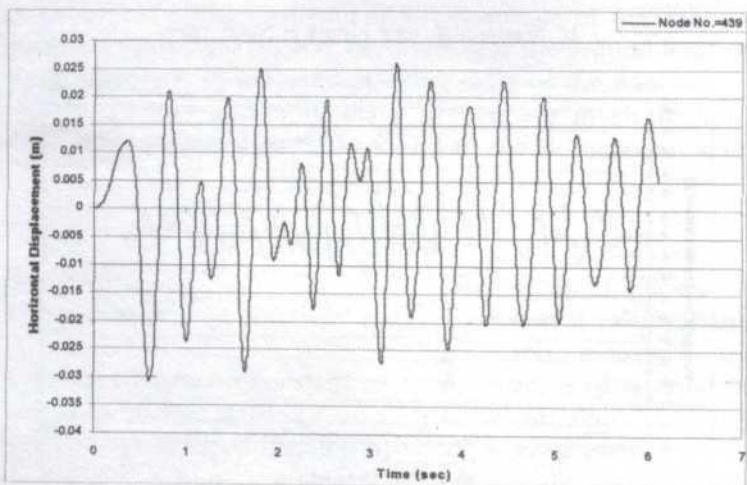
Fig. 5: Horizontal acceleration at Node 204, 326 and 439



a) Displacement time history at Node 204

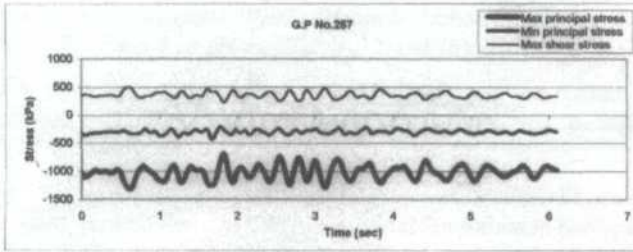


b) Displacement time history at Node 326

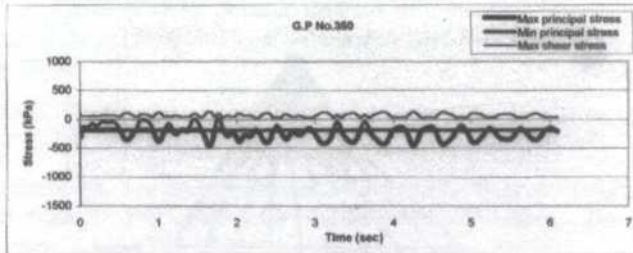
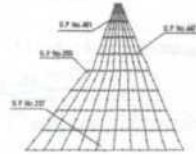


c) Displacement time history at Node 439

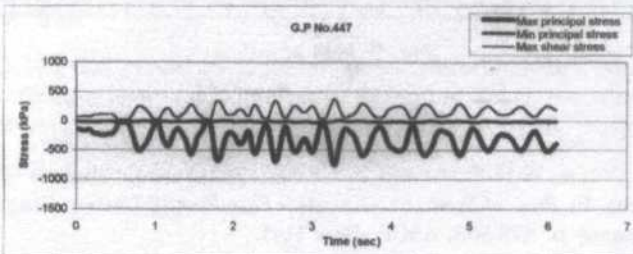
Fig. 6: Horizontal displacement at Node 204, 326 and 439



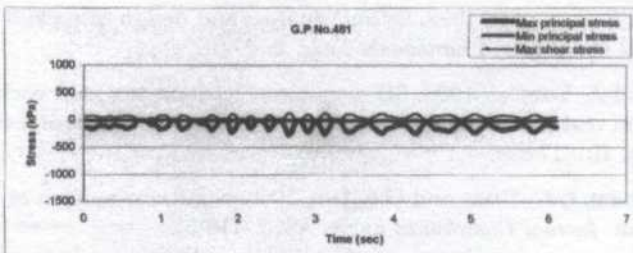
a) History of stresses in Gauss point No. 257



b) History of stresses in Gauss point No. 350



c) History of stresses in Gauss point No. 447



d) History of stresses in Gauss point No. 481

Fig. 7: Principle and shear stresses at critical G.P in the dam body

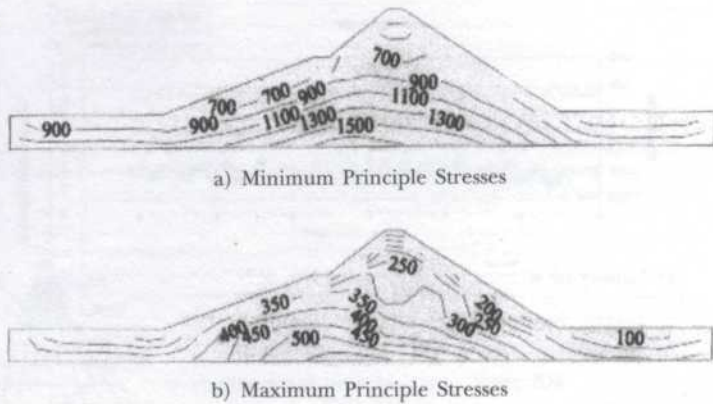


Fig. 8: Contours of peak absolute maximum and minimum principal stress (KPa)

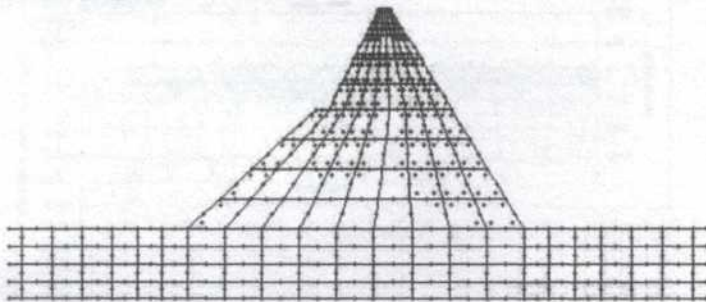


Fig. 9: Mod of failure

REFERENCES

- BUREAU, G., R.L. VOLPE, W.H. ROTH and T. UDAKA. 1985. Seismic analysis of concrete face rockfill dams. In *Proc. of Symp. on Concrete - Face Rockfill Dams - Design, Construction, and Performance*, p. 479-508, ASCE, New York.
- GAZETAS, G. and N. UDDIN. 1995. Dynamic response of concrete face rockfill dams to strong seismic excitation. *Journal of Geotechnical Engrg.* ASCE **121**(2): 185- 197.
- GAZETAS, G. and P. DAKOULAS. 1992. Seismic analysis and design of rockfill dams: state of the art. *Soil Dynamic and Earthquake Enng.* **2**: 27-61.
- JAFAZADA, F. and A. YAGHUBI. 1998. 3D dynamic behaviour of zoned rockfill dams with emphasis on real case study. In *Proced. Int. Symposium on New Trends & Guidelines on Dams Safety*, **II**: 817-824.
- KHALID, S., B. SINGH, G.C. NAYAK and O.P. JAIN. 1990. Nonlinear analysis of concrete face rockfill dam. *Journal Geotechnical Engrg.* ASCE **116**(5).
- MIRCEVSKA, V. and V. BICKOVSKI. 1998. Two-dimensional nonlinear dynamic analysis of rockfill dam. *Intenational Symposium on Dam Safety* **2**: 859-866.

- NOORZAEI, J. and E. MOHAMMADIAN. 1999. Dynamic behavior of the Kavar CFRD in southern Iran. *Int Journal of Hydropower and Dams* (6): 70-73.
- NOORZAEI, J. and E. MOHAMMADIAN. 2000. Modeling of concrete face rockfill dam via finite-infinite and interface elements. In *Proc. Int. Symp. on CFRD*, p. 361-370, 18 Sept, Beijing.
- NOORZAEI, J., M. KARAMI, T.A. WALEED and M.S. JAFAR. 2002. Elasto-plastic seismic response of Kavar rockfill dam. In *12th International Symposium in Earthquake Engineering*, I.I.T, Roorkee, India, Dec. (To be presented).
- NOSE M. and K. BABA. 1980. Dynamic behaviour of rockfill dams. In *Proceedings of Conference on "Dams & Earthquake"*, p. 69-78, Oct 1-2, London.
- OWEN, D.R.J and E. HINTON. 1980. *Finite Elements in Plasticity: Theory and Practice*. UK: Pineridge Press Limited.
- ROA, F.R. and L.A. GAMBOA. 1996. Seismic analysis of concrete – faced gravel-fill dams. In *Proceedings of the Int Symposium on Seismic and Environmental Aspects of Dams Design*, I, Santiago, Chile.
- SKERMER, N.A. 1973. Finite element analysis of el infiernillo dam. *Can. Geotech. Journal* 10(2).
- SEED, H.B., R.B. SEED, S.S. LAI and B. KHAMENEHPUR. 1985. Seismic design of concrete – face rockfill dams. In *Proc of Symp. on Concrete-face Rockfill Dams – Design, Construction and Performance*, p.459-478, ASCE, New York.
- THANOPOULOS, J. and J. TICOB. 1998. Erosion problems of concrete faced rockfill dams during construction. In *Proced. Int. Symposium on New Trends & Guidelines on Dams Safety*, II: 967-974.
- ZIENKIEWICZ, O.C. and G.C. NAYAK. 1972. Elasto - plastic stress analysis, a generalization for various constitutive relation including strain softening. *Int Journal Num. Meth. Energy*. 5(1): 113-135.

APPENDIX A

Shape functions for two-dimensional serendipity types of finite and infinite elements

Type of element	Element figure	Shape functions
Eight-nodes finite element		<p>For corner nodes :</p> $N_i = \frac{1}{4}(1 + \xi\xi_i)(1 + \eta\eta_i)(\xi\xi_i + \eta\eta_i - 1)$ <p>For midside nodes:</p> <p>a) $\xi = 0.0$</p> $N_i = \frac{1}{2}(1 - \xi^2)(1 + \eta\eta_i)$ <p>b) $\eta = 0.0$</p> $N_i = \frac{1}{2}(1 - \xi\xi_i)(1 + \eta^2)$
Five-nodes infinite element		$N_1 = \frac{\xi\eta(1-\eta)}{(1-\xi)} \quad N_4 = \frac{-\xi\eta(1+\eta)}{(1-\xi)}$ $N_2 = \frac{(1+\xi)(1-\eta)}{2(1-\xi)} \quad N_5 = \frac{-2\xi(1-\eta^2)}{(1-\xi)}$ $N_3 = \frac{(1+\xi)(1+\eta)}{2(1-\xi)}$

Studies of Equilibria Involving the Binary and Ternary Complexes of Aluminium with Eriochrome Cyanine R (ECR) and Cetylpyridinium Chloride (CP)

¹Musa Ahmad & ²Ramaier Narayanaswamy

¹*School of Chemical Sciences and Food Technology
Faculty of Science and Technology
Universiti Kebangsaan Malaysia
43600 Bangi, Selangor, Malaysia*

²*School of Chemical Engineering and Analytical Science,
The University of Manchester
P.O.Box 88, Sacville Street
Manchester M60 1QD, England*

Received: 19 May 2003

ABSTRAK

Kertas ini membincangkan kajian stoikiometri kompleks binari (aluminium-ECR) dan ternari aluminium-ECR-CP) bagi aluminium. Kedua-dua kompleks didapati hadir dalam larutan dan berada dalam keseimbangan antara satu sama lain. Pemalar pembentukan, kadar tindak balas dan stoikiometri kedua-dua kompleks telah ditentukan dalam kajian ini dan mekanisme tindak balas yang mungkin bagi pembentukan kompleks ternari telah dicadangkan dalam kertas ini.

ABSTRACT

This paper is concerned with the study of stoichiometry of binary (aluminium-ECR) and ternary (aluminium-ECR-CP) complexes of aluminium. Both complexes are shown to be present in the solution and in equilibrium with each other. The formation constant, the reaction rate and the stoichiometry of both complexes have been evaluated and a possible reaction mechanism of the ternary complex formation is proposed in this paper.

Keywords: Eriochrome cyanine R, aluminium, ternary complex, binary complex and equilibrium

INTRODUCTION

Spectrophotometric methods for the determination of aluminium based on the binary complex formation with eriochrome cyanine R (ECR) has been reported to exhibit moderate sensitivity (Marczenko 1976). Introduction of a third component such as a long quaternary base (ionic surfactant) to this binary system leads to the formation of a ternary complex with advantageous properties. Spectrophotometric analysis for aluminium ions based on this ternary system is far more sensitive than the method based on a binary system.

To date, there is no comprehensive study reported in the literature concerning the stoichiometry of the binary and ternary systems, and also the equilibrium associated with these systems. This paper reports the results on the

study of the stoichiometry of the binary and ternary complexes of aluminium with ECR, as well as the stoichiometry of the intermediates of these complexes formed at sub-stoichiometric amounts of cationic surfactant. This study was carried out in order to fully understand the characteristic of the ternary complex since we are interested in using the system for the development of optical fibre aluminium sensor. Our work on the development of optical fibre aluminium sensor by using this system has already been published (Musa and Norleen 2002; Musa and Narayanaswamy 2002). This study is also carried out to deduce possible mechanisms for this ternary complex formation.

MATERIALS AND METHODS

Reagents

Aluminium standard solution of 2.0×10^{-4} M was prepared by dissolving 0.0237g of amount of hydrated aluminium potassium sulphate, $\text{Al}_2(\text{SO}_4)_3 \cdot \text{K}_2\text{SO}_4 \cdot 24\text{H}_2\text{O}$ in deionised water and the solution was then diluted with deionised water to 250 mL. Aqueous solutions of 2.0×10^{-4} M ECR were prepared by dissolving required amounts of the reagent in deionised water and diluting it to 250 mL, to produce the 2×10^{-4} M solutions. A total weight of 0.0179 g cationic surfactant, cetyl-pyridinium chloride (CP) was dissolved in 250 mL deionised water to give CP standard solution of 2.0×10^{-4} M.

The ammonia-acetic acid buffer of pH 6.0 was prepared by mixing about 40 mL of 0.2 M ammonia solution with about 40 mL glacial acetic acid in deionised water. The pH value of this solution was adjusted to pH 6.0 using diluted ammonia solution or diluted glacial acetic acid solution, before dilution to 1 litre volume using deionised water.

Instrumentation

The absorbance of solutions was measured by using PERKIN-ELMER UV-Visible Spectrophotometer (λ V) and in all measurements, 1 cm cells were used. The pH measurements were carried out using an ECM 201 pH meter.

Procedures

Three methods have been used in this study to determine the stoichiometry of both binary and ternary complexes of the aluminium i.e. molar ratio method, continuous variation method (also known as Job's method) and slope ratio method. These are described below:

(i) Molar Ratio Method

In the molar ratio method, a series of solutions is prepared in which the analytical concentration of one reactant (usually the cation) is held constant while that of the other reactant varied (Skoog 1988). To determine the stoichiometric value of the reagent to the aluminium and that of the surfactant to the aluminium ion in the ternary complex, two approaches were used in this study. The first approach is where the concentration of the aluminium and the

reagent, as well as their molar ratio, were kept constant while the concentration of the surfactant was varied. In the second approach, the concentration of the aluminium and the surfactant, as well as their molar ratio, were kept constant while the concentration of the reagent was varied.

In the first approach, 1 mL of 2.0×10^{-4} M Al^{3+} solution and 5 mL 2.0×10^{-4} M of the reagent were used and added to a series of 25 mL volumetric flasks containing 2 mL buffer solution and different volumes of 2.0×10^{-4} M CP. All the solutions were then made to volume by using deionised water. In the second approach, 1 mL of 2.0×10^{-4} M Al^{3+} solution and 5 mL of 2.0×10^{-4} M CP were used. These solutions were added into a series of volumetric flasks containing 2 mL buffers and varied volumes of 2.0×10^{-4} M of the reagent. All the solutions were then made to 25 mL using deionised water before absorption measurements.

The same procedure was then applied to the binary complex but without surfactant added to the solution. In this case, the aluminium concentration was held constant and the reagent concentration varied.

(ii) Continuous Variation Method

In the method of continuous variation procedure, cation and reagent solutions of identical concentrations are mixed in such a way that the total volume and hence the total number of moles of reactants in each mixture is maintained at constant but the mole-ratio of reactants varies systematically (Skoog 1988).

For ternary complex, this method was applied for the determination of stoichiometry of aluminium to the reagent when the aluminium to CP ratio was held a constant. The aluminium, 2.0×10^{-4} M and the reagent 2.0×10^{-4} M solutions were then mixed in such a way that the total volume in each mixture was constant (6 mL) and the mole fraction of these reactants varied from 0.0 to 1.0. Two Job's plots with two different total volumes were needed in this study to enable the determination of the formation constant of the complex. Therefore, another set of solutions with total volume of 3 mL was also prepared in this study.

For binary complex, the same procedure was used but without the surfactant added to the solutions. Two sets of solutions with total volume of 3 mL and 6 mL were prepared, while the mole fractions of these reactants were varied from 0.0 to 1.0.

(iii) Slope Ratio Method

The slope ratio method is mainly used in the studies of weak complexes and requires that the formation of complex can be forced to completion with a large excess of either metal or reagent (4). Two sets of solutions were prepared. The first contained various amounts of metal ion each with the same large excess of ligand, while the second consisted of various amounts of reagent, each with the same quantity of large excess of metal.

For binary complex, the first set of solutions was prepared by adding 1 mL of 2.0×10^{-4} M aluminium to a series of 25 mL volumetric flasks containing 0

to 3 mL of 2.0×10^{-4} M of the reagent. The second set of solutions was simply prepared by adding 5 mL (2.0×10^{-4} M) of the reagent into a series of 25 mL volumetric flasks containing 0 to 3 mL of 2.0×10^{-4} M aluminium solution.

The same procedure was applied to ternary complex but in this case, the surfactant was added to the solution in such a way that the aluminium to CP ratio in both sets of solutions was held constant. In this experiment, two aluminium to CP ratios have been studied i.e. 1:3 and 1:6.

The stoichiometry of the binary and ternary complexes during the intermediate state from binary to ternary systems was determined by the three methods which have been mentioned earlier. The experimental procedures used were identical to that described above but the Al:CP ratios were held constant at 1:0.5; 1:1.0; 1:1.5; 1:2.0 and 1:2.5 for each of these.

An attempt was also made to determine the stoichiometry of the reagent to the surfactant in the absence and presence of aluminium. Since the complex of reagent-surfactant was very weak, the only method used in this study was the slope-ratio method.

In the absence of aluminium the first set of the solutions was prepared by adding 3 mL of 2.0×10^{-4} M into a series of solutions containing 0 to 3 mL of the reagent (2.0×10^{-4} M). The second set of solutions was prepared by addition of 3 mL of the reagent solution (2.0×10^{-4} M) into a series of solutions containing 0 to 3 mL of 2.0×10^{-4} M of CP solutions. In the presence of aluminium, the same procedures were applied but 1 mL of 2.0×10^{-4} M of aluminium solution is added into each set of the solutions.

RESULTS AND DISCUSSION

Absorption Spectra

Fig. 1 shows the effect of gradual addition of CP into the binary Al-ECR system. As can be seen from the spectra, addition of more CP will decrease the absorbance of the binary complex at 528 nm and increase the absorbance of the ternary complex at 606 nm. When the molar ratio of Al:CP reached 1:3, no absorption due to the binary complex at 528 nm was observed. The presence of a mixture of binary and ternary complex at low cationic surfactant concentration was also reported for Ga(III)-ECR-CTMA system (Marczenko and Kalowska 1979).

Stoichiometry of Binary Complex of Al-ECR

With binary complex, Al-ECR, all the methods used in this study revealed that the stoichiometry of this complex was 1:3. The graphs showing the stoichiometry of 1:3 for this complex are shown in Figs. 2 to 4. The stoichiometric ratio of 1:3 for binary complex of Al:ECR was also reported by Hill (1956).

Stoichiometry of Ternary Complexes of Al-CP-ECR

Figs. 5 to 7 show the graphs used to determine the stoichiometric ratio of Al:CP with the molar ratio of Al:ECR maintained a constant at 1:3. All these three methods gave identical results, i.e. the stoichiometric ratio of Al:CP as 1:3.

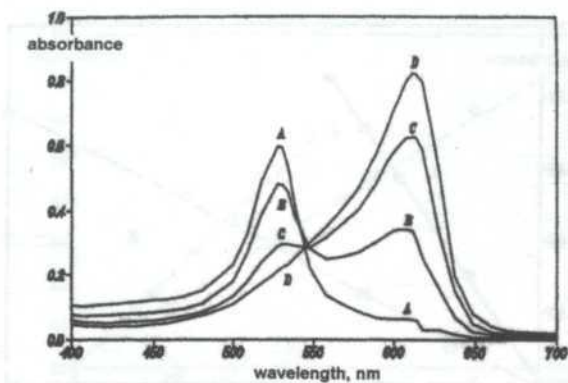


Fig. 1: The effect of addition of different amounts of CP into binary complex, Al-ECR. The molar ratios of Al:CP used 1:0 (A), 1:1.0 (B), 1:2.0 (C) and 1:3.0 (D)

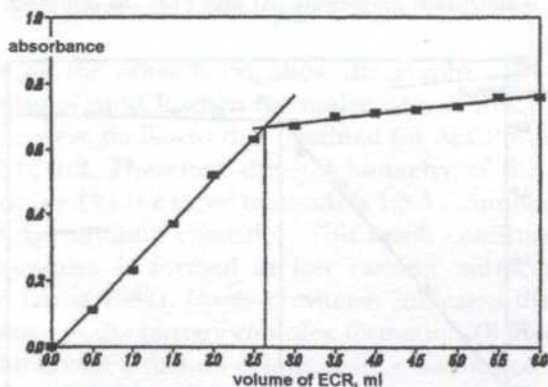


Fig. 2: Graph for stoichiometry determination of binary complex, Al-ECR by means of molar ratio method

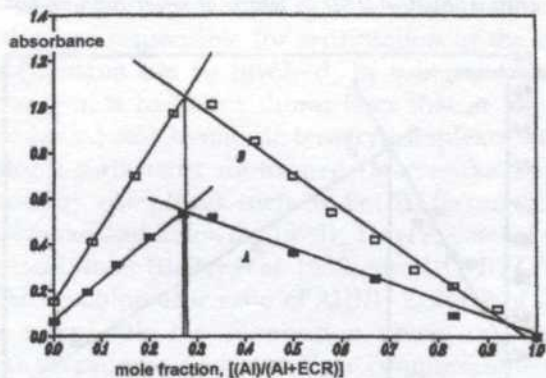


Fig. 3: Job's plots for stoichiometry determination of binary complex, Al-ECR by means of continuous variation method, when the total volume was maintained at 3 mL (A) and 6 mL (B)

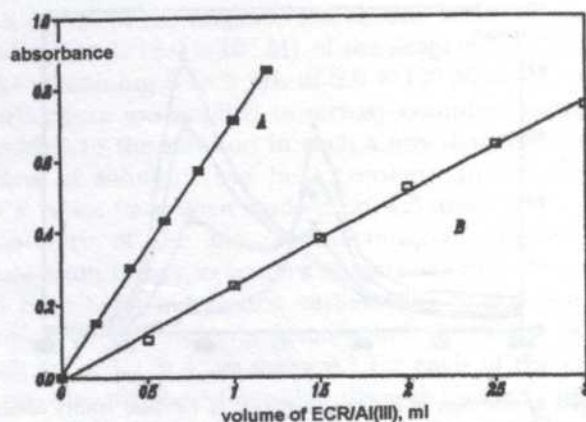


Fig. 4: Graph for stoichiometry determination of binary complex, Al-ECR by means of slope ratio method when aluminium (A) and ECR (B) concentration varies

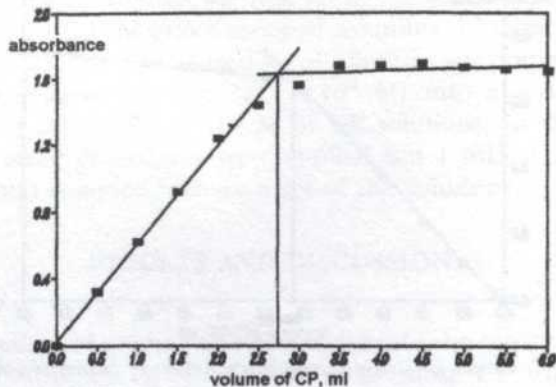


Fig. 5: Graph for stoichiometry ratio determination of Al:CP in the ternary complex, when Al:ECR = 1:3.0 by means of molar ratio method

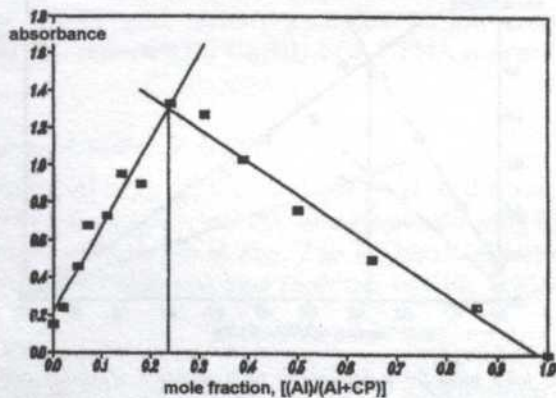


Fig. 6: Job's plot for stoichiometry ratio determination of Al:CP in the ternary complex, when Al:ECR = 1:3.0 by means of continuous variation

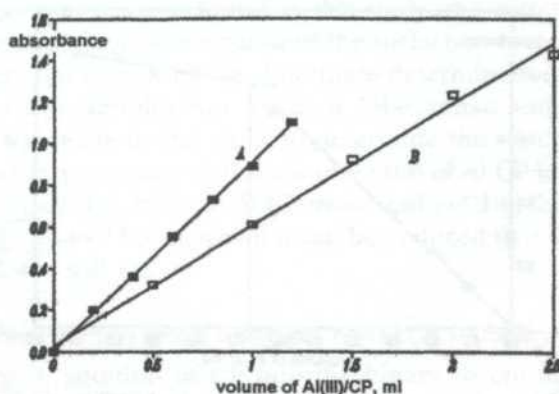


Fig. 7: Graphs for stoichiometry ratio determination of Al:CP in the ternary complex by means of slope ratio method, when aluminium (A) and CP (B) concentration varies. Aluminium concentration of 4.0×10^{-4} M was used

Figs. 8 to 10, on the other hand, show the graphs used to determine the stoichiometric ratio of Al:ECR when the molar ratio of Al:CP was kept constant at 1:3. The results were similar to that obtained for Al:CP with a stoichiometric ratio of Al:ECR of 1:3. Therefore the stoichiometry of the ternary complex, Al-ECR-CP determined by the three methods is 1:3:3 (aluminium to eriochrome cyanine R to cetylpyridinium chloride). This result confirms the belief that a stoichiometric complex is formed at low cationic surfactant concentration (Marczenko and Jarosz 1982). It was previously indicated that the presence of micelles is necessary in the ternary complex formation (Bailey *et al.* 1968). This is based on the observation that no colour change was noticed when quaternary ammonium salts such as tetraethyl- and tetrabutylammonium bromide were used instead of cationic surfactants. Since these compounds are not surfactants, they do not produce micelles. Klopff and Cook (1984) point out however, that in most systems it has not been established whether surfactant monomer or micellar interaction are responsible for sensitisation of the complex. In some systems, both phenomena can be involved. By using spectrophotometric and amperometric titration, it has been shown later that at low concentration of surfactant (below c.m.c.) stoichiometric ternary complexes which contain a few molecules of cationic surfactants are formed (Marczenko and Kalowska 1981). These include ternary complexes such as Fe(III)-ferron (Goto *et al.* 1982), Be(II)-ECR (Marczenko and Kalowska 1978), Tin(IV)-catecol violet (Bailey *et al.* 1968), Mo(II)-catecol violet (Bailey *et al.* 1968) and UO(II)-CAS in the presence of CTMA ion. The stoichiometric ratio of Al(III)-ECR-CP of 1:3:3 found in this study seems to agree with the observation above on the point that the favourable effects of cationic surfactants on complexation reactions are not solely due to the unusual environment on the surface of surfactant micelles as what it was previously believed (Goto *et al.* 1982). For Gd(III)-CAS-CP system, there was evidence that the sensitisation of the complex is due to monomer interaction (Klopff and Cook 1984). At this point however, the colour intensity

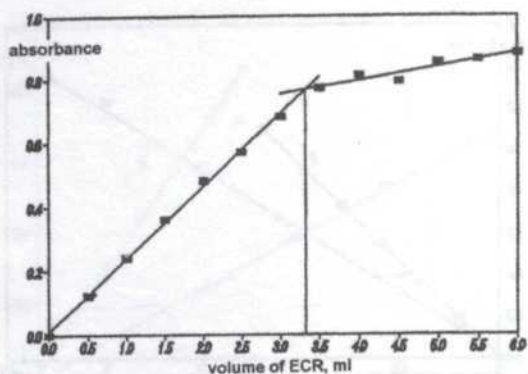


Fig. 8: Graph for stoichiometry ratio determination of Al:ECR in the ternary complex, when Al:CP = 1:3.0 by means of molar ratio method

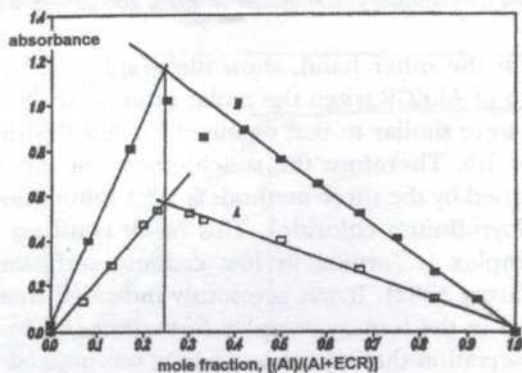


Fig. 9: Job's plot for stoichiometry ratio determination of Al:ECR in the ternary complex, when Al:CP = 1:3.0, by means of continuous variation. Total volume was maintained at 3 mL (A) and 6 mL (B)

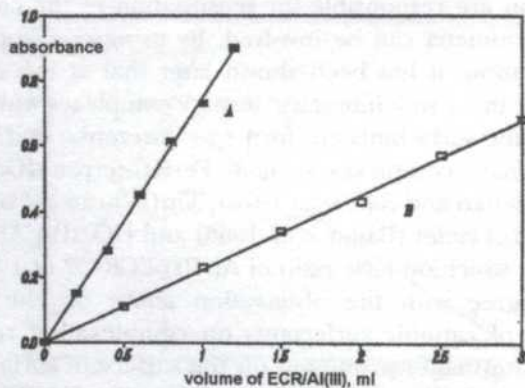


Fig. 10: Graph for stoichiometry ratio determination of Al:ECR in the ternary complex, when Al:CP = 1:3.0, by means of slope ratio method, when aluminium (A) and ECR (B) concentration varies

is not at its maximum since as found in this study, the colour intensity of the complex increases as the concentration of the surfactant increases. Though the Al-ECR-CP system has been used for aluminium determination, no result on the stoichiometry of this complex was reported (Marczenko and Jarosz 1982).

An attempt was made in this study to determine the stoichiometric ratio of Al:ECR in the ternary complex with the molar ratio of Al:CP kept a constant but at a higher value than 1:3. With an Al:CP molar ratio of 1:6, the results obtained are shown in Figs. 11 to 13 from which it can be deduced that the stoichiometric ratio of Al:ECR was still 1:3.

Stoichiometry of Binary and Ternary Complexes of Al-ECR in Binary-Ternary Transition

As shown in Fig. 1, addition of CP into the binary system at a concentration below the stoichiometric amount will be insufficient to completely transform

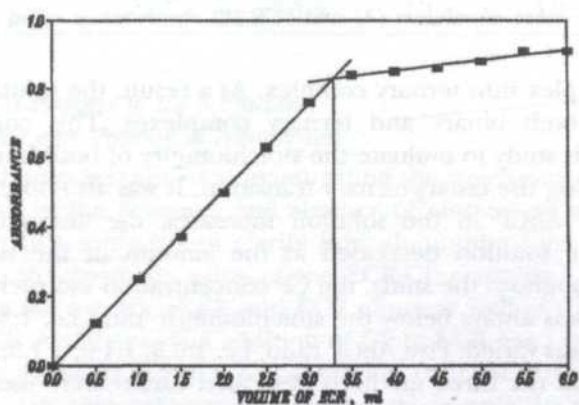


Fig. 11: Graph for stoichiometry ratio determination of Al:ECR in the ternary complex, when Al:CP = 1:6.0, by means of molar ratio method

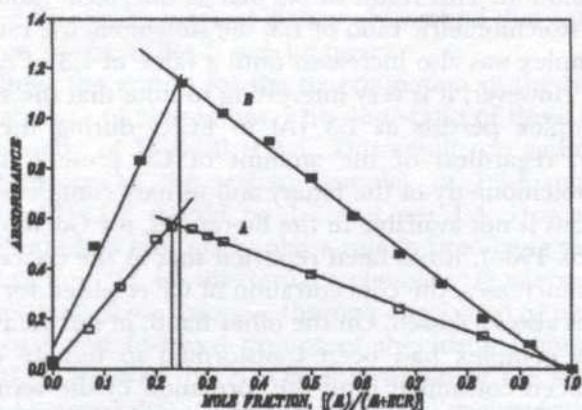


Fig. 12: Job's plot for stoichiometry ratio determination of Al:ECR in the ternary complex, when Al:CP = 1:6.0, by means of continuous variation. Total volume was maintained at 3 mL (A) and 6 mL (B)

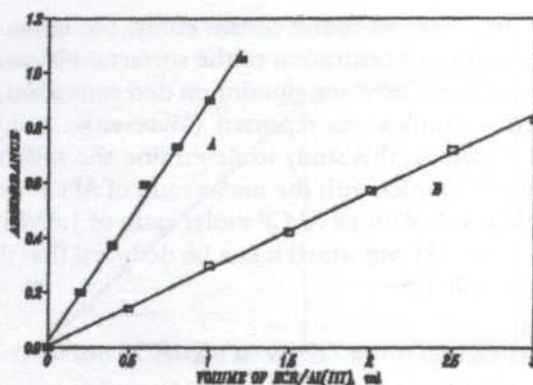


Fig. 13: Graph for stoichiometry ratio determination of Al:ECR in the ternary complex, when Al:CP = 1:6.0, by means of slope ratio method, when aluminium (A) and ECR (B) concentration varies

the binary complex into ternary complex. As a result, the solution will contain a mixture of both binary and ternary complexes. This condition will be exploited in this study to evaluate the stoichiometry of both binary and ternary complexes during the binary-ternary transition. It was also observed that as the molar ratio of Al:CP in the solution increases, the amount of the binary complex in the solution decreased as the amount of the ternary complex increased. Throughout the study, the CP concentration was such that the molar ratio of Al:CP was always below the stoichiometric ratio i.e. 1:3 while the ECR concentration was varied. Five Al:CP ratio, i.e. 1:0.5; 1:1.0; 1:1.5; 1:2.0 and 1:2.5, were chosen and the three methods described earlier were used to determine the stoichiometric ratio of the Al:ECR in these complexes.

Table 1 summarises the results obtained for the stoichiometric ratios determination of Al:ECR in both binary and ternary complexes when CP was gradually added to the solution. This result shows that as the Al:CP ratio increased and approached its stoichiometric ratio of 1:3, the stoichiometric ratio of Al:ECR in the ternary complex was also increased until a value of 1:3 of Al:ECR ratio has been achieved. However, it is very interesting to note that the stoichiometry of the binary complex persists at 1:3 (Al to ECR) during the binary-ternary transition state, regardless of the amount of CP present in the solution. Although the stoichiometry of the binary and ternary complexes in the binary-ternary transitions is not available in the literatures, for Gd(III)-CAS-CP system (Klopf and Cook 1984), it has been reported that as the concentration of the binary complex increases, the concentration of CP required for sensitisation of the complex was also increased. On the other hand, in this study we found that as more binary complex had been transformed to ternary complex, more surfactant has been consumed until the formation of the ternary complex is completed. Therefore, it can be inferred that for Gd(III)-CAS-CP system, the increases in CP concentration are necessary since more binary complex is available in the solution to be transformed to a ternary complex.

TABLE 1
Stoichiometric ratios of Al:ECR in the binary and ternary complexes determined by the methods of slope ratio, molar ratio and continuous variation

Al:CP ratio	1:0.5	1:1.0	1:1.5	1:2.0	1:2.5
molar-ratio method:					
(i) binary	1:3.1	1:3.3	1:3.3	1:3.4	-
(ii) ternary	1:0.8	1:1.3	1:1.6	1:2.2	1:2.6
continuous variation method:					
(i) binary	1:2.5	1:2.9	1:3.3	1:3.1	1:3.2
(ii) ternary	1:0.6	1:1.1	1:1.3	1:2.0	1:2.6
slope-ratio method:					
(i) binary	1:3.1	1:3.4	1:3.3	1:3.3	-
(ii) ternary	1:1.1	1:1.9	1:1.8	1:2.3	1:2.6

*Stoichiometry of the Reagent to the Surfactant,
ECR-CP in Absence and Presence of Aluminium*

In this section, the study is aimed at investigating the stoichiometry of any ECR-CP complex both in the presence and absence of aluminium in the solution. The result from this study would clarify how aluminium ions play a role in determining the stoichiometry value of the ECR-CP complex.

Fig. 14 shows the spectra of CP and ECR alone as well as that of the weak complex, ECR-CP at 480 nm. The addition of CP to ECR has a very small effect on the spectrum of the ECR and it has a very low contrast since the difference between the λ_{max} in their absorption spectra, $\Delta\lambda$ is only 30 nm. The same observation has been reported by Klopff and Cook (1984) for interactions between CAS and CP. This complex is so weak that attempts to use molar ratio method and continuous variation method to determine its stoichiometry were unsuccessful. The slope ratio method is the only method that could be used for the determination of the ECR-CP stoichiometry.

Fig. 15 (A) shows the graphs for the determination of the stoichiometry of ECR-CP in the absence of aluminium. The slope-ratio of these graphs showed that the stoichiometry of ECR-CP is 1:4. This result was rather unexpected, since the stoichiometry of the ternary complex of 1:3:3 suggests that the stoichiometry for ECR:CP should be 1:1 and not 1:4. However, this result suggested that aluminium ions might play a role in producing the ratio of 1:3:3 (therefore ECR:CP = 1:1) in the ternary complex. Quaternary bases were reported to form a kind of ion associate through dissociated or nearly dissociated sulphonic, carboxyl and hydroxyl groups of the triphenylmethane reagents (Savvin *et al.* 1978; Chernova 1977). On observation of the structure of ECR molecule, it can be noted that it has four functional groups with which the CP could be associated. Therefore, in the absence of aluminium in the solution, CP could be possibly associated with all of these functional groups and hence produce the stoichiometry of 1:4 for ECR:CP.

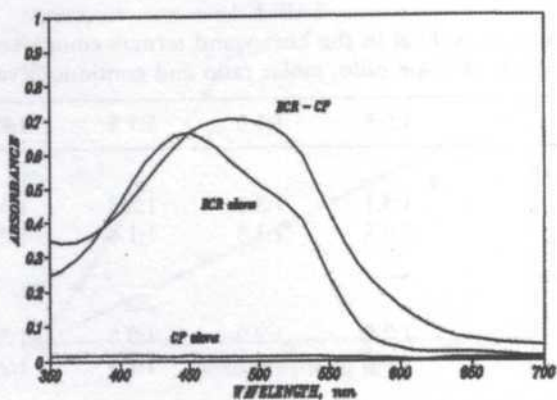
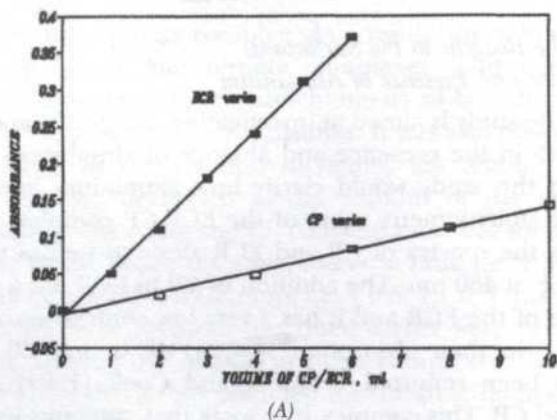
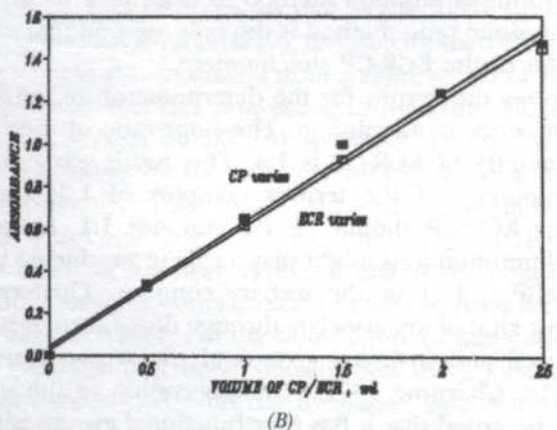


Fig. 14: Absorption spectra of CP, ECR and ECR-CP complex. CP = 10.0 mL, ECR = 10.0 mL of 2.0×10^{-4} M concentration



(A)



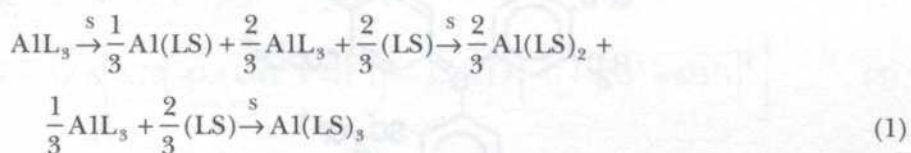
(B)

Fig. 15: Graphs for stoichiometry determination of ECR-CP complex in absence (A) and presence (B) of aluminium by method of slope ratio

Fig. 15 (B) shows the graphs for stoichiometry determination of ECR-CP in the presence of aluminium. The slope-ratio of these graphs showed that in the presence of aluminium the stoichiometry of ECR:CP is 1:1. This result suggests that the degree of the association between CP and the four functional groups in the ECR molecule in the presence and absence of aluminium in the solution, is not the same. As the aluminium ion approaches the ECR molecule, only one of these ion associations persist while the others dissociate to form a binding with the aluminium ion.

Proposal of a Reaction Mechanism for Al-ECR System

It is now established that the stoichiometry of the binary complex of Al-ECR is 1:3 while in the ternary complex of Al-ECR-CP, the stoichiometry is 1:3:3. In its binary-ternary transition state the stoichiometry of the binary complex persists at 1:3, while for the ternary complex, it increased gradually until the stoichiometry reached the value of 1:3:3. Fig. 16 shows the plots of Al:CP ratio versus Al:ECR ratio in the binary and ternary complexes based on the average values of the results shown in Table 1. This result suggested that the complexes will follow the sequence below:



where L = reagent

S = cationic surfactant

Other than binary complex, Eqn. (1) showed that before the ternary complex formation completed, the solution will also contain ECR-CP complex. The presence of ternary complex together with reagent-cationic surfactant complex in the solution was postulated by Wakamatsu and Otomo (1975) for Fe(III)-(2-bromo-4,5-dihydroxyazobenzene-4'-sulfonate)-CP system.

In the absence of aluminium, the preceding sections shows that the CP will be associated with all the functional groups available in the ECR molecule and will give stoichiometric ratio of 1:4 for ECR-CP complex. The structure of the ECR-CP complex could be as shown in Fig. 17.

The π -electron system in the sulphonic acid group of the ECR molecule is isolated from the rest of the conjugation system of the molecule (Marczenko and Kalowska 1981), therefore this explained why the association of this group with CP is "immune" to the presence of aluminium than the others. When aluminium ion approaches the ECR-CP complex, the repulsion between the aluminium and the CP which have the same positive charge, is believed to cause the dissociation of the CP-functional group other than the sulphonic acid group, in order to form a binding between the aluminium and these function

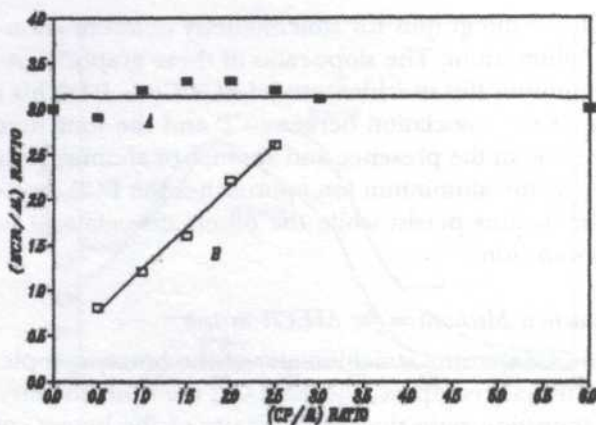


Fig. 16: Plots of ECR:Al ratio versus CP:Al ratio in the binary (A) and ternary complexes (B)

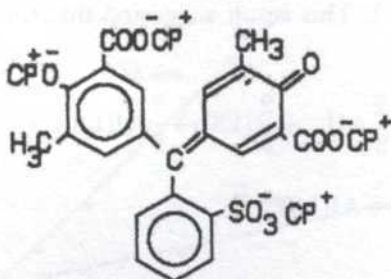


Fig. 17: Proposed structure of ECR-CP complex without the presence of aluminium in the solutions

groups. The possible structure of the ternary Al-ECR-CP complex based on these observations could be written as shown in Fig. 18.

By looking to the proposed structure of the Al-ECR-CP complex, it could be understood that the sensitisation of the binary complex by the CP could be in two ways:

- (i) Stabilising the negatively charged metal complex through electrostatic interaction between the negatively charged complex and the positively charged CP.
- (ii) The formation of a tautomer structure which further stabilised the complex.

While the first phenomena has also been suggested for other systems such as Gd(III)-CAS-CP (Klopf and Cook 1984) and niobium-morin-CTMA (Sanz-Medel and Alonso 1984), the second phenomena has never been reported in the literature and is a very interesting subject to pursue.

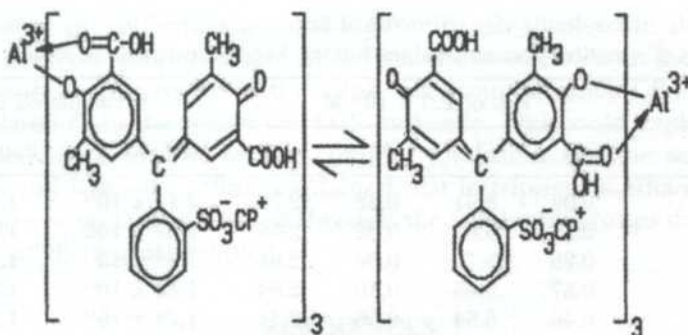


Fig. 18: Proposed structure of the ternary complex, Al-ECR-CP

Formation Constant of Aluminium Complexes with ECR

In this study, the formation constant of the binary and ternary complexes were determined from Job's plots by using the method described by Kirkbright *et al.* (1965). The following equations were used for the formation constant calculation:

$$K = x / (M - x)(L - 3x)^3 \quad (2)$$

$$x = 1/A \left[0.79 \left[-G + \sqrt{(G^2 + 4H^3)} \right]^{1/3} - 1.26H / \left[-G + \sqrt{(G^2 + 4H^3)} \right]^{1/3} \right] \quad (3)$$

where K = Formation constant

x = Some point on the curve corresponding to a certain concentration of the complex

M, L = The concentration of Al(M) and ECR(L) in the first Job's plot if no reaction had taken place between them.

M', L' = The concentration of Al(M') and ECR(L') in the second Job's plot if no reaction had taken place between them.

$$A = 27 (L' + M' - L - M) \quad (4)$$

$$H = AC - B^2 \quad (5)$$

$$G = A^2D - 3ABC + 2B^3 \quad (6)$$

where B = $9 (L^2 + 3LM - L'^2 - 3L'M')$

C = $(L'^3 + 9L'^2M' - L^3 - 9L^2M)$

D = $ML^3 - M'L'^3$

Substitution of x in the expression for K, provides the numerical values for the formation constant of binary and the ternary complexes as shown in Tables 2 to 4.

The results from these tables showed that the values of the formation constant for binary and ternary complexes are of the same order. This indicates

TABLE 2
Formation constant values for the binary complex, Al-ECR

Absorbance	mL of 2.0×10^{-4} M				K calculated from	
	M	L	M'	L'	1st Job's plot	2nd Job's plot
0.20	0.09	5.91	0.22	2.78	2.14×10^{11}	1.43×10^{11}
0.25	0.18	5.82	0.32	2.68	2.02×10^{11}	1.36×10^{11}
0.30	0.28	5.72	0.39	2.61	1.93×10^{11}	1.31×10^{11}
0.35	0.37	5.63	0.46	2.54	1.83×10^{11}	1.26×10^{11}
0.40	0.46	5.54	0.56	2.44	1.74×10^{11}	1.20×10^{11}
0.45	0.55	5.45	0.63	2.37	1.66×10^{11}	1.16×10^{11}
0.50	0.64	5.36	0.71	2.29	1.62×10^{11}	1.13×10^{11}
0.55	0.73	5.27	0.80	2.20	1.55×10^{11}	1.09×10^{11}

$$K_{\text{average}} = 1.53 \pm 0.34 \times 10^{11} \text{ M}^3$$

TABLE 3
Formation constant values for the ternary complex, Al-ECR-CP when
Al:CP constant at 1:3

Absorbance	mL of 2.0×10^{-4} M				K Calculated From	
	M	L	M'	L'	1st Job's Plot	2nd Job's Plot
0.10	0.13	2.87	0.09	5.91	1.39×10^{11}	2.06×10^{11}
0.20	0.26	2.74	0.22	5.78	1.31×10^{11}	1.93×10^{11}
0.30	0.39	2.61	0.35	5.65	1.24×10^{11}	1.82×10^{11}
0.40	0.52	2.48	0.49	5.51	1.18×10^{11}	1.71×10^{11}
0.50	0.65	2.35	0.62	5.38	1.13×10^{11}	1.62×10^{11}

$$K_{\text{average}} = 1.54 \pm 0.33 \times 10^{11} \text{ M}^3$$

TABLE 4
Formation constant values for the ternary complex Al-ECR-CP when
Al:CP constant at 1:6

Absorbance	mL of 2.0×10^{-4} M				K Calculated From	
	M	L	M'	L'	1st Job's Plot	2nd Job's Plot
0.10	0.10	2.90	0.07	5.93	1.39×10^{11}	2.08×10^{11}
0.20	0.22	2.78	0.19	5.81	1.33×10^{11}	1.97×10^{11}
0.30	0.34	2.66	0.31	5.69	1.27×10^{11}	1.86×10^{11}
0.40	0.46	2.54	0.43	5.57	1.21×10^{11}	1.76×10^{11}
0.50	0.58	2.42	0.55	5.45	1.16×10^{11}	1.67×10^{11}

$$K_{\text{average}} = 1.57 \pm 0.34 \times 10^{11} \text{ M}^3$$

that the surfactant molecules are not predominantly involved in the complex formation between aluminium and ECR. As mentioned earlier in the preceding section, the π -electron system of the sulphonic group at which CP is associated with, is isolated from the rest of the ECR molecule. This could explain why CP remains inactive during the ternary complex formation. For the same reason, Marczenko and Kalowska (1981) explained that in triphenylmethane reagents, the associates of surfactant formed through the sulphonic groups do not affect the colour of the metal complex.

REFERENCES

- BAILEY, B.W., J.E. CHESTER, R.M. DAGNALL and T.S. WEST. 1968. Analytical applications of ternary complexes VII: elucidation of mode of formation of sensitized metal-chelate systems and determination of molybdenum and antimony. *Talanta* **15**(12): 1359-1369.
- CHERNOVA, R.K. 1977. Effect of some colloidal surfactants on spectrophotometric characteristics of metal chelates with chromophoric organic reagents, *Zh. Anal. Khim.* **32**(8): 1477-86.
- GOTO K., S. TAGUCHI, K. MIYABE and K.I. HARUYAMA. 1982. Effect of cationic surfactant on the formation of ferron complexes. *Talanta*. **29**(7): 569-75.
- HILL, U.T. 1956. Direct photometric determination of aluminum in iron ores. *Anal. Chem.* **28**: 1419-1424.
- KIRKBRIGHT, G.F., T.S. WEST and C. WOODWARD. 1965. Spectrofluorometric determination of submicrogram amounts of aluminium and beryllium with 2-hydroxy-3-naphthoic Acid. *Anal. Chem.* **37**(1): 137-43.
- KLOPF and COOK. 1984. Surfactant effects on the spectrophotometry of the gadolinium-chrome azurol S complex. *Anal. Chim. Acta* **162**: 293-304.
- MARCZENKO, Z. 1976. *Spectrophotometric Determination of Elements*. Ellis Horward.
- MARCZENKO, Z. and H. KALOWSKA. 1978. Sensitive spectrophotometric determination of beryllium with eriochrome cyanine R and cetyltrimethylammonium ions. *Microchemical J.* **23**(1): 71-78.
- MARCZENKO, Z. and H. KALOWSKA. 1979. Sensitive spectrophotometric determination of gallium with eriochrome cyanine R and cetyltrimethylammonium ions. *Mikrochimica Acta* **2**(5-6): 507-514.
- MARCZENKO Z. and H. KALOWSKA. 1981. Spectrophotometric determination of iron(III) with chrome azurol S or eriochrome cyanine R and some cationic surfactants. *Anal. Chim. Acta* **123**: 279-87.
- MARCZENKO, Z. and M. JAROSZ. 1982. Formation of ternary complexes of aluminum with some triphenylmethane reagents and cationic surfactants. *Analyst* **107**(1281): 1431-1438.
- MUSA AHMAD and NORLEEN ABDUL MANAF. 2002. Bahan penderia untuk pengesanan aluminium berasaskan reagen kolorimetrik terdop dalam filem sol-gel. *Pertanika J. of Sci. and Technology* **10**(1): 99 - 109.

- MUSA AHMAD and R. NARAYANASWAMY. 2002. Optical fibre Al(III) sensor based on solid surface fluorescence measurement, sensors and actuators. *B: Chemical* **81(2-3)**: 259 - 266.
- SANZ-MEDEL, A and J.I.G. ALONSO. 1984. Spectrofluorometric determination of niobium with morin enhanced by cetyltrimethylammonium bromide micelles. *Anal. Chim. Acta* **165**: 159-69.
- SAVVIN, S.B., R.K. CHERNOVA and L. M. KUDRYAVTSEVA. 1978. Determination of traces of aluminium with chromazurol S in the presence of micelles of nonionic surfactants, *Zh. Anal. Khim.*, **33(11)**: 2127-33.
- SKOOG, W.H. 1988. *Fundamental of Analytical Chemistry*. New York: Saunders College Publishing International.
- WAKAMATSU, Y. and M. OTOMO. 1975. Spectrophotometric determination of iron(III) with sodium 2-bromo-4,5-dihydroxyazobenzene-4'-sulfonate in the presence of cetylpyridinium chloride. *Anal. Chim. Acta* **79**: 322-5.

A Cryptosystem Analogous to LUCELG and a Digital Signature Scheme

¹Choo Mun Yoong & ²Mohamad Rushdan Md Said

¹Inti College Malaysia,
Jalan BBN12/1, Bandar Baru Nilai
71800 Nilai, Negeri Sembilan, Malaysia

²Institute for Mathematical Research and Department of Mathematics
Universiti Putra Malaysia, 43400 UPM Serdang, Selangor, Malaysia
E-mail: cmyoong@yahoo.com, mrushdan@fsas.upm.edu.my

Received: 9 June 2003

ABSTRAK

ElGamal dan LUC adalah dua contoh sistem kriptografi awam. Berdasarkan kepada dua sistem ini, LUCELG dibangunkan dengan mengambil kira kekuatan kedua-dua sistem tersebut. Gabungan ElGamal dan sistem kriptografi beranalog kubik kepada RSA (LUC₃) menghasilkan satu sistem kriptografi yang baru. Mengikut kaedah (Smith94), satu skema tandatangan digital dicadangkan. Aspek keselamatan sistem dikaji dan walaupun sistem-sistem ini bergantung pada kesukaran pemfaktoran atau masalah logaritma diskrit, namun sistem-sistem ini tidak boleh dibanding secara terus.

ABSTRACT

ElGamal and LUC are examples of a public-key cryptosystem. Based on these two systems, LUCELG that depends on the strength of the two systems was constructed. The combination of ElGamal and the cubic analogue of the LUC cryptosystem (LUC₃) produces a new public-key cryptosystem. Following (Smith94), a new digital signature scheme is proposed. The security aspects of the system are also looked into and although all these systems appear to depend on the intractability of factorization or of the discrete logarithm problem, the systems do not seem to be readily comparable.

Keywords: Public-key cryptosystem, lucas functions, encryption, decryption

PUBLIC-KEY CRYPTOSYSTEMS

Public-key cryptosystem is a concept invented by Diffie and Hellman (1976). They presented the concept but not the practical implementation of a system. Since 1976, numerous public-key systems have been proposed but many of these are insecure and impractical such as Knapsack public-key encryption and Merkle-Hellman knapsack encryption (Men). Only a few are secure and practical. One such example presented by Rivest *et al.* (1978) as a practical way to implement a public-key cryptosystem is the well-known RSA cryptosystem (RSA). Smith & Lennon (1993), following cryptographic application of Lucas function (Lucas), proposed an analogue to RSA, known as the LUC cryptosystem (Smith 93).

Let α, β be the roots of the quadratic equation

$$x^2 - Px + Q = 0.$$

Two particular solutions of the general second-order linear recurrence relation denoted by U_n and V_n , are defined by

$$V_n = \alpha^n + \beta^n$$

and

$$U_n = \frac{\alpha^n - \beta^n}{\alpha - \beta}$$

These are sequences of integers since we have:

$$U_0 = 0, U_1 = 1, V_0 = 2, \text{ and } V_1 = P.$$

These sequences depend only on the integers P and Q , and the terms are called the Lucas functions of P and Q . They are sometimes written as $U_n(P, Q)$ and $V_n(P, Q)$, in order to show their dependence on P and Q . They were first discussed by Lucas (1878) and satisfy the second-order linear recurrence relations

$$V_n(P, Q) = PV_{n-1} - QV_{n-2} : U_n(P, Q) = PU_{n-1} - QU_{n-2}.$$

If N is any positive integer, then

$$\begin{aligned} V_n(P \bmod N, Q \bmod N) &= V_n(P, Q) \bmod N \\ U_n(P \bmod N, Q \bmod N) &= U_n(P, Q) \bmod N, \end{aligned}$$

because this result is certainly true when n is 0 or 1, and for every n which is 2 or greater, we have

$$V_n(P \bmod N, Q \bmod N) = P \bmod N (V_{n-1}(P, Q) \bmod N) - Q \bmod N (V_{n-2}(P, Q) \bmod N).$$

Similarly

$$U_n(P \bmod N, Q \bmod N) = P \bmod N (U_{n-1}(P, Q) \bmod N) - Q \bmod N (U_{n-2}(P, Q) \bmod N).$$

If we take $Q = 1$, we then get the simple relationship

$$V_{nk}(P, 1) = V_n(V_k(P, 1), 1).$$

This composition result is important as it is a clear generalization of the rule for composition of power, with the subscript of a Lucas function playing the role of a power, thus enabling Smith to construct an analogous system to RSA. He then went on to introduce an analogue to the ElGamal cryptosystem (Elg), naming it LUCELG (Smith94) and a digital signature system, LUCELG DS.

LUCELG PUBLIC-KEY SYSTEM

In LUCELG, the receiver chooses a prime p and the initial values P , and $Q = 1$ which are publicized such that $P^2 - 4Q \pmod p$ is a quadratic non-residue, and

$$V_{\frac{(p+1)}{t}}(P, Q) \not\equiv 2 \pmod p,$$

for all $t > 1$ dividing $(P + 1)$. Let us say Alice wants to send a message to Bob, so Bob (receiver) must choose the private key x , and publish the public key $y \equiv V_x(P, Q) \pmod p$.

A message m is an integer satisfying $1 < m < p-1$. To encrypt a message, Alice needs to choose a secret number k , which is an integer satisfying $1 < k < p-1$, calculates $G \equiv V_k(y, Q) \pmod p$, $e_1 \equiv V_k(P, Q) \pmod p$ and $e_2 \equiv Gm \pmod p$. The encrypted message is the pair (e_1, e_2) .

To decrypt the message, Bob needs to compute

$$V_x(e_1, Q) \equiv V_x(V_k(P, Q), Qk) \equiv V_{kx}(P, Q) \equiv G \pmod p$$

and the inverse of G . Then Bob can find the message m , because $m \equiv e_2 G^{-1} \pmod p$.

It is very important that Q is chosen so that $Q \equiv 1 \pmod p$; the recipient needs to know $Q^k \pmod p$ for the secret value k in order to compute $V_{kx}(P, Q)$ from $V_k(P, Q)$ using

$$V_{kx}(P, Q) = V_k(V_x(P, Q), Q^k)$$

This problem can be solved by taking $Q \equiv 1 \pmod p$.

Let $a = \frac{1}{2} \left[P + \sqrt{P^2 - 4Q} \right]$, and $\Delta = P^2 - 4Q$; Legendre symbol $(\Delta/p) = -1$, then

$\mathbb{O}\Delta/P \in F_{p^2}$, the finite field of p^2 element, via an isomorphism that we denote by ϕ_p . The condition $(\Delta/p) = -1$ is to make sure that one is working in the finite field F_{p^2} rather than F_p . The condition that $V_c(P, Q) \not\equiv 2 \pmod p$ for proper divisors c of $p + 1$ is to ensure that the multiplicative order of the image $\phi_p(\alpha) \in F_{p^2}$ is equal to $p + 1$. If $\phi_p(\alpha^n) = 1$ then $V_n(\alpha) \equiv 2 \pmod p$ and $U_n(\alpha)$, which does not happen for any proper divisor of $p + 1$ by this condition.

THE EXTENDED LUCAS FUNCTIONS

In [SL], Said and Loxton (2003) obtained two results, using the extended theory of the Lucas function by Lehmer (1930) [Leh], which were used to develop a public-key cryptosystem analagous to LUC. These are the higher order analogues of the two equations that were used in the LUC system: the extension of the rule for the composition of powers and the extension of Euler totient function for the elements of the sequence of the third order linear recurrence relation.

Let α, β, γ be the roots of the polynomial equation $x^3 - Px^2 + Qx - R = 0$. By analogy with the Lucas sequence and referring to the cubic equation above, the extended Lucas sequence of numbers are defined as

$$\begin{aligned} V_n(P,Q,R) &= \alpha^n + \beta^n + \gamma^n, \\ U_n(P,Q,R) &= \alpha^n + \omega\beta^n + \omega^2\gamma^n, \\ W_n(P,Q,R) &= \alpha^n + \omega^2\beta^n + \omega\gamma^n, \end{aligned}$$

where $\omega = \frac{1}{2}(-1 + \sqrt{-3})$ is a cube root of unity. Then the sequences (V_n) , (U_n) and (W_n) all satisfy the linear recurrence with characteristic equation $X_{n+3} + PX_{n+2} - QX_{n+1} + RX_n$. All the V_n must be integers, as the first three of the numbers are integers, that is

$$\begin{aligned} V_0(P,Q,R) &= 3 \\ V_1(P,Q,R) &= P \end{aligned}$$

and

$$V_2(P,Q,R) = P^2 - 2Q.$$

The term $V_{nd}(P,Q,R)$ can be written as the d -th term of another sequence of functions defined by integers $V_e(P,Q,R)$, $V_e(Q,PR,R^2)$, and R^k , that is $V_{nd}(P,Q,R) = V_d(V_e(P,Q,R), V_e(Q,PR,R^2), R^k)$.

If we let $R = 1$ the expression can be simplified to

$$\begin{aligned} V_{nd}(P,Q,1) &= V_d(V_e(P,Q,1), V_e(Q,P,1), 1) \\ &= V_d(V_e(P,Q,1), V_{-e}(P,Q,1), 1) \end{aligned}$$

Let N be a product of two distinct odd primes p and q . If we pick a number e such that $(e, \Phi(N)) = 1$, then we can solve

$$ed \equiv 1 \pmod{\Phi(N)}$$

for d where d is the inverse of e modulo $\Phi(N) = \bar{p} \bar{q}$ the function defined in [SL]. Therefore

$$\begin{aligned} V_d(V_e(P,Q,1), V_e(Q,P,1), 1) &= V_{ed}(P,Q,1) \\ &= V_{k\Phi(N)+1}(P,Q,1) \text{ for some integer } k \\ &= P \pmod N \end{aligned}$$

and in a similar manner, we have

$$V_d(V_e(Q,P,1), V_e(P,Q,1), 1) \equiv Q \pmod N.$$

A NEW PUBLIC-KEY CRYPTOSYSTEM

In this system, a prime p and the initial values of P , Q and R are publicized. Each user chooses a private key x , and publishes the public keys

$$\begin{aligned} y &\equiv V_x(P,Q,1) \pmod p \\ y' &\equiv V_x(P,Q,1) \pmod p \end{aligned}$$

A message m is an integer satisfying $1 \leq m \leq p-1$. To encrypt the message for user, the sender needs to choose a secret k , such that $1 \leq k \leq p-1$, and compute

$$\begin{aligned} G &\equiv V_k(y,y',1) \pmod p, \\ d_1 &\equiv V_k(P,Q,1) \pmod p, \\ d_2 &\equiv V_k(Q,P,1) \pmod p, \\ d_3 &\equiv Gm \pmod p. \end{aligned} \tag{1}$$

The encrypted message consists of (d_1, d_2, d_3) . To decrypt the message, the user computes

$$\begin{aligned} V_x(d_1, d_2, 1) &\equiv V_x(V_k(P,Q,1), V_k(Q,P,1), 1) \pmod p \\ &\equiv V_{xk}(P,Q,1) \pmod p, \\ &\equiv G \end{aligned}$$

and then calculates G^{-1} . The extended Euclidean algorithm can be applied to calculate G^{-1} . He then inverts the result modulo p and recovers $m \equiv d_3 G^{-1} \pmod p$.

Example 1:

Let us choose a prime $p = 101$ and we will use small parameters for P , Q as an example. Suppose we take the initial values $P = 6$, $Q = 9$, $R = 1$; the equation of a cubic is $f(x) \equiv x^3 - 6x^2 + 9x - 1 \pmod{101}$. Bob chooses a secret key, $x = 2$, and computes the values $V_2(6,9,1) = 18$ and $V_2(9,6,1) = 69$, and these values are the public keys. If Alice wants to send a message, she needs to choose a secret random key, $k = 3$. She then computes

$$\begin{aligned} G &\equiv V_k(V_x(P,Q,1), V_x(Q,P,1), 1) \pmod{101} \\ &\equiv V_3(V_2(6,9,1), V_2(9,6,1), 1) \pmod{101} \end{aligned}$$

$$\begin{aligned} &\equiv V_3(18,69,1) \pmod{101} \\ &\equiv 2109 \pmod{101} \\ &\equiv 89 \end{aligned}$$

and

$$\begin{aligned} d_3 &\equiv mV_3(18,69,1) \pmod{101} \\ &\equiv 100x(89) \pmod{101} \\ &\equiv 12 \end{aligned}$$

The encryption messages are $(V_3(6,9,1), V_3(9,6,1), d_3) = (57,570,12)$. If Bob wants to decrypt the encrypted message, he needs to compute

$$\begin{aligned} G &\equiv V_2(V_3(6,9,1)V_3(9,6,1),1) \pmod{101} \\ &\equiv V_2(57,570,1) \pmod{101} \\ &\equiv 2109 \pmod{101} \\ &\equiv 89 \end{aligned}$$

and calculate for G^{-1} : Using the extended Euclidean algorithm, we get

$$\begin{aligned} 89y &\equiv 1 \pmod{101} \\ 101 &= 89(1) + 12 \\ 89 &= 12(7) + 5 \\ 12 &= 5(2) + 2 \\ 5 &= 2(2) + 1 \end{aligned}$$

Working from the bottom to the top

$$\begin{aligned} 1 &= 5 - (2) \\ &= 5 - [12 - 5(2)](2) \\ &= (5)5 - 12(2) \\ &= (5)[89 - 12(7)] - 12(2) \\ &= (5)89 - 12(37) \\ &= (5)89 - (37)[101 - 89(1)] \\ &= (42)89 - (37)101, \end{aligned}$$

and thus $G^{-1} = 42$. From equation (1),

$$\begin{aligned} d_3 &\equiv Gm \pmod{101} \\ m &\equiv G^{-1}d_3 \pmod{101} \\ &\equiv 504 \pmod{101} \\ &\equiv 100 \end{aligned}$$

In conclusion, Bob can decrypt the message, $m = 100$ from Alice.

LUCELG DS DIGITAL SIGNATURE SCHEME

A signature scheme is a method of signing a message stored in electronic form. It consists of two components: a signing algorithm and a verification algorithm. Let us say Alice sends a message to Bob, after Bob has signed the message; he sends back the message to Alice to verify it. So, Alice then knows that Bob has received the message.

Now, let us see how Bob computes the signed message. Bob computes his 'signature' S for the M message using D_B :

$$S = D_B(M)$$

Then Bob encrypts S using E_A and sends $E_A(S)$ to Alice. He does not need to send M , because it can be computed from S . After getting the $E_A(S)$, Alice decrypts the ciphertext with D_A to get S . She knows who the sender of the signature is (in this case Bob). Later, Alice can obtain the message M with the encryption procedure of the sender, $M = E_B(S)$, where $E_B(S)$ is available on the public file.

She can possess a message-signature pair which is similar to a signed paper document. Bob cannot deny sending this message to Alice, because no one else could create $S = D_B(M)$. To create $S = D_B(M)$, we need the secret key which is kept by Bob. Finally, Alice can confirm that Bob signed the document. And Alice cannot modify M , since she needs to create the corresponding signature $S = D_B(M')$ as well.

To sign a message, we need to satisfy some requirements. Let B be the recipient of a message M signed by A. Then A's signature must satisfy the following requirements:

- B must be able to validate A's signature.
- It must be impossible for anyone, including B, to forge A's signature.
- If A denies signing message M, it must be possible for a third party to resolve a dispute arising between A and B.

LUCELG DS

In this digital signature scheme [Smith94], two public key values are needed. They are

$$y \equiv V_x(P,1) \pmod{p}$$

and

$$y' \equiv U_x(P,1) \pmod{p}$$

Similarly, two values for the part of the signature are needed. A secret key k , must be chosen for each message, m .

$$r \equiv V_k(P,1) \pmod{p}$$

and

$$r' \equiv U_k(P,1) \pmod{p}$$

The s component of the signature is calculated similar to ElGamal [Elg], except that the equation is solved modulo $(p+1)$ rather than modulo $(p-1)$. Using the extended Euclidean algorithm we can solve for s by using

$$s \equiv k^{-1}(m - xr) \pmod{(p+1)} \quad (2)$$

To verify a LUCELG DS signature, we need to check

$$V_m \equiv V_{s_{k+sr}} \pmod{p}$$

that is the right hand side (RHS) must be the same with the left hand side (LHS). The left hand side

$$\text{LHS} \equiv V_m(P,1) \pmod{p}$$

The right hand side (RHS) equation is more complicated than in ElGamal. From the equation above we know that

$$\begin{aligned} 2V_{s_{k+sr}} &\equiv V_{sk} V_{sr} + DU_{sk} U_{sr} \pmod{p} \\ \text{RHS} &\equiv \frac{1}{2} \{V_r(y,1) V_x(r,1) + Dy'U_r(y,1)r'U_x(r,1)\} \pmod{p} \end{aligned} \quad (3)$$

where

$$D \equiv P^2 - 4 \pmod{p}$$

If $\text{RHS} = \text{LHS}$ then the quadruple (m, r, r', s) is an authentic LUCELG DS signature.

A NEW DIGITAL SIGNATURE SCHEME

The main idea of the protocol described below is to generate a new digital signature scheme. In this scheme, two public-keys are necessary. The public-keys are set up as follow:

- (i) Choose a large prime p of at least 512-bit length.
- (ii) Choose a random number k in the range $1 \leq k \leq p$. A random key should be chosen for each message (or message block),
- (iii) Choose m as a document to be signed, where $0 \leq m \leq p$.

The public keys are

$$y \equiv V_x(P, Q, 1) \pmod{p}, \text{ and } y' \equiv V_x(Q, P, 1) \pmod{p}$$

The Signing Procedure

The signing procedure of a message say, consists of the following steps:

Σ Alice computes a signing using a secret value key, x . Say Alice publishes the value $y \equiv V_x(P, Q, 1) \pmod p$ and $y' \equiv V_x(Q, P, 1) \pmod p$.

Σ User Alice chooses a random k with $\gcd(k, p + 1) = 1$, is a secret value. If k is chosen such that $\gcd(k, p + 1)$, then the equation (2) has a solution for s . By the equation above, we have

$$r \equiv V_k(P, Q, 1) \pmod p, \text{ and } r' \equiv V_k(Q, P, 1) \pmod p$$

- Using the extended Euclidean algorithm, s can be solved by using

$$s \equiv k^{-1}(m - xr) \pmod{(p + 1)}. \tag{4}$$

- User Alice calculates the left hand side

$$Vm \equiv V_{xrsk} \pmod p.$$

From the properties of the extended Lucas functions [SL], we have

$$3V_{n+m} \equiv V_n V_m + W_n U_m + W_m U_n \pmod p$$

thus

$$V_{xrsk} \equiv \frac{1}{3} \{y, y', 1\} V_s(r, r', 1) W_r(y, y', 1) U_s(r, r', 1) + W_s(r, r', 1) U_r(y, y', 1) U_r(y, y', 1) \pmod p \tag{5}$$

where

$$\begin{aligned} U_{sk} &= U_s(V_k(P, Q, R), V_k(Q, P, 1), 1) = U_s(r, r', 1) \\ W_{sk} &= W_s(V_k(P, Q, R), V_k(Q, P, 1), 1) = W_s(r, r', 1) \\ V_{sk} &= V_s(V_k(P, Q, R), V_k(Q, P, 1), 1) = V_s(r, r', 1) \end{aligned}$$

This is the same as

$$\begin{aligned} U_{rx} &= U_r(y, y', 1) \\ W_{rx} &= W_r(y, y', 1) \\ V_{rx} &= V_r(y, y', 1) \end{aligned}$$

Verification Procedure

To verify a signature (m, r, r', s) , we examine whether

$$Vm \equiv V_{xrsk} \pmod p$$

because $m \equiv xr + sk \pmod{p+1}$. The right hand side (RHS) is more complicated than the LUCELG DS. If RHS = LHS, then the signature is valid.

Example 2:

Suppose Bob wants to sign the message $m = 5$, and he chooses the random value and the secret key $x = 2$, (note that $\gcd(3,8) = 1$). The value for $P = 6$, $Q = 9$ and the function f is given by

$$f(x) = x^3 - 6x^2 + 9x - 1.$$

Let p be a prime, $p = 7$, and α, β, γ are roots of $f(x)$. By using the Cardan's formulae [Tig], we can calculate

$$\begin{aligned}\alpha &= 2 + u + v \\ \beta &= 2 + \omega u + \omega^2 v \\ \gamma &= 2 + \omega^2 u + \omega v\end{aligned}$$

where $u^3 = \frac{1}{2}(-1 + \sqrt{-3})$ and $v^3 = \frac{1}{2}(-1 - \sqrt{-3})$. The public keys are

$$\begin{aligned}y &\equiv V^2(6,9,1) \pmod{7} \\ &\equiv 18 \pmod{7} \\ &\equiv 4 \pmod{7}\end{aligned}$$

$$\begin{aligned}y &\equiv V^2(9,6,1) \pmod{7} \\ &\equiv 69\end{aligned}$$

Bob chooses the random value $k = 3$, and computes

$$\begin{aligned}r &\equiv V_3(6,9,1) \pmod{7} \\ &\equiv 57 \pmod{7} \\ &\equiv 1 \pmod{7}.\end{aligned}$$

$$\begin{aligned}r' &\equiv V_3(9,6,1) \pmod{7} \\ &\equiv 570 \pmod{7} \\ &\equiv 3 \pmod{7}.\end{aligned}$$

and from equation (4), we know

$$\begin{aligned}s &\equiv k^{-1}(m - xr) \pmod{p+1} \\ &\equiv 3^{-1}(5 - 2) \pmod{8} \\ &\equiv 3(3) \pmod{8} \\ &\equiv 1\end{aligned}$$

To verify the signature $(m, r, r', s) = (5, 1, 3, 1)$, we check whether

$$V_m \equiv V_{xr+sk} \pmod{p}.$$

To check the right hand side, from equation (5) we have

$$\begin{aligned}
 V_{x+r,sk} &\equiv \frac{1}{3} \{V_r(y,y',1) V_s(r,r',1) W_r(y,y',1) U_s(r,r',1) \\
 &+ Ws(r,r',1)Ur(y,y',1) \text{ mod } p \\
 &\equiv \frac{1}{3} \{V_1(4,6,1) V1(1,3,1)+W_1(4,6,1) U_1(1,3,1) W_1(1,3,1) U_1(4,6,1)\} \text{mod } 7 \\
 &\equiv \frac{1}{3} \{V_1(18,69,1) V_1(57,570,1)+W_1(18,69,1) U_1(57,570,1) \\
 &+ W_1(57,570,1) U_1(18,69,1)\} \text{ mod } 7 \\
 &\equiv \frac{1}{3} \{V_2(6,9,1) V_3(6,9,1)+W_2(6,9,1) U_3(6,9,1)+W_3(6,9,1) U_2(6,9,1)\} \text{mod } 7 \\
 &\equiv \frac{1}{3} \{(\alpha^2+\beta^2+\gamma^2) (\alpha^3+\beta^3+\gamma^3)+(\alpha^2+\omega^2\beta^2+\omega\gamma^2) (\alpha^3+\omega\beta^3+\omega^2\gamma^3) \\
 &+ (\alpha^3 + \omega^2\beta^3 + \omega\gamma^3) (\alpha^2 + \omega\beta^2 + \omega^2\gamma^2)\} \text{ mod } 7 \\
 &\equiv \{\alpha^5 + \beta^5 + \gamma^5 + \alpha^2\beta^3 + \alpha^2\gamma^3 + \beta^2\alpha^3 + \beta^2\gamma^3 + \gamma^2\alpha^3 + \gamma^2\beta^3\} \\
 &+ \{\alpha^5 + \beta^5 + \gamma^5 + \omega^2\alpha^2\beta^3 + \omega\alpha^2\gamma^3 + \omega\beta^2\alpha^3 + \omega^2\beta^2\gamma^3 + \omega^2\gamma^2\alpha^3 + \omega\gamma^2\beta^3\} \\
 &+ \{\alpha^5 + \beta^5 + \gamma^5 + \omega\alpha^2\beta^3 + \omega^2\alpha^2\gamma^3 + \omega^2\beta^2\alpha^3 + \omega\beta^2\gamma^3 + \omega\gamma^2\alpha^3 + \omega^2\gamma^2\beta^3\} \text{mod } 7 \\
 &\equiv \alpha^5 + \beta^5 + \gamma^5 \text{ mod } 7 \\
 &\equiv 5.
 \end{aligned}$$

To check the left hand side, we calculate $V_m = V_5$. We know that $V_0 = 3, V_1 = 6, V_2 = 18$, and

$$\begin{aligned}
 V_3 &\equiv 6V_2 - 9V_1 + V_0 \text{ mod } 7 \\
 &\equiv 6(18) - 9(6) + 3 \text{ mod } 7 \\
 &\equiv 108 - 54 + 3 \text{ mod } 7 \\
 &\equiv 1 \text{ mod } 7
 \end{aligned}$$

By using the same method, $V_4 \text{ mod } 7 \equiv 4$, and

$$\begin{aligned}
 V_5 &\equiv PV_4 - QV_3 + V_2 \text{ mod } 7 \\
 &\equiv 6(4) - 9(1) + 18 \text{ mod } 7 \\
 &\equiv 5 \text{ mod } 7
 \end{aligned}$$

Since $V_5 \equiv V_{x+r,sk} \text{ mod } 4$, so the quadruple (5,1,3,1) of Bob signature is an authentic signature.

CRYPTOGRAPHIC STRENGTH

There are two ways to discuss the security of a cryptosystem. These are computational security and unconditional security. We call a cryptosystem 'computationally secure' if the best-known method of breaking the cryptosystem needs a large amount of computer time, such as Shift Cipher and Substitution

Cipher. Another approach is to give some evidence of computational security by reducing the security of the cryptosystem to some difficult problems. We know that RSA and its variants depend on the intractability of factorization but this only provides a proof of security relative to some other problems, not an absolute proof of security. The same is true for LUCELG and the proposed system which depend on the intractability of the discrete logarithm problem. A cryptosystem is defined to be 'unconditionally secure' if it cannot be broken, even with infinite computational resources.

Randomized Encryption

The proposed cryptosystem is a randomized encryption. The randomized encryption techniques increases the cryptographic security of an encryption process through the following methods [Men]:

- Increasing the effective size of the plaintext message space.
- Decreasing the effectiveness of chosen plaintext attacks by virtue of a one to many mappings of plaintext to ciphertext.
- Decreasing the effectiveness of statistical attack by leveling the *a priori* probability distribution of inputs.

Discrete Logarithm Problem

The discrete logarithm problem (DLP) is the following [Men]: given a prime p , a generator α of Z_p and an element $\beta \in Z_p$, find the integer x , $0 \leq x < p-2$, such that $\alpha^x \equiv \beta \pmod{p}$.

The best algorithm for solving the Discrete Logarithm (DLP) problem relies on combining congruences multiplicatively [Smith94]. This cannot be done with extended Lucas functions because extended Lucas functions are not closed under multiplication. Hence these subexponential algorithms cannot be applied to our proposed system. Breaking the system is equivalent to solving for x in equation $V_x(P, Q, 1)$, where P , C and p are known. To find $V_x(P, Q, 1)$ we need to compute $(\alpha^2 + \beta^2 + \gamma^2)$, $(\alpha^3 + \beta^3 + \gamma^3)$, ... and therefore inefficient if x is large.

The most powerful method for computing discrete logarithms is the index-calculus algorithm. This algorithm cannot be applied to the proposed encryption algorithm. But let us see how the index-calculus method works to ElGamal cryptosystem [Stin]. The method uses a factor base, which is a set B of 'small' prime. Suppose $B = \{p_1, p_2, \dots, p_b\}$. The first step is to find the logarithms of the B primes in factor base. The second step is to compute a discrete log of element β . We construct $C = B + 10 \pmod{p}$,

$$\alpha^{X_j} \equiv P_1^{A_{1j}} P_2^{A_{2j}} \dots P_b^{A_{bj}} \pmod{p}$$

with $1 \leq j \leq C$, and

$$X_j \equiv A_{1j} \log_{\alpha} P_1 + A_{2j} \log_{\alpha} P_2 + \dots + A_{bj} \log_{\alpha} P_b \pmod{p-1}$$

Then we take the random value x , compute $\alpha^x \pmod{p}$, and then determine if

$\alpha^s \bmod p$ has all its factors in B . If we have successfully carried out the precomputation step, we choose a random integer, s where $(1 \leq s \leq p - 2)$ and compute

$$y \equiv m\alpha^s \bmod p$$

Factor y over the factor base B . If this can be done, we obtain a congruence of the form

$$m\alpha^s \equiv P_1^{A_{1j}} P_2^{A_{2j}} \dots P_B^{A_{Bj}} \bmod p$$

This can be written equivalently as

$$(\log_\alpha m) + s \equiv A_{1j} \log_\alpha P_1 + A_{2j} \log_\alpha P_2 + \dots + A_{Bj} \log_\alpha P_B \bmod p - 1.$$

since everything is known, except $\log_\alpha m$. But this cannot apply to the proposed system because we have $(\alpha^x + \beta^x + \gamma^x)$

CONCLUSIONS

The proposed system is a combination of ElGamal and the cubic analogue of the RSA cryptosystem. The security of this cryptosystem, as does LUCCELG, depends on the intractability of the discrete logarithm problem. Further research can be continued to discuss the complexity of the algorithms and the efficiency of the proposed cryptosystem. Other aspects of security could also be investigated.

REFERENCES

- DIFFIE, W. and M.E. HELLMAN. 1976. New directions in cryptography. *IEEE Transactions on Information Theory* **IT-22(6)**: 644-654.
- ELGAMAL, T. 1985. A public-key cryptosystem and a signature scheme based on discrete logarithms. *IEEE Transaction on Information Theory* **31**: 469-472.
- LEHMER, D.H. 1930. An extended theory of Lucas functions. *Annals of Math.* 419-448.
- LUCAS, F.E.A. 1878. Theorie des fonctions numeriques simplement periodiques. *American Jnl Math.* **1**: 184-240, 289-321.
- MENEZES, A., P.V OORSCHOT and S. VANSTORE. *HandBook of Applied Cryptography*. Boca, Raton, London: Tokyo CRC Press.
- RIVEST, L., A. SHAMIR and L. ADLEMAN. 1978. A method for obtain digital signatures and public key cryptosystem. *Communications of the ACM* **21(2)**: 120-126.
- SAID, M.R.M. and J. LOXTON. 2003. A cubic analogue of the RSA cryptosystem. *Bulletin of The Australian Mathematical Society* **68**: 21-38.
- SMITH, P. and M. LENNON. 1993. LUC: A new public key system. In *Ninth IFIP Symposium on Computer Security* ed. E. G. Douglas, pp. 103-117. Elsevier Science Publishers.

- SMITH, P. and C. SKINNER. 1994. A public-key cryptosystem and a digital signature systems based on the Lucas function analogue to discrete logarithms. *Pre-proceedings Asia Crypt'94*, pp. 298-306.
- STINSON, R.D. 1990. *Cryptography: Theory and Practice*. Boca Raton, FL: CRC Press.
- SHANNON, C. E. 1949. Communication theory of secrecy system. *Bell Syst. Tech. J.* **28**: 656-715.
- SHANNON, C.E. 1984. A mathematical theory of communication. *Bell Syst. Tech. J.* **27**: 379-423 (July),623-656 (Oct) .
- TIGNOL, J.P. 1988. *Galois' Theory of Algebraic Equations*. Longman Group UK Limited.

Kaedah Kolorimetri untuk Analisis Kuantitatif Kapsaisin Secara Pencaman Corak Menggunakan Jaringan Neural Tiruan

¹Mohamad Nasir Mat Arip, ^{*1}Musa Ahmad, ¹Ahmed Mahir Mokhtar,
²Mohd. Nasir Taib & ¹Lee Yook Heng

¹Pusat Pengajian Sains Kimia & Teknologi Makanan,

Fakulti Sains dan Teknologi

Universiti Kebangsaan Malaysia

43600 Bangi, Selangor, Malaysia

²Fakulti Kejuruteraan Elektrik

Universiti Teknologi Mara

40450 Shah Alam, Selangor, Malaysia

Diterima: 9 Julai 2003

ABSTRAK

Analisis kuantitatif kapsaisin menggunakan reagen 2,6-dikloro-p-benzokuinon-4-klorimida (reagen Gibbs) dan jaringan neural tiruan telah dilakukan. Pencirian yang dilakukan termasuklah pengoptimuman pH, kesan kepekatan reagen, julat dinamik kepekatan kapsaisin, analisis kestabilan foto reagen, penentuan had pengesanan dan analisis kebolehulangan. Nilai optimum untuk kepekatan reagen Gibbs dan nilai pH masing-masingnya adalah 2.96×10^{-4} M dan 11.0. Nilai sisihan piawai relatif (RSD) kebolehulangan kaedah adalah memuaskan iaitu 3.55%, 2.44% dan 4.52%, masing-masingnya pada kepekatan kapsaisin 200 ppm, 500 ppm, dan 800 ppm. Reagen Gibbs juga menunjukkan kestabilan foto yang baik dengan nilai RSD 0.013% untuk tempoh kajian selama 38 jam. Jaringan neural tiruan dengan tiga lapisan suapan hadapan dilatih menggunakan algoritma perambatan balik. Untuk penentuan kepekatan kapsaisin, rangkaian neural tiruan dengan 20 neuron terlindung, kadar pembelajaran 0.00001% dan melakukan latihan menggunakan 47,738 kitaran, memberikan keputusan yang memuaskan. Rangkaian neural ini berupaya memanjangkan julat dinamik kepekatan kapsaisin dari 0-200 ppm kepada 0-600 ppm. Purata ralat interpolasi yang diberikan oleh rangkaian neural ini adalah kira-kira 0.06%.

ABSTRACT

A quantitative study for capsaicin based on the use of 2,6-dichloro-p-benzoquinone-4-chlorimide (Gibbs reagent) and artificial neural network (ANN) has been carried out. The characterization include pH optimization, effect of reagent concentration, dynamic range of capsaicin concentration, photo stability, limit of detection and reproducibility. The optimum response was obtained at pH 11.0 and Gibbs reagent concentration of 2.96×10^{-4} M. The reproducibility of the method was very satisfactory with RSD values of 3.55%, 2.44% and 4.52% for capsaicin concentration of 200 ppm, 500 ppm and 800 ppm, respectively. Photostability test showed that the reagent was very stable with RSD value of 0.013% for the duration of 38 hours. A three layer feed-forward neural network was used and network training was performed by using back propagation algorithm. For the determination of capsaicin, a neural network with 20 hidden neurons, 0.00001% learning rate and trained over 47,738 cycles produced the

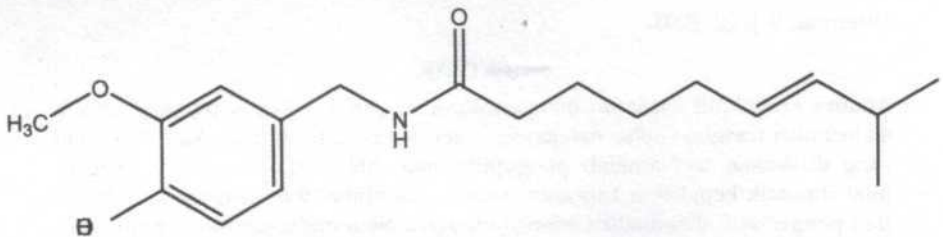
* Corresponding author

best result. This network was able to extend the narrow dynamic range of capsaicin from 0 – 200 ppm to 0-600 ppm. The average interpolation error produced by this network was approximately 0.06 %.

Kata kunci: Tahap kepedasan, kapsaisin, reagen Gibbs, jaringan neural tiruan

PENGENALAN

Kapsaisin (*Rajah 1*) adalah komponen yang bertanggungjawab memberikan rasa kepedasan di dalam cili telah ditemui oleh Bucholtz pada tahun 1816 (Govindarajan 1985). Kapsaisin atau tatanama IUPAC (E)-N-[(4-Hidroksi-3-metoksifenil)-metil]-8-metil-6-nonenamida (Budavari 1989) adalah ahli kepada kumpulan kapsaisinoid dan merupakan sejenis alkoholoid.



Rajah 1: Struktur kapsaisin

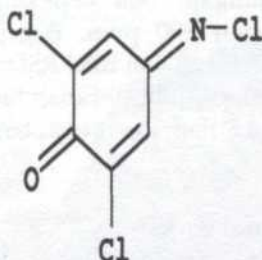
Sehingga kini, terdapat beberapa reagen telah dikemukakan oleh penyelidik untuk bertindak balas dengan kapsaisin. Pada tahun 1959, Joint Committee (PS/SAC) mencadangkan penggunaan asid diazobenzena sulfanilik, 2,6-diklorokuinonklorimida (reagen Gibbs) dan 4-aminoantipairin (4-AAP) (Joint committee (PS/SAC)1959). Lain-lain reagen yang dicadangkan adalah vanadium oksiklorida, fosfomolibdik-fosfo-tungsten, kalium ferrisianida-ferrik klorida, dan natrium nitrat molibdat (Palacio 1977; 1979) Bajaj (1980) telah mencadangkan penggunaan reagen Folin Ciocalteu untuk pengesanan kapsaisin.

Kaedah kolorimetri menggunakan reagen 4AAP merupakan kaedah piawai untuk pengesanan fenol (Mohler and Jacob 1957). Walau bagaimanapun ia tidak sesuai digunakan untuk pengesanan kapsaisin kerana ia sangat tidak stabil apabila bertindak balas dengan kapsaisin. Ini adalah kerana perubahan warna berlaku dengan pantas dan ia tidak memberikan satu perubahan warna yang stabil untuk satu tempoh yang panjang (Join committee (P/S SAC) 1959; 1963)

Jaringan Neural Tiruan (ANN), merupakan sistem yang dimodelkan berasaskan otak manusia. Ia terdiri daripada lapisan berganda elemen pemprosesan mudah yang dipanggil neuron. Setiap neuron disambungkan kepada neuron yang bersebelahan dengan pelbagai koefisien yang menggambarkan kekuatan sambungan ini. Proses latihan dilakukan terhadap ANN dengan memberikan input tertentu untuk melaraskan koefisien ini sehingga output yang dikehendaki terhasil. Pada masa kini penerokaan teknologi ANN dalam bidang kimia telah mencakupi kepada pelbagai penggunaan termasuklah penentuan spektrum, ramalan dan kawalan proses kimia serta pencaman corak (Billings *et al.* 1991).

Walau bagaimanapun bilangan penyelidikan yang dilakukan masih sedikit dan hanya tertumpu di negara-negara maju memandangkan ia agak baru terutamanya di rantau Asia.

Objektif kajian ini adalah untuk melakukan analisis kuantitatif bagi menentukan kepekatan kapsaisin menggunakan ANN. Reagen Gibbs (*Rajah 2*) telah dipilih untuk digunakan di dalam kajian ini kerana memberikan perubahan warna yang jelas apabila bertindak balas dengan kapsaisin dan sangat stabil seperti yang dilaporkan oleh Joint Committee (PS/SAC) (1959; 1963). Walaupun reagen Gibbs telah digunakan dalam kajian terdahulu, pencirian secara menyeluruh tindak balas di antara reagen Gibbs dan kapsaisin terutamanya untuk melihat potensinya sebagai bahan untuk sensor kimia belum pernah dilakukan. ANN digunakan dalam kajian ini untuk membantu proses automasi dalam perolehan data bagi menentukan kepekatan kapsaisin di samping memanjangkan julat kepekatan dinamik kapsaisin.



Rajah 2: Struktur reagen Gibbs (2,6-dikloro-p-benzokuinon-4-klorimida).

EKSPERIMEN

Bahan Kimia dan Peralatan

Bahan-bahan kimia yang digunakan dalam kajian ini adalah kapsaisin (Fluka Chemika, >>99.0 %), etanol (BDH HPLC grade. 99 %), 2,6-dikloro-p-benzokuinon-4-klorimida, kalium klorida, asid hidroklorik, kalium dihidrogen fosfat, natrium hidroksida, asid borik dan natrium hidrogen karbonat. Semua bahan kimia ini digunakan tanpa penulenan lanjut. Air yang digunakan dalam penyediaan ini adalah air nyah ion yang diperolehi daripada alat Maxima Ultra Pure Water Elga, model Elga Stat Maxima UF.

Cara Kerja

(i) Penyediaan Larutan

Larutan stok kapsaisin 1000 ppm disediakan dengan melarutkan 250 mg serbuk kapsaisin dalam 250 mL pelarut etanol. Larutan kapsaisin dalam julat kepekatan 50-800 ppm disediakan melalui pencairan larutan stok ini. Larutan stok reagen Gibbs (0.01971 M) disediakan dengan melarutkan 0.1037 g serbuk reagen Gibbs ke dalam 10 mL etanol. Larutan ini kemudiannya dimasukkan ke dalam kelalang isi padu 25 mL dan dicairkan hingga ke senggatan dengan etanol. Larutan penimbal pH 1.0 hingga 13.0 disediakan mengikut tatacara Dean

(1989). Alat meter pH (Witeg W-500) telah digunakan untuk mengukur pH setiap larutan penimbal yang telah disediakan.

(ii) Tatacara Kaedah

Dalam kajian pengoptimuman pH, larutan kapsaisin 200 ppm digunakan. Serapan larutan ini direkodkan menggunakan Spektrofotometer UL-Nampak (Varian Cary-100) pada julat panjang gelombang 190-800 nm. Nilai-nilai perbezaan serapan antara larutan kompleks kapsaisin-reagen Gibbs dan larutan reagen Gibbs sahaja pada larutan penimbal berbeza diplotkan melawan nilai pH yang dikaji (pH 1.0 -13.0).

Untuk melihat kesan kepekatan reagen Gibbs ke atas serapan kompleks, kepekatan larutan kapsaisin ditetapkan pada 200 ppm, manakala kepekatan reagen Gibbs diubahkan dalam julat $0.0 - 6.0 \times 10^{-4}$ M. Dalam penentuan julat dinamik kepekatan kapsaisin, kepekatan larutan kapsaisin dalam julat 50 - 600 ppm digunakan. Kepekatan reagen Gibbs ditetapkan pada 2.96×10^{-4} M.

Dalam kajian keboleholungan, tiga kepekatan kapsaisin yang berbeza digunakan iaitu 200, 500 dan 800 ppm. Bagi setiap kepekatan kapsaisin, pengukuran diulangi sebanyak 8 kali dan nilai RSD ditentukan. Kajian kestabilan foto pula dilakukan dengan mengambil serapan larutan reagen Gibbs pada pH 11.00 secara berterusan pada panjang gelombang 600 nm untuk tempoh selama 38 jam.

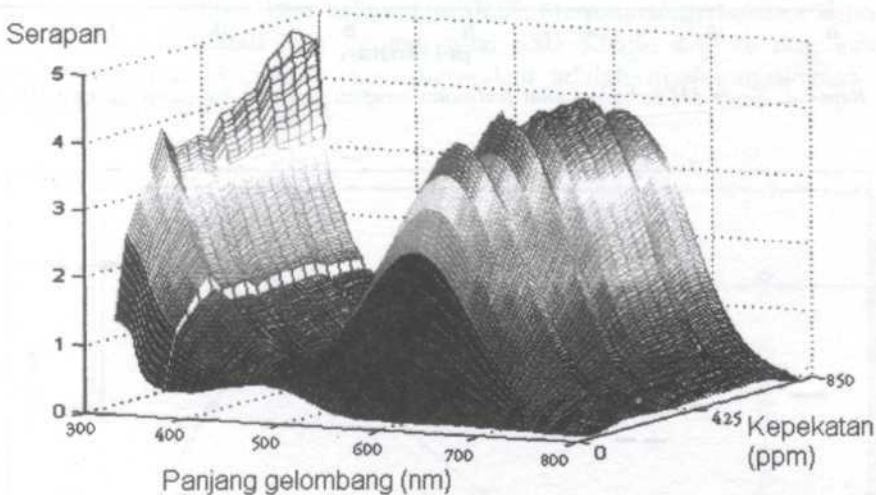
(iii) Arkitektur Jaringan Neural Tiruan

Jaringan neural tiruan (ANN) yang digunakan dalam penyelidikan ini ialah jenis rangkaian suapan-hadapan dengan satu lapisan terlindung dan menggunakan algoritma perambatan balik. Lapisan input yang digunakan adalah bergantung kepada bilangan bacaan serapan pada beberapa panjang gelombang yang dipilih untuk setiap spektrum. Untuk tindak balas kapsaisin dalam reagen Gibbs, sebanyak 7 neuron dalam lapisan input digunakan untuk mewakili 7 nilai serapan pada 7 panjang gelombang berbeza, untuk setiap spektrum serapan. Lapisan output mempunyai 1 neuron sahaja yang mewakili nilai kepekatan kapsaisin yang ingin ditentukan. Bilangan neuron dalam lapisan terlindung tidak tetap dan ditentukan secara cuba jaya sehingga suatu rangkaian neuron yang dapat memberi keputusan ramalan yang baik diperolehi. Selain itu, bilangan kitaran iaitu bilangan kali kitaran latihan dilakukan turut dioptimumkan. Latihan dan simulasi algoritma ini dilakukan dengan menggunakan program Matlab versi 5.3 di bawah pemprosesan Intel Pentium IV berkelajuan 1.3 GHz dan mengandungi 128MB RAM. Raimundo dan Narayanaswamy (2001) melaporkan bahawa bilangan lapisan terlindung, bilangan neuron dalam lapisan terlindung dan kadar pembelajaran adalah nilai-nilai yang perlu diubah untuk mendapatkan satu keputusan yang baik dalam satu latihan rangkaian neural. Ini di sokong oleh Faiz *et al.* (2003) yang mendapati bahawa hasil yang memuaskan diperolehi dengan mengubah nilai-nilai ini. Dalam kaedah ini, kaedah cubajaya digunakan dengan mengubah bilangan neuron terlindung, bilangan kitaran dan kadar pembelajaran sehingga satu

arkitektur rangkaian neural yang mempunyai ralat latihan (SSE) yang rendah diperolehi. Rangkaian neural tiruan dengan satu lapisan terlindung digunakan dalam kajian ini.

KEPUTUSAN DAN PERBINCANGAN

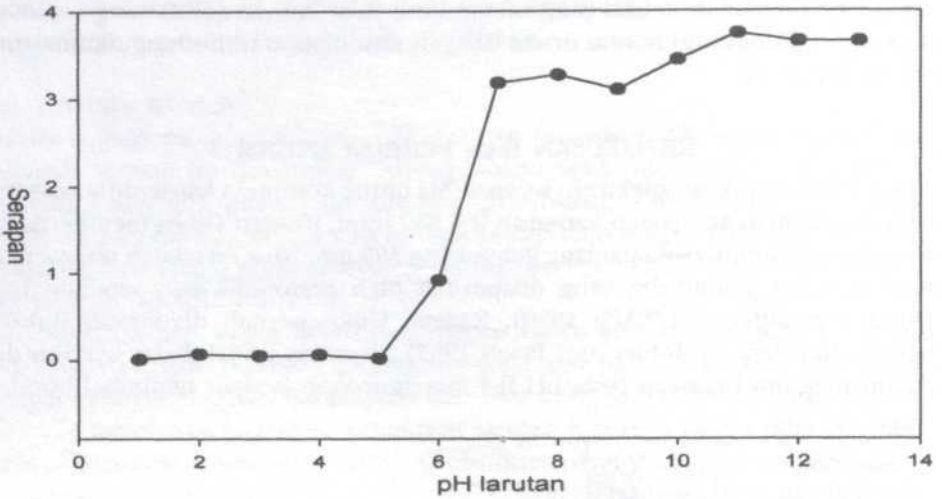
Rajah 3 menunjukkan spektrum serapan 3D untuk kompleks kapsaisin – reagen Gibbs pada julat kepekatan kapsaisin 0 – 850 ppm. Reagen Gibbs memberikan serapan maksimum pada panjang gelombang 595 nm. Nilai ini adalah menyamai nilai panjang gelombang yang dilaporkan oleh penyelidik lain sebelum ini (Joint committee (PS/SAC) 1959). Reagen Gibbs pernah digunakan untuk pengesanan fenol (Mohler and Jacob 1957), di mana tindak balas berlaku di dalam medium beralkali pada pH 9.4 menggunakan larutan penimbal borat.



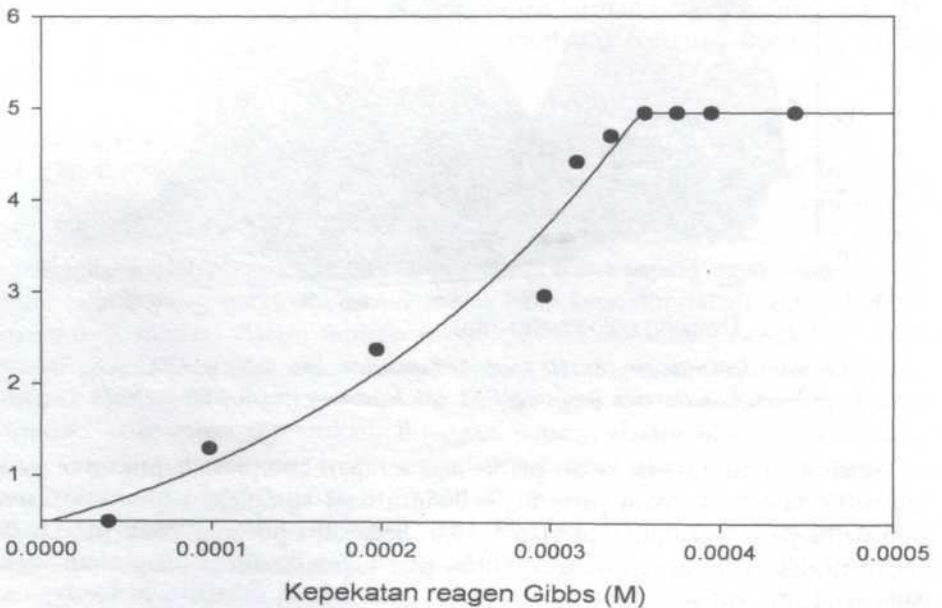
Rajah 3: Spektrum serapan 3D kompleks kapsaisin-reagen Gibbs pada keadaan optimum iaitu larutan dengan pH 11 dan kepekatan reagen 2.96×10^4 M

Rajah 4 menunjukkan kesan pH ke atas serapan kompleks kapsaisin-reagen Gibbs. Perbezaan serapan pada $\lambda_{\text{maks}} = 595\text{nm}$ bagi kompleks kapsaisin-reagen Gibbs didapati maksimum pada pH 11.0. Serapan optimum pada pH alkali untuk tindak balas antara reagen Gibbs dan kapsaisin turut dilaporkan oleh Palacio (1977; 1979).

Rajah 5 menunjukkan kesan kepekatan reagen Gibbs semasa pembentukan kompleks kapsaisin-reagen Gibbs. Peningkatan serapan kompleks kapsaisin – Gibbs dengan peningkatan kepekatan reagen Gibbs adalah disebabkan oleh kepekatan kompleks kapsaisin – Gibbs yang terbentuk semakin meningkat. Serapan kompleks kapsaisin – Gibbs menjadi hampir malar apabila kepekatan reagen Gibbs mencapai 3.55×10^4 M kerana semua kapsaisin yang ada dalam larutan telah digunakan untuk membentuk kompleks dengan reagen Gibbs. Pada keadaan ini, reagen Gibbs berada dalam keadaan berlebihan. Nor Azah



Rajah 4: Kesan pH terhadap nilai perbezaan serapan kompleks kapsaisin-reagen Gibbs



Rajah 5: Graf kesan kepekatan reagen Gibbs terhadap serapan kompleks kapsaisin-reagen Gibbs

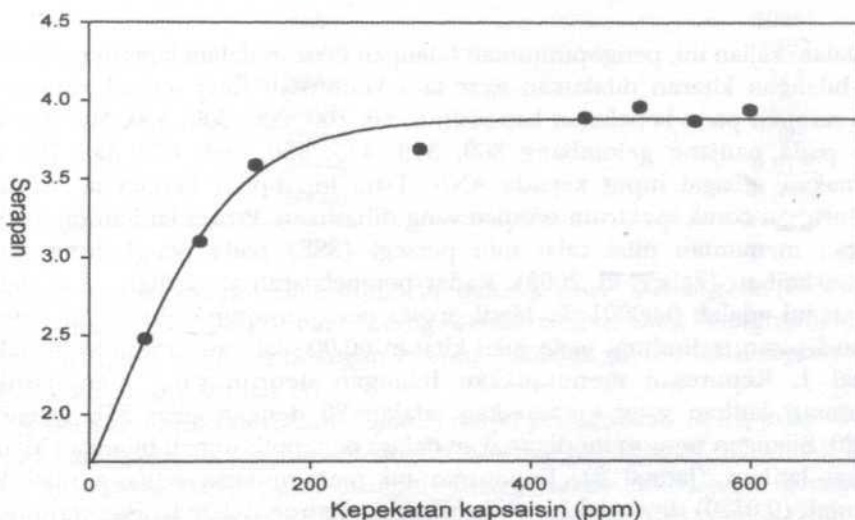
dan Musa (2002) turut melaporkan bentuk graf yang sama apabila mengkaji kepekatan reagen galosianin terhadap respon penerima kimia gentian optik untuk ion plumbum.

Rajah 6 menunjukkan kesan kepekatan kapsaisin ke atas serapan kompleks kapsaisin-reagen Gibbs. Keamatan serapan kompleks kapsaisin-reagen Gibbs didapati meningkat dengan peningkatan kepekatan kapsaisin dan menjadi hampir

malar apabila kepekatan kapsaisin mencapai 250 ppm. Pada keadaan ini, semua reagen Gibbs telah digunakan dalam pembentukan kompleks kapsaisin-reagen Gibbs manakala kapsaisin berada dalam keadaan berlebihan.

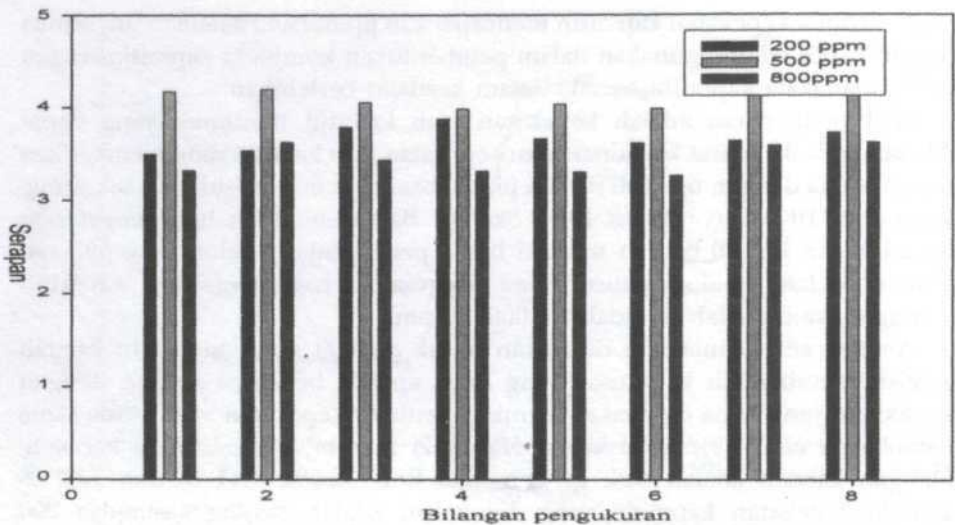
Had pengesanan adalah kepekatan atau kuantiti minimum yang dapat dikesan pada 95 % aras keyakinan iaitu kepekatan atau kuantiti yang memberikan bacaan sama dengan tiga kali sisihan piawai bagi satu siri pengukuran sekurang-kurangnya 10 kali (Christian 1994; Skoog). Bagi penentuan had pengesanan dalam kajian ini, 10 bacaan serapan blank pada panjang gelombang 595 nm diukur. Melalui analisis statistik, had pengesanan bagi penentuan kapsaisin menggunakan kaedah ini adalah 0.00097 ppm.

Analisis kebolehulangan dilakukan untuk melihat sama ada suatu kaedah analisis memberikan keputusan yang sama apabila beberapa reagen dengan kepekatan yang sama digunakan untuk penentuan kepekatan analit yang sama (Alabbas *et al.* 1989). Hasil kajian (*Rajah 7*) menunjukkan bahawa kebolehulangan kaedah adalah baik dengan nilai RSD 3.55%, 2.44 % dan 4.52 % apabila kepekatan kapsaisin yang digunakan adalah masing-masingnya 200 ppm, 500 ppm dan 800 ppm.



Rajah 6: Kesan kepekatan kapsaisin (0 – 850 ppm) terhadap serapan kompleks kapsaisin-reagen Gibbs pada panjang gelombang 595 nm

Kajian terhadap kestabilan foto reagen Gibbs dilakukan untuk melihat sama ada reagen akan mengalami penguraian foto apabila didedahkan kepada cahaya untuk satu jangka masa yang panjang. Sumber cahaya dari lampu deuterium digunakan dalam kajian ini. Serapan reagen pada panjang gelombang 595 nm diukur pada sela masa 1 jam dalam tempoh 38 jam. Hasil kajian terhadap kestabilan foto reagen Gibbs menunjukkan kestabilan foto yang baik dengan nilai RSD 0.010 %. Nilai RSD yang kecil ini menunjukkan reagen Gibbs agak stabil secara foto dalam larutan akues.



Rajah 7: Kebolehulangan penggunaan reagen Gibbs untuk penentuan kepekatan kapsaisin pada kepekatan kapsaisin yang berbeza iaitu 200 ppm, 500 ppm dan 800 ppm

Dalam kajian ini, pengoptimuman bilangan neuron dalam lapisan terlindung dan bilangan kitaran dilakukan agar satu keputusan yang terbaik diperolehi. Data serapan pada kepekatan kapsaisin 0, 50, 100, 200, 300, 400, 500 dan 600 ppm pada panjang gelombang 309, 349, 445, 550, 594, 672 dan 765 nm digunakan sebagai input kepada ANN. Data ini dipilih kerana ia mewakili keseluruhan corak spektrum serapan yang dihasilkan. Proses latihan dijalankan dengan memantau nilai ralat min persegi (SSE) pada penghujung setiap kitaran latihan (Faiz *et al.* 2003). Kadar pembelajaran yang digunakan dalam latihan ini adalah 0.00001 %. Hasil proses pengoptimuman bilangan neuron dalam lapisan terlindung pada nilai kitaran 60,000 kitaran ditunjukkan dalam Jadual 1. Keputusan menunjukkan bilangan neuron yang menghasilkan keputusan latihan yang memuaskan adalah 20 dengan nilai SSE terendah 0.0120. Bilangan neuron ini digunakan dalam pengoptimuman bilangan kitaran semasa latihan (Jadual 2). Keputusan ini menunjukkan bahawa nilai SSE terendah (0.0120) diperolehi apabila bilangan neuron dalam lapisan terlindung dan bilangan kitaran adalah masing-masingnya 20 dan 47,738.

Untuk mendapatkan arkitektur jaringan yang paling sesuai bagi aplikasi penentuan kepekatan larutan kapsaisin yang tidak diketahui, semua jaringan terlatih ini diuji dengan data daripada lima kepekatan kapsaisin yang berlainan untuk melihat keupayaan peramalan oleh jaringan terlatih tersebut. Data keamatan serapan setiap larutan kapsaisin dijadikan input kepada jaringan terlatih tersebut dan bacaan bagi setiap data diambil pada dua panjang gelombang terpilih. Keupayaan ramalan pada kepekatan kapsaisin yang berbeza oleh ANN berbanding kepekatan kapsaisin sebenar pada bilangan kitaran yang berbeza ditunjukkan dalam Jadual 3. Bilangan kitaran yang memberikan peratus ralat terendah (0.06 %) adalah 10,000 dan 47,738 kitaran. Data dalam Jadual

JADUAL 1
 Pengoptimuman bilangan neuron terlindung bagi kaedah kolorimetri untuk penentuan kepekatan kapsaisin menggunakan reagen Gibbs

Bilangan neuron terlindung	SSE
5	3979
10	1.5128
12	0.1382
15	0.0354
20	0.0120
25	0.2000

JADUAL 2
 Pengoptimuman bilangan kitaran dengan 20 neuron terlindung bagi kaedah kolorimetri untuk penentuan kepekatan kapsaisin menggunakan reagen Gibbs

Bilangan kitaran	SSE
5000	10685
10000	2567
20000	113
30000	4.80
40000	0.300
47738	0.0120
60000	0.0120

2 walau bagaimanapun menunjukkan bahawa nilai SSE bagi 47,738 adalah lebih rendah iaitu 0.0120 berbanding 10,000 kitaran yang menghasilkan SSE sebanyak 2,567. Oleh itu bilangan kitaran sebanyak 47,738 telah dipilih untuk digunakan dalam latihan ini.

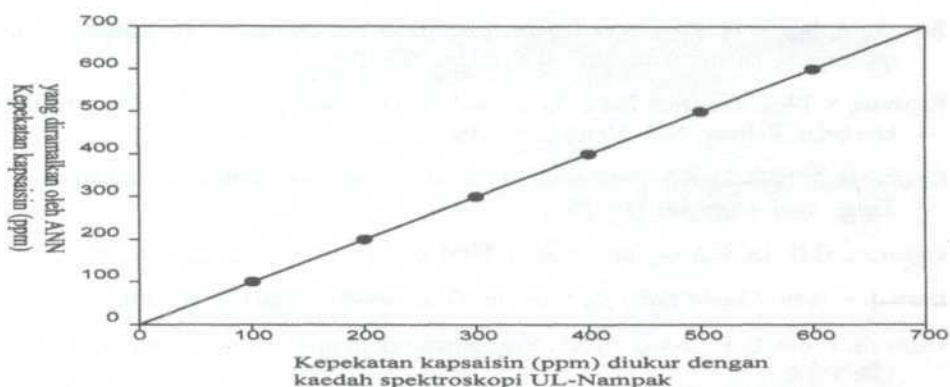
Seperti ditunjukkan dalam *Rajah 5*, tanpa penggunaan ANN, julat dinamik kepekatan kapsaisin yang boleh ditentukan dengan kaedah ini adalah dalam julat kepekatan 0-200 ppm. Dengan menggunakan ANN, julat dinamik ini boleh ditingkatkan kepada julat yang lebih besar iaitu di antara 0-600 ppm (*Rajah 8*). Walaupun terdapat kaedah kemometrik yang boleh digunakan untuk pemilihan data (Cirovic 1997; Despaigne and Massart 1998), pemilihan data input dalam kajian ini dilakukan dengan mengambil kira rangsangan, dan kebolehannya untuk digandingkan dengan diod pemancar cahaya (LED). Ciri terakhir ini perlu dipertimbangkan memandangkan terdapat kemungkinan pembinaan peralatan penerima kapsaisin mudah alih pada kajian yang akan datang. Selain daripada itu, panjang gelombang yang dipilih ini turut menggambarkan ciri dan identiti keseluruhan spektrum serapan yang telah direkodkan.

Dalam proses latihan ANN, fungsi penukar sigmoid digunakan dalam lapisan terlindung dan output. Hanya satu lapisan terlindung sahaja yang

JADUAL 3

Keupayaan ramalan kepekatan kapsaisin oleh ANN berbanding kepekatan kapsaisin sebenar pada bilangan kitaran yang berbeza

Bilangan kitaran	Kepekatan sebenar kapsaisin, ppm										Ralat kalibrasi purata	Peratus
	150		250		350		450		550			
	Ramalan	Ralat	Ramalan	Ralat	Ramalan	Ralat	Ramalan	Ralat	Ramalan	Ralat		
5,000	160	10	232	18	413	63	476	26	495	55	34	0.10
10,000	161	11	221	29	399	49	461	11	540	10	22	0.06
20,000	169	19	230	20	395	45	443	7	573	23	23	0.07
30,000	167	17	223	27	406	56	442	8	579	29	27	0.08
40,000	166	16	228	22	403	53	452	2	581	31	25	0.07
47,738	158	8	241	9	398	48	444	6	580	30	20	0.06



Rajah 8: Graf penentuan data latihan dan kalibrasi oleh jaringan yang mempunyai 20 neuron terlindung bagi kapsaisin dalam reagen Gibbs

digunakan dalam kajian ini memandangkan ia telah terbukti berkesan dalam menyelesaikan berbagai masalah analisis (Svozil *et al.* 1997). Latihan jaringan dijalankan dengan menggunakan kaedah latihan pertambahan, di mana pemberat dibetulkan selepas ralat latihan rangsangan diukur (Bos and Van der Linden 1993).

KESIMPULAN

Penentuan kepekatan kapsaisin menggunakan reagen Gibbs telah dilakukan dalam kajian ini menggunakan ANN dengan 20 neuron terlindung, kadar pembelajaran 0.00001 % dan melakukan latihan menggunakan 47,738 kitaran. ANN berupaya memanjangkan julat dinamik kepekatan kapsaisin dari 0 - 200 ppm hingga 0 - 600 ppm. Purata ralat yang diberikan oleh ANN adalah 0.06 %.

PENGHARGAAN

Penyelidik ingin merakamkan penghargaan kepada Kementerian Sains, Teknologi dan Alam Sekitar kerana sumbangan gran penyelidikan IRPA 01-02-02-0030 dan IRPA 09-03-03-0006NBD untuk kajian ini.

RUJUKAN

- ALABBAS, S.H., D.C. ASHWORTH dan R. NARAYANASWAMY. 1989. Design and performance features of an optical fibre reflectance pH sensor. *Analytical Proceedings* 26. 373-375.
- BAJAJ, K. L. 1980. Colorimetric determination of capsaicin in capsicum fruits. *J. Assoc. Off. Anal. Chem.* **63(6)**: 1314-1316.
- BILLINGS, S. A., H. B. JAMALUDDIN dan S. CHEN. 1991. A comparison of the back-propagation and recursive prediction error algorithms for training neural network. *Mech. Syst. Signal. Proc.* **5**: 233-255.

- Mohamad Nasir Mat Arip, Musa Ahmad, Ahmed Mahir Mokhtar, Mohd Nasir Taib & Lee Yok Heng
- BOS, A. M. BOS & W. E. VAN DER LINDEN. 1993. Data processing by neural networks in quantitative chemical analysis. *Analyst* **118**: 323-328.
- BUDAVARI, S. 1989. *The Merck Index. An Encyclopedia of Chemical, Drugs, and Biologicals*. Edisi kesebelas. Rahway, N. J. Merck & Co. Inc.
- CIROVIC, D. A. 1997. Feed-forward artificial neural networks: Applications to spectroscopy. *Trend. Anal. Chem.* **16**: 148-155.
- CHRISTIAN, G.D. 1994. *Analytical Chemistry*. Edisi keenam. New York: John-Wiley & Son.
- DEAN, J.A. 1989. *Chemist Ready Reference Handbook*. New York: McGraw-Hill Inc.
- DESPAGNE, F. dan D. L. MASSART. 1998. Neural network in multivariate calibration. *Analyst* **123**: 157R.
- FAIZ BUKHARI MOHD SUAHI, MUSA AHMAD dan MOHD NASIR TAIB. 2003. Optimisation of the range of an optical fibre pH sensor using feed-forward artificial neural network. *Sensors and Actuators B.* **90**:175 – 181.
- GOVINDARAJAN, V. S. 1985. Capsicum – production, technology, chemistry and quality. I. History, botany, cultivation and primary processing. *Crit. Rev. Food Sci. Nutr.* **22**: 109.
- Joint Committee (PS/SAC). 1959. Recommended methods of analysis of crude drugs. The determination of capsaicin content of capsicum and its preparations I. *Analyst.* **84**: 603-617.
- Joint Committee (PS/SAC). 1963. Recommended methods of analysis of crude drugs. The determination of capsaicin content of capsicum and its preparations II. Content of Capsicum and its Preparations (Part II). *Analyst.* **89**: 377-388.
- MOHLER, E. F. dan L. N. Jacob. 1957. Determination of phenolic type compound in water and industrial waste water: comparison of analytical method. *Anal. Chem.* **29**: 1369-1374.
- PALACIO, J.J.R. 1977. Spectrophotometric determination of capsaicin. *J. Assoc. Off. Anal. Chem.* **60**: 970.
- PALACIO, J.J.R. 1979. Further study of spectrophotometric determination of capsaicin. *J. Assoc. Off. Anal. Chem.* **62**: 1168.
- RAIMUNDO, Jr, I. M. dan R. NARAYANASWAMY. 2001. Simultaneous determination of relative humidity and ammonia in air employing an optical fibre sensor and artificial neural network. *Sens. Actuators. B.* **74**: 60-68.
- SKOOG, A.D., D.M. WEST dan F.J. HOLLER. 1996. *Analytical Chemistry*. Edisi ketujuh. New York: Saunders College Publishing.
- SVOZIL, D., V. KVASNICKA dan J. POSPICHAL. 1997. Introduction to multi-layer feed-forward neural network. *Chemom. Intell. Lab. Sys.* **39**: 43-62.
- YUSOF, N.A dan M. AHMAD. 2002. A flow cell optosensor for lead based on immobilized gallicin in chitosan membrane. *Talanta* **58**: 459-466.

Effect of Specimen Size and Shape on the Compressive Strength of High Strength Concrete

Alaa S. Malaikah

*Civil Engineering Department, College of Engineering, King Saud University,
PO Box 800, Riyadh 11421, Saudi Arabia
E-mail: malaikah@ksu.edu.sa*

Received: 10 September 2003

ABSTRAK

Pengaruh bentuk dan saiz spesimen ke atas kekuatan mampat yang diukur telah dikaji untuk konkrit berkekuatan tinggi yang berbeza dicampur. Lebih 260 spesimen daripada 30 campuran konkrit berkekuatan tinggi dituang dan diuji. Didapati bahawa secara purata nisbah kekuatan mampat silinder 150×300 mm kepada kiub 150 mm adalah 0.80; manakala untuk silinder 100×200 mm kepada kiub 150 mm adalah 0.93. Juga, secara purata, nisbah kekuatan mampat silinder 150×300 mm kepada silinder 100×200 mm adalah 0.86.

ABSTRACT

The influence of specimen size and shape on the measured compressive strength was investigated for different high strength concrete mixes. Over 260 specimens from 30 high strength concrete mixtures were cast and tested. It was found, that on average, the ratio of the compressive strength of 150×300 mm cylinders to 150 mm cubes was 0.80; while for 100×200 mm cylinders to 150 mm cubes was 0.93. Also, on average, the ratio of the compressive strength of 150×300 mm cylinders to 100×200 mm cylinders was 0.86.

Keywords: High strength concrete, compressive strength, size effect, shape effect

INTRODUCTION

In Saudi Arabia concrete is the dominant construction material for all types of buildings and other structures. Most of the structural concrete elements are made with a compressive strength of 20 to 35 MPa. Lately, there is an increase in use of high strength concrete (HSC) in major construction projects such as high-rise buildings and bridges. The advances in the quality control of concrete production are enabling ready mixed, pre-stressed, and pre-cast concrete plants to achieve higher strength concretes.

Locally, the characteristic compressive strength is usually measured based on 150 mm cubes. But in design practice, the design compressive strength is usually based on the standard 150×300 mm cylinders. The use of 100×200 mm cylinders gained more acceptance locally as the need to test high strength concrete increases. This is expected since most testing machines used locally have a full capacity of 1300 kN. Hence, to test a standard specimen having a compressive strength of 80 MPa would require a test machine with a capacity greater than 1300 kN.

Several researchers have compared measured strengths achieved with different sizes of cubical and cylindrical specimens for high strength concrete. For cylindrical specimens comparisons were usually made between the compressive strength of 150 × 300 mm cylinders and that of 100 × 200 mm cylinders. Carrasquillo *et al.* (1981) reported that the average ratio of compressive strength of 150 × 300 mm to 100 × 200 mm cylinders was 0.9 regardless of strength and test age. A contradiction to this finding was later reported by Carrasquillo *et al.* (1988) which reported that compressive strength of 100 × 200 mm cylinders were 7 percent lower than those of 150 × 300 mm cylinders. French *et al.* (1993) observed in their study that on average 100 × 200 mm cylinders tested showed 6 percent higher strength than that of their companion 150 × 300 mm cylinders. Aitcin *et al.* (1994) reported that larger cylinder sizes gave rise to lower apparent compressive strength, and that compressive strength is not sensitive to cylinder size for very high strength concrete.

For comparison between compressive cube strength and compressive cylinder strength (diameter/height = 1/2), a factor of 0.8 to the cube strength is often applied for normal strength concrete (FIP-CEB 1990). The same reference also cited a study that indicated that the cylinder/cube compressive strength ratio is not only a function of the strength grade but also of the mix design parameters. In a recent study, Alsayed (1997) reported that the ratio of 0.8 that is applied for normal strength concrete remains the same for high strength concrete.

In this paper, results of an ongoing research on high strength concrete were presented. A comparison of the compressive strength between 150 mm cubes, 150 × 300 mm and 100 × 200 mm cylinders was performed. These sizes were chosen because it represented the sizes that are most commonly used locally in the construction industry and research. The results were obtained from 30 high strength mixes, 3 of which were provided from a local ready-mixed concrete plant. The study suggested compressive strength conversion factors between the different specimen sizes and shapes used in the study.

METHODOLOGY

Materials

The use of locally available materials from different sources in the Riyadh area was emphasized in this study. For the cases where locally available materials were not attainable, commercially available materials were used. For the ready-mixed concrete, the material properties used were not collected. The following are the details for the materials used in the laboratory mixes.

Cement: Commercially available Portland cement Type I conforming to ASTM C 150 specification.

Coarse Aggregates: Locally available crushed limestone was used for coarse aggregates. These aggregates were procured from different sources around the city of Riyadh. The physical properties of the coarse aggregates are listed in Table 1. The mineral composition was obtained by Energy Dispersal X-Ray

(EDX) analysis. The crushed limestone typically had Calcite (Ca more than 96%), and clay which provided Potassium (K 1.8%), and Iron (Fe 1.3%).

Fine Aggregates: Locally available crushed sand and white natural silica sand were used in the overall study. These aggregates were also procured from different sources as the case for the coarse aggregates. The physical properties of the fine aggregates are given in Table 2. The crushed sand had typically the following mineral composition: Calcite (Ca more than 90%), and clay which provided Potassium (K 4%), and Iron (Fe 3%). The natural silica sand known as Quartz Arenite typically had Quartz (Si more than 95%), and Clay which provided Potassium (K 3%), and Iron and Calcium (1% each).

TABLE 1
Physical properties of coarse aggregates

Property	Group I		Group II	Group III
	LM 1-A	LM 1-B	LM 2	LM 3
Maximum size aggregate, mm	10	20	10	10
Dry unit weight, kg/m ³	1650	1550	1616	1536
Absorption, percent	1.95	3.02	1.03	1.83
Specific gravity:				
a. Bulk oven-dry	2.58	2.54	2.57	2.61
b. Bulk saturated surface dry	2.60	2.58	2.63	2.66

Note: Limestone = LM

TABLE 2
Physical properties of fine aggregates

Property	Group I		Group II		Group III	
	silica sand	washed sand	silica sand	washed sand	silica sand	washed sand
Dry unit weight, kg/m ³	1800	1680	1730	1570	1616	1536
Absorption, percent	0.2	3.02	0.42	1.69	1.03	1.83
Specific gravity:						
a. Bulk oven-dry	2.66	2.54	2.56	2.59	2.59	2.62
b. Bulk saturated surface dry	2.68	2.58	2.57	2.66	2.60	2.66
Fineness modulus*	2.8		2.9		2.8	

* combined 50% silica sand and 50% washed sand

Silica Fume: Commercially available powder silica fume was used in the study. The silica fume had a specific gravity of 2.3.

Admixture: Commercially available sulphonated naphthalene-based high performance superplasticizer conforming to ASTM C 494 as Type F.

Mix Proportions

During the course of this study, around 30 high strength mixtures with 28-day compressive strength in the range of 35 to 90 MPa (cylinder strength) and 40 to 102 MPa (cube strength) were cast and tested. Details of the mix proportions for all the mixtures except for the ready-mixed concrete are tabulated in Tables 3 through 5. The composition of cementitious material used for the laboratory mixes were Portland cement ranging from 350 to 550 kg/m³ and silica fume 0, 10, and 15% replacement by weight of cement. The water-cementitious ratio (w/cm) ranged from 0.22 to 0.35.

Casting and Curing

All laboratory batches of concrete were cast inside the laboratory in a small capacity drum mixer, (except for 2 mixes II-7R and II-13R) a heavy duty pan mixer was used to check if silica fume was properly mixed during initial mixes.

TABLE 3
Mix proportions of group I

Ref. No.	water (kg/m ³)	cement, Type I (kg/m ³)	silica fume (kg/m ³)	coarse aggregate 20mm (kg/m ³)	coarse aggregate 10mm (kg/m ³)	washed sand (kg/m ³)	silica sand (kg/m ³)	super-plasticizer (L/m ³)	w/cm ratio	Slump (mm)
I-1	145	495	49.5	1070	0	290	290	18.75	0.26	230
I-2	122.5	350	0	845	280	372.5	0	8.75	0.35	230

TABLE 4
Mix proportions of group II

Ref. No.	water (kg/m ³)	cement, Type I (kg/m ³)	silica fume (kg/m ³)	coarse aggregate (kg/m ³)	washed sand (kg/m ³)	silica sand (kg/m ³)	super-plasticizer (L/m ³)	w/cm ratio	Slump (mm)
II-1	145	495	0	1070	290	290	7.50	0.283	220
II-2	182	550	0	1050	271	271	5.50	0.331	35
II-3	182	495	55	1050	263	263	7.85	0.331	55
II-4	169	550	0	1050	287	287	7.35	0.307	25
II-5	169	495	55	1050	278	278	13.75	0.307	130
II-6	158	550	0	1050	302	302	10.00	0.287	85
II-7	158	495	55	1050	293	293	15.00	0.287	110
II-7R	158	495	55	1050	293	293	15.00	0.287	250
II-8	149	550	0	1050	314	314	13.37	0.271	150
II-9	149	495	55	1050	305	305	17.37	0.271	110
II-10	149	468	83	1050	301	301	20.12	0.270	100
II-11	138	550	0	1050	328	328	16.50	0.251	200
II-12	138	495	55	1050	319	319	19.75	0.251	160
II-13	138	468	83	1050	315	315	22.60	0.25	145
II-13R	138	468	83	1050	315	315	22.60	0.25	220

TABLE 5
Mix proportions of group III

Ref. No.	water (kg/m ³)	cement, Type I (kg/m ³)	silica fume (kg/m ³)	coarse aggregate (kg/m ³)	washed sand (kg/m ³)	silica sand (kg/m ³)	super-plasticizer (L/m ³)	w/cm ratio	Slump (mm)
III-3	121	550	0	1070	295	295	21.75	0.22	70
III-4	121	495	55	1070	295	295	30.00	0.22	70
III-5	132	550	0	1070	295	295	13.50	0.24	55
III-6	132	495	55	1070	295	295	21.25	0.24	75
III-7	143	550	0	1070	295	295	11.25	0.26	110
III-8	143	495	55	1070	295	295	18.63	0.26	80
III-9	154	550	0	1070	295	295	7.25	0.28	25
III-10	154	495	55	1070	295	295	13.95	0.28	62
III-11	165	550	0	1070	295	295	6.63	0.30	45
III-12	165	495	55	1070	295	295	12.00	0.30	90

The mixing, casting, and curing conformed to ASTM C192. Each batch was used to cast the 3 standard size 150 × 300 mm cylinders, 3 medium size 100 × 200 mm cylinders, and 3 standard 150 mm cubes to obtain the compressive strength. The cylindrical and cubical samples were cast in steel molds to eliminate any effect that could result from plastic or cardboard molds. The standard size cylindrical and cubical specimens were cast in two layers with each layer vibrated in a vibrating table for 35 to 45 seconds. The medium size cylindrical samples were cast in two layers with each layer vibrated in a vibrating table for 30 to 35 seconds. After the compaction operation, the top of the specimen was smooth finished by means of a trowel. The cylindrical specimens were covered by polyethylene bags and the cubical specimens were covered by means of a plastic cover. The specimens were demolded after 24 hours, and then subjected for 28 days to standard moist curing by immersing them in curing tanks containing lime saturated water at 23 C.

Test Procedure

At the age of 28 days, the specimens were taken out from the curing tank. The cylindrical specimens were end-capped with a vitrobond sulfur based capping compound. The compressive strength was measured in compliance with ASTM C39. To perform compression tests, a 3000 kN Auto Comp 2 compression machine manufactured by Controls was used. The load accuracy of this machine is ±1%. The machine used has a high stiffness frame with four pre-stressed columns to ensure maximum rigidity and stability and is suitable for cylinder and cube testing.

TEST RESULTS AND DISCUSSION

During the course of this study, over 260 specimens from 30 high strength concrete mixtures were tested in which 3 of those mixes were obtained from

ready-mixed plants. The average 28-day compressive strength for 150 × 300 mm, 100 × 200 mm cylinders and 150 mm cubes are shown in Table 6. The observed strength ratios of 150 × 300 mm cylinders to 150 mm cubes, 100 × 200 mm cylinders to 150 mm cubes, and 150 × 300 mm cylinders to 100 × 200 mm cylinders for each concrete mixture tested are shown in columns 5, 6, and 7, respectively.

The ratio of the 150 × 300 mm cylinder to the 150 mm cube was between 0.66 and 0.97. As expected, the 150 mm cubes are always stronger than the 150 × 300 mm cylinders. This is usually attributed to having an overlapped restrained zone in cubes while testing under uniaxial compression, hence a zone of

TABLE 6
Average Compressive strength of 150x300 mm and
100x200 mm cylinders and 150 mm cubes

Ref. No.	$f'_c(150 \times 300)$ (MPa)	$f'_c(100 \times 200)$ (MPa)	$f'_c(150 \text{ cube})$ (MPa)	$\frac{f'_c(150 \times 300)}{f'_c(150 \text{ cube})}$	$\frac{f'_c(100 \times 200)}{f'_c(150 \text{ cube})}$	$\frac{f'_c(150 \times 300)}{f'_c(100 \times 200)}$
(1)	(2)	(3)	(4)	(5)	(6)	(7)
I-1	56	—	70	0.80	—	—
I-2	46	—	57	0.81	—	—
II-1	64.5	72.8	78.7	0.82	0.93	0.89
II-2	53.1	55.9	60.9	0.87	0.92	0.95
II-3	55.0	56.4	69.1	0.80	0.82	0.98
II-4	52.9	64.3	67.2	0.79	0.96	0.82
II-5	68.0	86.3	86.5	0.79	1.00	0.79
II-6	62.6	81.0	71.5	0.88	1.13	0.77
II-7	66.4	69.8	78.4	0.85	0.89	0.95
II-8	71.5	74.3	81.4	0.88	0.91	0.96
II-9	80.6	82.1	92.9	0.87	0.88	0.98
II-10	82.1	84.2	94.0	0.87	0.90	0.98
II-11	58.7	65.4	73.0	0.80	0.90	0.90
II-12	74.0	91.6	91.1	0.81	1.01	0.81
II-13	83.5	86.1	85.7	0.97	1.00	0.97
II-7R	66.9	—	91	0.73	—	—
II-13R	79.7	—	102	0.78	—	—
III-3	58.9	65.5	81.6	0.72	0.80	0.90
III-4	74.6	82.4	92.0	0.81	0.90	0.90
III-5	62.2	76.0	82.7	0.75	0.92	0.82
III-6	72.1	85.8	87.0	0.83	0.99	0.84
III-7	66.8	79.9	87.1	0.77	0.92	0.84
III-8	59.9	72.9	82.1	0.73	0.89	0.82
III-9	47.8	65.3	70.5	0.68	0.93	0.73
III-10	59.6	84.8	87.8	0.68	0.96	0.70
III-11	44.9	65.2	68.0	0.66	0.96	0.69
III-12	49.4	71.8	70.9	0.70	1.01	0.69
RM-1	35.5	—	38	0.93	—	—
RM-2	37	41	47	0.79	0.87	0.90
RM-3	47.5	51	55	0.86	0.93	0.93

triaxial compression develops. On the other hand, cylinders with length/diameter ratio of 2 have an unrestrained zone away from the ends. The comparison of the 150 × 300 mm cylinder to the 150 mm cube compressive strength test results are plotted in Fig. 1. As shown in the figure, from the test results, the ratio of the 150 × 300 mm cylinder to the 150 mm cube compressive strength was on average about 0.80. This result agrees with previously reported results.

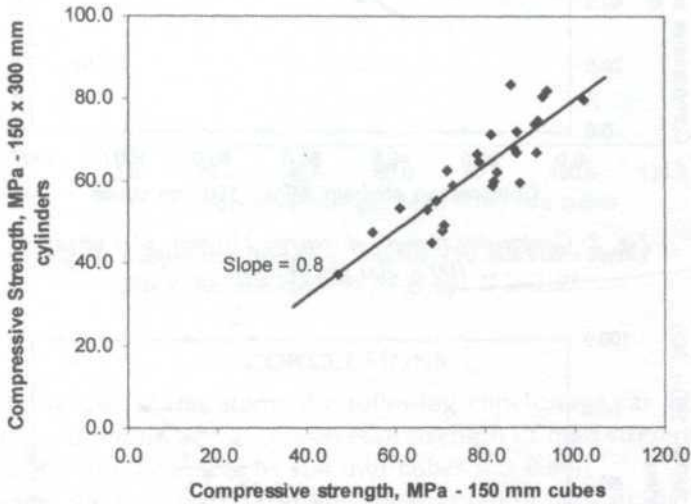


Fig. 1: Compressive strength of concrete 150 mm cubes versus 150 × 300 mm cylinders

Comparison of the compressive strength test results from 100 × 200 mm cylinders and 150 mm cubes are shown in column 6 of Table 6 and plotted in Fig. 2. The ratios ranged from 0.8 to 1.13. The 1.13 ratio was only from one data point and all other data points were less than 1.0. Hence, one could comfortably expect that 150 mm cube compressive strength would be higher than 100 × 200 mm cylinders. On average, the ratio of the 100 × 200 mm cylinders to the 150 mm cube was 0.93, as can be seen in Fig. 2.

Similarly, comparison of the compressive strength test results of the 150 × 300 mm cylinders versus the 100 × 200 mm cylinders are shown in column 7 of Table 6 and plotted in Fig. 3. On average, the ratio of the 150 × 300 mm to 100 × 200 mm cylinders was 0.86, as can be seen in Fig. 3. This also confirms the presence of a size effect where the nominal compression strength at failure decreases as the specimen size increases (Sener 1997).

A plot of the compressive strength of 150 mm cubes versus 150 × 300 mm cylinders for concrete mixture groups II and III is shown in Fig. 4. Each of the mixes within the group had the same source of coarse and fine aggregates and each group had a different source of aggregate. It can be seen from Fig. 4 that each group had a different but close ratio of compressive strength of 150 × 300

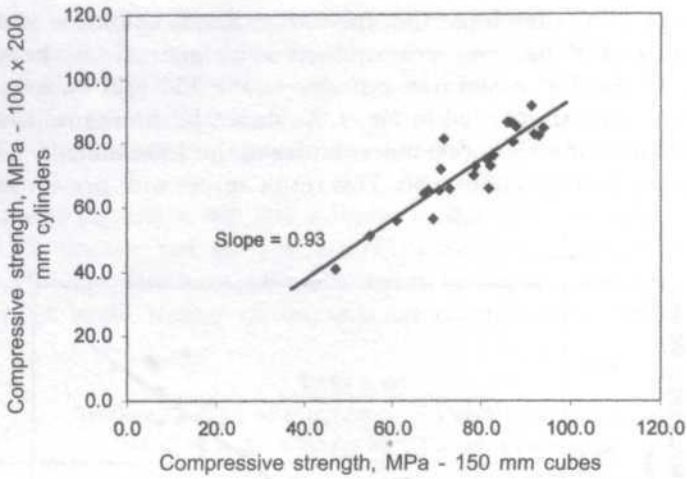


Fig. 2: Compressive strength of concrete 150 mm cubes versus 100 × 200 mm cylinders

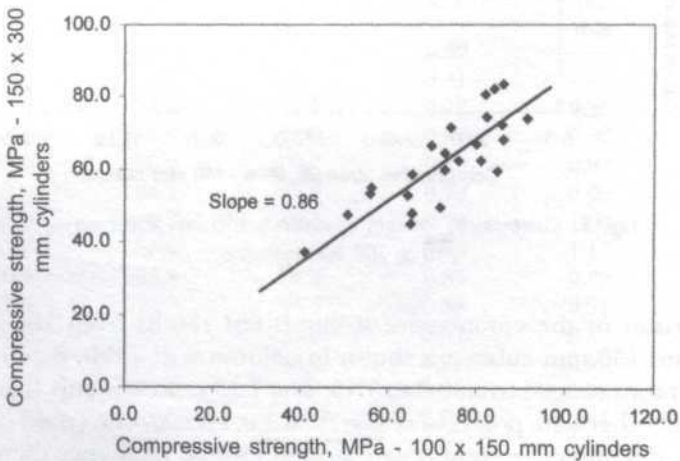


Fig. 3: Compressive strength of concrete cylinders cast in 100 × 200 mm versus 150 × 300 mm

mm cylinders to 150 mm cubes. This seems to indicate that the mix design parameters influence the cylinder/cube strength ratio. A recent study using locally available materials indicated that the quality of coarse aggregate has a significant effect on the compressive strength of high strength concrete (Beshr *et al.* 2003).

Although conversion factors between the standard sizes and shapes are obtained, it is strongly recommended that in reporting the compressive strength values of high strength concrete, the size and shape used for strength determination must be specified.

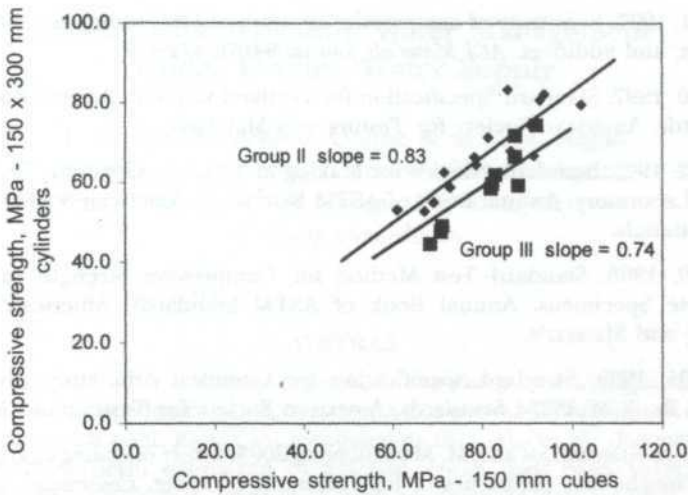


Fig. 4: Compressive strength of concrete 150 mm cubes versus 150 x 300 mm cylinders for groups II and III

CONCLUSIONS

Based on the results of this study, the following conclusions can be made.

1. On average, the ratio of the compressive strength of high strength concrete of 150 x 300 mm cylinders to 150 mm cubes was 0.80.
2. On average, the ratio of the compressive strength of high strength concrete of 100 x 200 mm cylinders to 150 mm cubes was 0.93.
3. On average, the ratio of the compressive strength of high strength concrete of 150 x 300 mm cylinders to 100 x 200 mm cylinders was 0.86.
4. The obtained results indicate that mix design parameters influence the strength ratios of cylinder to cube.

ACKNOWLEDGEMENTS

The author would like to acknowledge the financial support given by the Research Center, College of Engineering King Saud University through research grant No. 10/423. The experimental program was carried out at the structure and concrete laboratories of the Civil Engineering Department, King Saud University. The author would also like to express his gratitude to Dr. Abdulrahman Alhozaimy for his thoughtful suggestions and his contribution in this study.

REFERENCES

- AİTCİN, P.C., B. MIAO, W. D. COOK and D. MITCHELL. 1994. Effects of size and curing on cylinder compressive strength of normal and high-strength concretes. *ACI Materials Journal* 91(4): 349-354.

- ALSAYED, S.H. 1997. Sensitivity of compressive strength of HSC to hot-dry climate, curing regimes, and additives. *ACI Materials Journal* **94(6)**: 472-477.
- ASTM C 150. 1997. Standard Specification for Portland Cement. Annual Book of ASTM Standards. American Society for Testing and Materials.
- ASTM C 192. 1995. Standard Practice for Making and Curing Concrete Test Specimens in the Laboratory. Annual Book of ASTM Standards. American Society for Testing and Materials.
- ASTM C 39. 1996. Standard Test Method for Compressive Strength of Cylindrical Concrete Specimens. Annual Book of ASTM Standards. American Society for Testing and Materials.
- ASTM C 494. 1999. Standard Specification for Chemical Admixtures for Concrete. Annual Book of ASTM Standards, American Society for Testing and Materials.
- BESHR, H., A. A. ALMUSALLAM and M. MASLEHUDDIN. 2003. Effect of coarse aggregate quality on the mechanical properties of high strength concrete. *Construction and Building Materials* **17**: 97-103.
- CARRASQUILLO, P.M. and R.L. CARRASQUILLO. 1998. Evaluation of the use of current concrete practice in the production of high-strength concrete. *ACI Materials Journal* **85(1)**: 49-54.
- CARRASQUILLO, R., A. NILSON and F. SLATE. 1981. Properties of high strength concrete subject to short-term loads. *ACI Journal* **78(3)**: 171-178.
- FRENCH, C.W. and A. MOKHTARZADEH. 1993. High strength concrete: effects of material, curing and test procedures on short-term compressive strength. *PCI Journal* **38(3)**: 76-87.
- Joint FIP-CEB Working Group on High Strength Concrete. 1990. High Strength Concrete: State of the Art Report. CEB Bulletin No. 197 (FIP SR 90/1), Federation Internationale de la Prescontrainte, London, England.
- SENER, SIDDIK. 1997. Size effect tests of high strength concrete. *Journal of Materials in Civil Engineering* **9(1)**: 46-48.

In-time Rice Irrigation Water Management Under Limited Water Supply

T. S. Lee, M. Aminul Haque & M.M.M. Najim
*Faculty of Engineering, Universiti Putra Malaysia,
Serdang, 43400 Selangor DE, Malaysia
tslee@eng.upm.edu.my*

Received: 14 Oktober 2003

ABSTRAK

Edaran air pengairan bertahap tepat-masa kepada petani merupakan suatu masalah utama kepada pengurus, perancang dan penyelidik berkenaan dengan pengairan sawah padi. Kajian ini menganalisis cara edaran air dan pelepasan air tepat-masa perlu diamalkan di kawasan sawah padi pada jangka masa pratetepuan dan jangka masa bekalan pengairan biasa. Analisis dibuat menggunakan data terkumpul di Projek Pengairan Besut, terletak di negeri Terengganu, Malaysia. Projek tersebut ini terbentuk daripada dua kawasan, berjumlah luasan pengairan 5,164 hektar. Berdasarkan keperluan air di ladang dan aliran yang wujud, simulasi saluran dibuat dan keputusan menunjukkan bahawa tugas persediaan ladang tidak digalakkan secara berterusan sekiranya terdapat kadar sumber aliran sungai kurang daripada 9.00 meter isi padu sesaat dan 3.00 meter isi padu sesaat masing masing di Empangan Besut dan Empangan Angga. Sekiranya kadar aliran kurang daripada jumlah tersebut, maka tugas persediaan ladang baik dilakukan dalam dua fasa berturut-turut. Akan tetapi, sekiranya aliran berada pada tahap 5.00 hingga 5.50 meter isi padu sesaat di Empangan Besut, tugas persediaan ladang disyorkan dilakukan dalam tiga fasa berturut-turut. Pada jangka masa pengairan biasa, kadar aliran 6.00 dan 1.75 meter isi padu sesaat masing masing di Empangan Besut dan Empangan Angga mesti wujud bagi mengairi keseluruhan projek berturut-turut dan sekiranya aliran kurang daripada tersebut, maka pengairan berpilihan atau pengairan bergiliran terpaksa dikuatkuasakan. Apabila wujudnya kadar aliran 7.20 sehingga 9.00 meter isi padu sesaat dan 1.70 sehingga 3.00 meter isi padu sesaat masing masing di Empangan Besut dan Angga, maka air perlu dilepaskan masuk ke saluran utama dan sekunder dua hari sebelum tugas persediaan ladang dimulakan. Demikian juga, air dilepaskan masuk tiga hari sebelum permulaan tugas persediaan ladang jika kadar aliran di antara 5.00 dan 7.00 meter isi padu sesaat di Empangan Besut. Lepas air masuk ke saluran perlu dimulakan lima jam terlebih dahulu pada jangka masa pengairan biasa demi untuk memenuhi jadual pengairan bertahap tepat-masa.

ABSTRACT

In-time water distribution of canal water to the farmers has been a major concern of managers, planners and researchers involved in irrigation. This study analyzed the ways for water distribution and timely water release in a rice-growing area during the pre-saturation period and the normal irrigation supply periods. The analyses were carried out using field data collected at the Besut Irrigation Scheme located in the northeastern corner of Peninsular Malaysia in the state of Terengganu. The scheme comprises two sub-schemes, giving a total

irrigation area of 5, 164 ha for the overall Besut Irrigation Scheme. Based on field water requirements and available flows at the intake gates, canal simulations were performed and results show that land preparation should not be done continuously unless flow rates are at least 9.00 m³/s and 3.00 m³/s at the Besut Barrage and Angga Barrage respectively. If the respective flow rates fall below these values, then land preparation should be done in two phases. However, when the flow rate is between 5.00 and 5.50 m³/s at the Besut Barrage, land preparation is recommended to be carried out over three phases. During the normal irrigation supply period, flow rates of 6.00 m³/s and 1.75 m³/s for the Besut and Angga Barrage respectively, are to be maintained for the entire irrigation scheme, otherwise selective irrigation or irrigation on a rotational basis has to be enforced. When flow rates are 7.20 – 9.00 m³/s and 1.70 – 3.00 m³/s at the Besut and Angga Barrage respectively, then water should be released two days before the beginning of the pre-saturation period for the filling main and secondary canals. However, water should be released three days before the beginning of the pre-saturation period when flow rates are between 5.00 and 7.00 m³/s at the Besut Barrage. But irrigation water should release 5.00 hours before beginning the normal supply period in order to maintain the in-time irrigation schedule.

Keywords: Canal flow simulation, water allocation, canal filling time, and rice irrigation.

INTRODUCTION

Malaysia is a rice-growing country and with the sophistication in rice cultivation practices, emphasis has been placed on farm water management. Rice has been cultivated in the coastal plains in Malaysia for a long time. Rice cultivation was carried out once in a year using local traditional systems. Double cropping of rice was fully implemented in 1988. The efficient utilization of water resources needs information, such as annual effective rainfall, runoff, consumptive use, and water release policy, etc. and this is possible through the application of computer modeling system in water management.

Ideal water management may be defined as the delivery of the right amount of irrigation water at the right time to the fields to increase crop yield. A lot of water is needed, especially during the critical time of the double cropping planting when the 'pre-saturation' and 'saturation' requirements have to be met. This requirement happens to be fulfilled at one peak time with the limited water resource. The Department of Irrigation and Drainage (DID) of Malaysia introduced the practice of 'Rotational Irrigation' for rotating the supply from plot to plot in the granary irrigation schemes. It is difficult to irrigate one big scheme especially when shortage of water occurs. Water losses are very critical due to the increasing rate of evaporation from the surface of the earth during the hot dry season, whence the production of rice needs more water. This means that we need to provide double the amount of water during the drought season when the storage of water has in fact decreased. The key to saving water and achieving high efficiency is through proper management and distribution of water. But the problem is how to distribute the water equitably to all rice

fields with high distribution efficiency. In time water management is one technique that can be implemented in rice irrigation schemes. This technique involves the effective use of irrigation water, reduction of operation loss (raise in efficiency) and increase of crop production. This will lead to savings in costs for operation and management.

Study Area

The area of study, Besut Irrigation Scheme, is located in the northeastern corner of Peninsular Malaysia in the state of Terengganu. The scheme consists of 2 sub-schemes, namely Angga Barrage sub-scheme and Besut Barrage sub-scheme. These sub-schemes are further sub-divided into 4 compartments, which are one compartment in the Angga sub-scheme (Compartment 2) and three compartments in the Besut sub-scheme (Compartment 1, 3, and 4). There are two sources of water supply for the scheme namely the Sungai Angga and Sungai Besut River. Compartments 1, 3 and 4 (totaling 4017 ha) receive irrigation supply by gravity from the Besut River System, while compartment 2 (1147 ha) receives irrigation supply also by gravity from the Angga River System. Moreover, the scheme area is divided into 39 irrigation blocks or water users' group as shown in *Fig. 1*. The main canals convey water downstream and the water is diverted to secondary and tertiary canals through discharge measuring offtake structures. Check gates are provided along the main as well as secondary canals to increase the water levels in the canals, when necessary. Irrigation infrastructure of this scheme has been provided for double cropping with a canal density of 48 m/ha, a drain density of 46 m/ha and farm road density of 24 m/ha (Teh and Mat, 1999). Water supply adequacy is sensitive to the water levels at the Besut and Angga barrages. When the water levels (above mean sea level) of Besut and Angga rivers are above 13.9 m and 16.5 m respectively, then the whole scheme is irrigated continuously. On the other hand, when the water levels fall below the above desired levels, the scheme is irrigated on a rotational basis. When drought occurs, the drains become supplementary sources of water. At present, water management problems are the most important constraints confronting the scheme in the fulfillment of its goal. Hence, the primary objective of this study is to investigate methods of in-time allocation of available water in order to achieve higher water productivity.

METHODS

Description of the Hydraulic Model

The *CanalMan* (Canal Management Software) model was used for performing hydraulic simulations of unsteady flow in branching canal networks. The *CanalMan* model was developed by Utah State University, Logan, Utah, USA (Merkley 1995). This model is based on partial differential equations (the Saint-Venant equations for one-dimensional flow) that allow the flow rate and water level to be computed as functions of space and time. The advantage of the model is that it computes the flow rate and water level simultaneously, so that

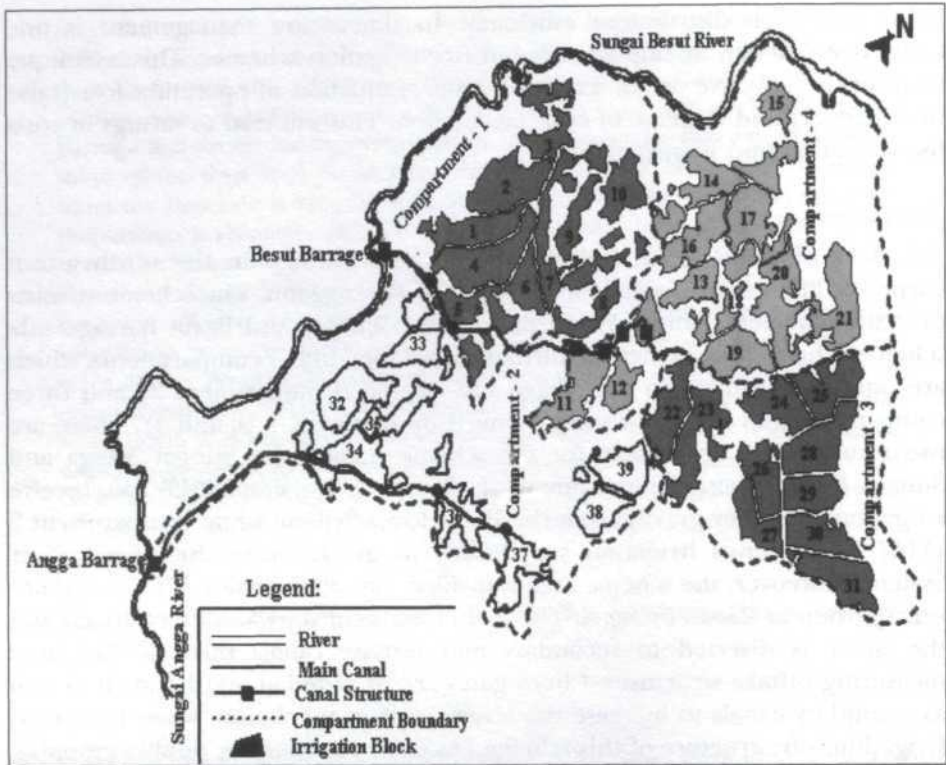


Fig. 1: Schematic map of the Besut Irrigation Scheme, Terengganu

the model more closely approximates the actual unsteady non-uniform nature of flow propagation in a canal. The model is highly interactive and includes integrated data editing capabilities, with numerous options for canal system configuration, hydraulic simulations, and output of results. Internal data cross-checking and input range restrictions on individual parameters help prevent unfeasible configurations and operating conditions. Canal networks are built interactively by inserting and arranging *nodes* graphically in a system layout window on-screen, where nodes represent locations of flow control structures and canal bifurcations.

The model determines approximate travel (or lag) times in canal reaches by applying a simplified equation for the celerity of a shallow-water wave (French 1985);

$$c = \sqrt{\frac{gA}{T}} \quad (1)$$

where c is wave speed or celerity (m/s), A is cross-sectional area of flow (m^2), T is top width of flow (m), and g acceleration due to gravity (approximate $9.81 m/s^2$).

The top width of flow is a function of the cross-sectional area and the channel shape and size. Eqn. [1] gives a wave speed that is equivalent to the mean flow velocity for critical flow in a section because it is the same as setting the Froude number equal to unity. The model determines the celerity for each canal reach using the current average values of flow area, A , and top width, T , then divides the reach length by the celerity to yield the lag time in seconds. The largest lag time of all reaches is multiplied by a coefficient between 1.0 and 2.0 (as a safety factor), and is taken as the minimum period between calculations of reach inflows by the gate scheduling algorithms, as discussed above.

Crop Water Requirements

Double cropping of rice is an activity that uses plenty of water. In rice irrigation, more than half of the water supplied is used for pre-saturation; i.e. to pre-saturate and inundate fields before planting of crop. Reducing the pre-saturation period may lead to saving water. For that reason, during the pre-saturation period the system should be in delivery mode at maximum capacity in order to reach all the fields as fast as possible so that planting of rice could be done without delay. The water requirement for pre-saturation is theoretically 150 – 200 mm, but can be as high as 650 – 900 mm when its duration is prolonged, i.e. 24 – 48 days (De Datta 1981; Bhuiyan *et al.* 1995). The water required during land soaking and land preparation period can be calculated as follows:

$$S_k = \frac{\frac{d_s}{t_s} + E_v + DP + Re_k}{8.64E_a} \quad (2)$$

where, S_k is land soaking water requirement (l/s/ha), d_s is depth of water required to saturate the soil (mm), E_v is evaporation rate (mm/day), t_s is time required to saturate the soil (days), Re_k is effective rainfall during the time period k (mm/day), DP is percolation rate [mm/day] and E_a is the application efficiency.

$$P_k = \frac{\frac{d_p}{t_p} + E_v + DP + Re_k}{8.64E_a} \quad (3)$$

where P_k is land preparation requirement (l/s/ha), d_p is depth of water required for crop submergence (mm), t_p is time required for land preparation (days).

The correct amount of irrigation delivery is the key element to improving irrigation management of the scheme. Irrigation supply for a field block through a gate can be estimated according to field water requirements. In

normal irrigation supply period, water required can be calculated on the basis of the formula (JICA 1998) shown below.

$$DWR = (ET_o \times K_c + SP - ERF) / E_s \quad (4)$$

where DWR is diversion water requirement, ET_o is reference evapotranspiration, K_c is crop coefficient, SP is seepage, ERF is effective rainfall and E_s is overall irrigation efficiency. The value of E_s , the overall irrigation efficiency includes irrigation efficiency and conveyance efficiency along the secondary canals, is believed to be 45% (JICA 1998). For soil saturation depth, the Department of Irrigation and Drainage (DID), Malaysia standard value of 150 mm is applied. For standing water depth, 100 mm is used for the pre-saturation period. Percolation values were obtained from operation and maintenance manuals collected from the DID local office.

Crop evapotranspiration (ET_c) is a key factor to determine a proper irrigation schedule and to improve water use efficiency in irrigated agriculture. ET_c can be estimated by a reference crop evapotranspiration (ET_o) and crop coefficient (Doorenbos and Pruitt 1977; Kang 1986; Kang *et al.* 1992 and Kerr *et al.* 1993). ET_o can be estimated by many methods (Jensen 1974; Hill *et al.* 1985 and Kang *et al.* 1994). These methods range from the complex energy balance equations (Allen *et al.* 1989) to simpler equations that require limited meteorological data (Hargreaves and Samani 1985). According to Smith *et al.* (1992), the Penman-Monteith (Monteith 1965) method gives more consistently accurate ET_o estimates than other ET_o methods. Md Hazrat *et al.* (2000) also recommended this method after applying it the Muda Irrigation Scheme in northwest Malaysia. Therefore, reference evapotranspiration was estimated by using the Penman-Monteith equation as follows:

$$ET_o = \frac{0.408\Delta(R_n - G) + \gamma \frac{900}{T + 273} u_2 (e_s - e_a)}{\Delta + \gamma(1 + 0.3u_2)} \quad (5)$$

where ET_o is reference crop evapotranspiration (mm/day), R_n is net radiation at the crop surface (MJ/m²/day), G is soil heat flux density (MJ/m²/day), T is air temperature at 2 m height (°C), u_2 is wind speed at 2 m height (m/s), e_s is mean saturation vapour pressure of the air [kPa], e_a is mean actual vapour pressure of the air (kPa), $(e_s - e_a)$ is saturation vapour pressure deficit (kPa), Δ is slope vapour pressure curve (k Pa °C⁻¹), γ is psychrometric constant (k Pa °C⁻¹) and 900 is conversion factor. The data of temperature, relative humidity, wind speed and sunshine hours were used for estimating reference evapo-transpiration. The crop water requirement was then determined from the product of the reference evapotranspiration and the respective crop coefficient. The crop coefficient K_c values given in published sources for the study area were used (Chan and Cheong 2001). The weather data such as temperature, relative

humidity, wind speed and sunshine hours of the study area were also collected for a period of 16 years, i.e. 1985-2000. The recent 40 years daily rainfall data (from 3 rainfall stations in the scheme) used in this study was obtained from the Central Data Information Section, Hydrological Branch, Department of Irrigation and Drainage (DID) Malaysia Headquarters in Kuala Lumpur. Water delivery information was obtained during a field survey.

Canal Flow Simulation

Data required for the canal simulations were canal bed width, side slope, canal length, gate structure and specification, water depth, canal cross-section, elevations, Manning's n and seepage rate. *CanalMan* input parameters include those data to be supplied to the *CanalMan* database files in order to run the model. These data were obtained from the Map Unit, DID Headquarters Malaysia in Kuala Lumpur. Canal simulation was performed for the pre-saturation and normal irrigation supply periods. Different flow rates for the Besut and Angga Barrages were used in the canal simulation process because flow rates change during the main season and off-season. The full supply discharges are $9.00 \text{ m}^3/\text{s}$ and $3.00 \text{ m}^3/\text{s}$ for the Besut and Angga Barrage respectively. Thus, canal simulation was started with full supply capacity and then with a step-by-step decreased flow capacity approach for the Besut and Angga Barrages. In each simulation process, simulated flow values were compared to design canal flow values (main and secondary canals) to obtain the water distribution area. Tertiary canal gates were adjusted with estimated field water requirements. Moreover, canal gate openings were adjusted whenever the simulation flow rate was higher than the demand. Finally, all simulation results were analyzed and possible water distribution area identified for pre-saturation period in phases and also repeated for the irrigation supply period for the whole scheme.

Canal Filling Time

The canals in the irrigation system must be filled in the order of first, the main, then the secondary and finally the tertiary canal. The canals were filled from downstream to upstream. When the last reach is full, the control drop or check at the head of the reach is set according to the design full supply level (FSL). All the secondary offtake gates were closed during the time of filling the main canals. When the main canal is filled to FSL, all tertiary offtakes and all direct field offtakes along the secondary canals are closed before filling secondary canals. Therefore, the model estimated the filling time of the main and secondary canals during the pre-saturation period. Tertiary canals filling time was not estimated due to small canal length. However, lag time was also estimated during normal supply period in order to make decisions on in-time water release from the barrages.

RESULTS AND DISCUSSION

Water Demand

A huge quantity of information is available and is needed for management decisions. Land preparation consists of soaking, ploughing and puddling of the soil. The study revealed that 250 mm water is needed for land preparation in both the main season and off-season. The mean monthly general weather conditions and water requirements for each month of the year are shown in Fig. 2. The average evapotranspiration was found to be 4.20 mm/day and 3.99 mm/day for off-season and main season crop respectively. Crop water requirements were higher during off-season crop compared to the main season crop, mainly as a result of prevailing weather conditions. The average seasonal consumptive use of water for rice cultivation was 795 mm, out of which 572 mm (72%) was accounted for ET and 223 mm (28%) for percolation. On the other hand, the average seasonal water supply was 1045 mm of which 732 mm (70%) was supplied by irrigation and 313 mm (30%) by rainfall. The water requirement was especially high for pre-saturation compared to supplementary supply in the main and off-season.

Water Allocation and Distribution

For the the period considered for canal simulation, in the first two weeks, the requirement comprises only the water requirement for land preparation. During this period, various flow rates for the Besut and Angga Barrages were used in the canal simulation process. The simulation results, when compared to the canal design capacity were satisfactory. Table 1 shows a canal simulation

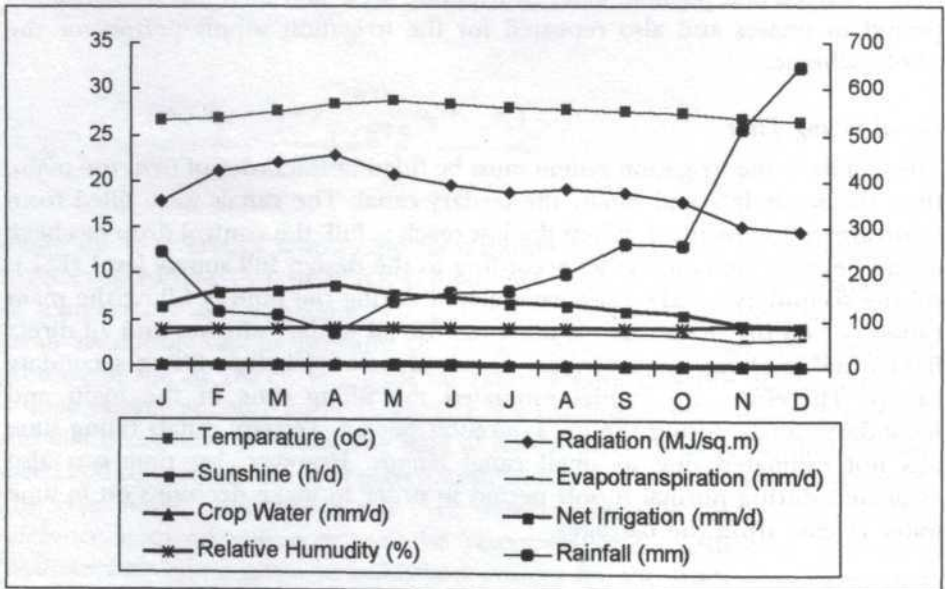


Fig. 2: General mean monthly weather conditions and crop water for the study area

TABLE 1
Example showing canal simulation results in the pre-saturation period during the main season and off-season

Compartment & Canal Name	Design Q_p	Simulated Q_p	Canal Name	Design Q_p	Simulated Q_p
	(l/s)	(l/s)		(l/s)	(l/s)
Besut Barrage (Compartment 1, 3, 4) Barrage Flow Rate = 9.00 m ³ /s					
Comp - 1					
Lubuk Kawah	1075	1080	Lubuk Agu	456	457
FC1/CD	80	80	FC2/CD	80	81
FC1/DE	41	40	FC2/DE	55	56
FC3/DE	80	80	Gong Lawan	46	48
FC4/DE	60	62	Telaga Nibong	1464	1467
Tok Nga	94	94	Kayu Kelat	133	134
Gong Kulim	205	206	Kubang Depu	256	256
Pulau Ribu	254	255	Tok Bugis	124	125
Chenerong	96	97	Gong Rengas	126	126
Comp - 3					
NN1	275	277	NOa	177	178
FC1/NO	155	155	OO1	567	570
PP1	572	571	QQ1	415	416
QQ2	944	945	Q2a	262	260
Q2b	286	285	Q2c	396	396
Comp - 4					
Apal	118	119	FC1/FG	262	262
M1a	264	266	M1b	213	215
HH1	168	170	II1	525	528
IJ	719	719	JK	455	456
KK1	107	110	KL	152	150
LL1	64	66			
Angga Barrage (Compartment 2) Barrage Flow Rate = 3.00 m ³ /s					
Comp - 2					
Padang Baloh	756	760	Melintang	86	86
Awek	555	555	RR1	80	81
FC1/RS	32	33	FC2/RS	56	55
SS1	227	230	ST	750	752

for the case of 9.00 m³/s and 3.00 m³/s for the Besut and Angga Barrage respectively. This serves as a check on the design values that were computed much earlier by designers of the scheme.

During the land preparation period, it was found that the total scheme area could not be inundated continuously in a single operation unless flow rates are at least $9.00 \text{ m}^3/\text{s}$ and $3.00 \text{ m}^3/\text{s}$ for Besut and Angga Barrage respectively. It was also noted that if flow rates fall below these values then pre-saturation should be done in two phases. Accordingly, the areas recommended for receiving water are identified and are presented in Table 2. The Phase I area is supplied first for pre-saturation time of 14 days at 2.10 l/s/ha . After 14 days, the same rate is supplied to the Phase II area. But if flow rate is between 5.00 and $5.50 \text{ m}^3/\text{s}$ in Besut Barrage, then pre-saturation should be done in three phases. In this case, each phase is supplied for pre-saturation time of 21 days at 1.38 l/s/ha . However, when the flow rate falls below $5.00 \text{ m}^3/\text{s}$ and $1.50 \text{ m}^3/\text{s}$ for Besut and Angga Barrage respectively, then pre-saturation inundation should be supplemented using recycling pumps. In this case, the drains would be utilized as supplementary sources of water, and pumped up to irrigation canals by six (6) recycling pumps. No study on the pumping requirements was carried out in this study.

After pre-saturation, from the fifth week onwards, the irrigation water supply period commences for the next 100 days. During the normal growth period, continuous supplementary irrigation is required to sustain losses due to seepage and percolation as well as evapotranspiration. The standing depth of water in each block is maintained at 100 mm and this depth is necessary for direct seeding rice. During this normal irrigation supply period, $6.00 \text{ m}^3/\text{s}$ and $1.75 \text{ m}^3/\text{s}$ flow rate for Besut and Angga Barrage respectively must be maintained throughout the entire period. Should available flows fall below the expected values stated above, then the simulation process must be repeated to identify optimal areas for irrigation and also areas where it may be best to leave alone in view of inadequate flows available.

Gate Operation and Water Release

Since available irrigation water in the scheme is quite limited, proper operation of diversion gates as well as even timely water distribution is essential for water saving. The study reveals that the farmers in the lower reaches (Compartment 3) get much less water per unit area than the farmers in the upper reaches (Compartment 1) resulting in an inequitable distribution of water. It has also been observed that few gates supply excess amount of water into the canals, which cause overflow into the fields. For proper functioning of the gates in controlling water, the gates must be opened adequately. This has led to the development of gate openings schedule for pre-saturation period and is presented in Table 3. On the other hand, the time lag of water traveling in the system is an important factor that determines the losses of irrigation water in the system itself. Thus, the model was used to calculate the required time in filling the main and secondary canals during the pre-saturation period. The average time for filling canals are summarized in Table 4. The details pertaining to each canal, though computed, are not reported in this table due to limitation of space. It has been observed that when flow rates are $7.20 - 9.00 \text{ m}^3/\text{s}$ and 1.70

TABLE 2
Water distribution area during pre-saturation and normal irrigation supply periods derived from water demand and water availability

Intake Gate Flow	Irrigable Area (KPA* Unit)		
(m ³ /s)	Pre-saturation Period – Besut Barrage (Compartment 1, 3, 4)		
	Phase - I	Phase - II	
> = 9.00	C - 1 (KPA - All); C - 3 (KPA - All); C - 4 (KPA - All)		
8.20 - 8.80	C - 1 (KPA - All); C - 3 (KPA - 26 - 31);	C - 4 (KPA - All); C - 3 (KPA - 22 - 25);	
7.20 - 8.00	C - 1 (KPA - All); C - 3 (KPA - 22 - 25);	C - 4 (KPA - 11 - 20); C - 4 (KPA - 21); C - 3 (KPA - 26 - 31);	
6.20 - 7.00	C - 1 (KPA - All); C - 4 (KPA - All);	C - 3 (KPA - All);	
5.70 - 6.00	C - 4 (KPA - All); C - 3 (KPA - 22 - 25);	C - 1 (KPA - All); C - 3 (KPA - 26 - 31);	
	Phase - I	Phase - II	Phase - III
5.00 - 5.50	C - 4 (KPA - 11- 20); C - 3 (KPA - 22 - 23);	C - 1 (KPA - All)	C - 4 (KPA - 21); C - 3 (KPA - 24 - 31);
< 5.00	Start recycling pumps for irrigation		
	Pre-saturation Period – Angga Barrage (Compartment 2)		
> = 3.00	C - 2 (KPA - All);		
2.20 - 2.80	C - 2 (KPA - 32 - 35);	C - 2 (KPA - 36 - 39);	
1.70 - 2.00	C - 2 (KPA - 32, 33, 35);	C - 2 (KPA - 36 - 39);	
< = 1.50	Start recycling pumps for irrigation		
	Irrigation Period – Besut Barrage (Compartment 1, 3, 4)		
6.00	C - 1 (KPA - All); C - 4 (KPA- All); C - 3 (KPA - All);		
	Irrigation Period - Angga Barrage (Compartment 2)		
1.75	C - 2 (KPA - All);		

*KPA- Kumpulan Pengguna Air (local Name; i.e. irrigation water user's group)
All denotes all KPA units, C denotes compartment, KPA- 22 - 25 denotes from unit KPA 22 to unit KPA 25 etc.

- 3.00 m³/s at the Besut and Angga Barrages respectively, then the starting date of water supply for the season should be two days before the beginning of the pre-saturation date in order to maintain irrigation scheduling in time. But water should be released three days before beginning of the pre-saturation period of season when flow rates are between 5.00 and 7.00 m³/s at the Besut

TABLE 3
Gate opening schedules in pre-saturation period

Barrage Flow (m ³ /s)	Canal Name		Gate Opening (%)		Canal Name		Gate Opening (%)	
	Existing	Suggested	Existing	Suggested	Existing	Suggested	Existing	Suggested
Besut Barrage (Compartment 1, 3, 4)								
>= 9.00	TLK	100	80	L. Agu	100	80		
	FC1/CD	100	70	FC3/DE	100	70		
	T.Nibong	100	75	FC4/TG	100	70		
	FC2/TLA	100	75	Tok Nga	100	70		
	Kayu Kelat	100	70	G. Kulim	100	80		
	K. Depu	100	75	P. Ribu	100	75		
	Tok Bugis	100	50	Chenrong	100	70		
	G. Rengas	100	70	Apal	100	70		
	FC1/FG	100	50	FC1/TG	100	70		
	FC1/GM	100	70	FC2/GM	100	70		
	HH1	100	70	III	100	70		
	FC1/MN	100	50	NOa	100	70		
	FC1/NO	100	70	FC3/PP1	100	75		
	FC1/QQ1	100	70	FC2/QQ1	100	70		
	Q2a	100	60					
8.2 - 8.80	TLK	100	80	L. Agu	100	80		
	T.Nibong	100	75	FC2/TLA	100	75		
	Tok Nga	100	70	Kayu Kelat	100	70		
	G. Kulim	100	80	K. Depu	100	75		
	P. Ribu	100	75	Tok Bugis	100	50		
	Chenrong	100	70	Apal	100	70		
	FC1/FG	100	50	FC1/GM	100	70		
	FC2/GM	100	70	HH1	100	70		
	III	100	70	FC1/MN	100	50		
	NOa	100	70	FC1/NO	100	70		
7.0 - 8.00	L. Agu	100	80	T.Nibong	100	75		
	Tok Nga	100	70	Kayu Kelat	100	70		
	G. Kulim	100	80	K. Depu	100	75		
	P. Ribu	100	75	Tok Bugis	100	50		
	Chenrong	100	70					
Angga Barrage (Compartment 2)								
3.00	TPB	100	75	Awek	100	70		
	FC1/Awek	100	50	FC2/RS	100	70		
	SS1	100	70					

TABLE 4
Average filling time in main and secondary canals during pre-saturation period

Barrage Name/ Flow (m ³ /s)	Compartment Name	Pre-saturation Period	
		Main Canals	Secondary Canals
Besut Barrage 9.00	Comp- 1	15.00	24.00
	Comp- 4	21.00	35.00
	Comp- 3	24.00	40.00
Angga 3.00	Comp- 2	17.00	24.00
Besut Barrage 8.20 - 8.80	Comp- 1	16.00	26.00
	Comp- 4	22.50	40.00
	Comp- 3	26.00	42.00
Angga 2.20 - 2.80	Comp- 2	19.00	26.00
Besut Barrage 7.20 - 8.00	Comp- 1	17.50	28.00
	Comp- 4	25.00	44.50
	Comp- 3	27.00	46.00
Angga 1.70 - 2.00	Comp- 2	22.00	29.00
Besut Barrage 6.20 - 7.00	Comp- 1	19.00	31.00
	Comp- 4	27.00	48.50
	Comp- 3	30.00	51.00
Besut Barrage 5.70 - 6.00	Comp- 1	21.50	33.50
	Comp- 4	30.00	50.00
	Comp- 3	32.00	53.50
Besut Barrage 5.00 - 5.50	Comp- 1	23.00	33.50
	Comp- 4	31.00	50.00
	Comp- 3	33.00	55.00

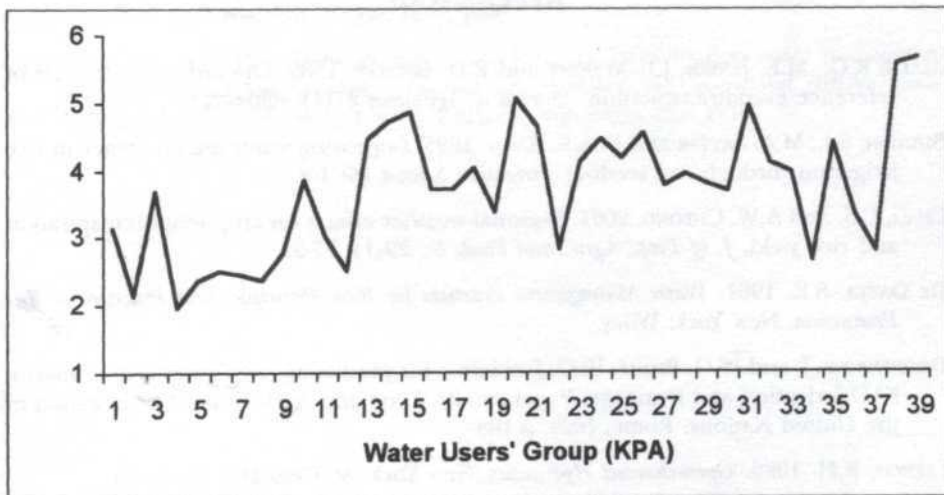


Fig. 3: Water travel time in irrigation blocks during normal supply period

Barrage. The time of arrival of water in irrigation blocks (KPA) from the Besut and Angga barrages during normal supply period are shown in *Fig. 3*. During the normal supply period, water should be released 5.00 hours before flow rates are 5.00 – 6.00 m³/s and 1.75 – 2.00 m³/s at the Besut and Angga Barrages respectively. In order to save water, irrigation supply should be reduced if there is rainfall. However, the amount to be reduced must be determined based on rainfall and canal discharge. This can be done through reducing the flow at the intake gate and adjustment of the orifice gate of secondary constant head.

CONCLUSIONS

Depending on water availability, land preparation can be done in one continuous stretch for all the compartments or over different phases as suggested by the simulation. During the irrigation period, should water resources in the river system be deemed inadequate, then the hydraulic simulation can be pursued, to identify the units and compartments that are best irrigated given that not all units can be supplied in view of the circumstances. The gate at each canal is constructed to permit the water flow to serve the unit adequately and equally among the farmers. Thus, gate operation must be managed properly. Time required in filling canals during pre-saturation are important for making decisions on water release from barrages. The canal simulation results therefore can have major implications in relation to future management programs directed toward more decision-making and water efficient rice culture. The use of *CanalMan* model to simulate irrigation canals as a means of improving in-time water management in rice double cropping systems through proper gate settings and establishing the extent of choice irrigated areas is therefore recommended.

REFERENCES

- ALLEN, R.G., M.E. JENSEN, J.L. WRIGHT and R.D. BURMAN. 1989. Operational estimates of reference evapotranspiration. *Journal of Agronomy* **81**(4): 650-662.
- BHUIYAN, S.I., M.A. SATTAR and M.A.K. KHAN. 1995. Improving water use efficiency in rice irrigation through wet seeding. *Irrigation Science* **16**: 1-8.
- CHAN, C.S. and A.W. CHEONG. 2001. Seasonal weather effects on crop evapotranspiration and rice yield. *J. of Trop. Agric. and Food. Sc.* **29**(1): 77-92.
- DE DATTA, S.K. 1981. *Water Management Practices for Rice. Principles and Practices of Rice Production*. New York: Wiley.
- DOORENBOSE, J. and W.O. PRUITT. 1977. Guideline for predicting crop water requirements. FAO Irrigation and Drainage, Paper no. 24. Food and Agricultural Organization of the United Nations, Rome, Italy, p.193
- FRENCH, R.H. 1985. *Open-channel Hydraulics*. New York: McGraw-Hill Book Co.
- HARGREAVES, G.H. and Z.A. SAMANI. 1985. Reference crop evapotranspiration from temperature. *Trans. ASAE* **1**(2): 96-99.

- HILL, R.W., R.J. HANKS and J.L. WRIGHT. 1985. Crop yield models adapted to irrigation scheduling. Utah Agriculture Experimental Station Report no. 99. Utah State University, Logan, Utah, p.198.
- JENSEN, M.E. 1974. *Consumptive Use of Water and Irrigation Water Requirements*. New York: Irrig. Drain. Am. Soc. Civil. Eng.
- JICA. 1998. The study on modernization of irrigation water management system in the granary area of Peninsular Malaysia. Draft Final Report, Volume –II March, Annexes.
- KANG, S.Z. 1986. Calculation and prediction of actual winter wheat evapotranspiration in condition of soil water deficit. *Acta Univ. Agric. Boreali-Occidentalis* **14**(1): 93-102.
- KANG, S.Z., Z.Z. HE and X. ZHANG. 1992. *Crop Water Requirement and Irrigation Models in Shaanxi Province*. Chinese Hydraulic and Hydro-Power Press, Beijing, p. 299.
- KANG, S.Z., X.M. LIU and Y.Z. XIONG. 1994. *Theory of Water Transport in Soil-Plant-Atmosphere Continuum and its Application*. p.228. Beijing: Chinese Hydraulic and Hydro-Power Press.
- KERR, G., L. POCHOP, K.J. FORNSTROM, J.M. KRALL and D. BROWN. 1993. Soil water and ET estimates for a wide range of rainfed and irrigated conditions. *Agric. Water Management* **24**: 147-159.
- MD. HAZRAT ALI, T.S. LEE, C.Y. KWOK and A.F. ELOUBAIDY. 2000. Modelling evaporation and evapotranspiration under temperature change in Malaysia. *Pertanika J. of Sci. and Technol.* **8**(2): 191-204.
- MERKLEY GARY, P. 1995. CanalMan (Version 5.30): *A Hydraulic Simulation Model for Unsteady Flow in Branching Canal Networks*. Utah State University, USA.
- MONTEITH, J.L. 1965. Evaporation and the environment. *Symp. Soc. Expt. Biol.*, **19**: 205-234.
- SMITH, M., R. ALLEN, J.L. MONTEITH, A. PERRIER, L. SANTOS PEREIRA and A. SAGEREN. 1992. Expert consultation on revision of FAO methodologies for crop water requirements. Food and Agricultural Organization of the United Nations, Land and Water Development Division, Rome, Italy, p.60.
- TEH, S.K. and M.Z. MAT. 1999. Promotion of Farmers' participation water management in Besut Irrigation Scheme, Malaysia. In *Workshop on Government Actions towards Effective Irrigators' Organizations*, 1-6 March, Vientiane, Lao PDR.

Enhancing Design for Aesthetics Based on Product Platform Architecture

Ahmad Baharuddin Abdullah & Zaidi Mohd Ripin
*School of Mechanical Engineering, Universiti Sains Malaysia
Engineering Campus, 14300, SPS, Pulau Pinang, Malaysia
E-mail: mebaha@eng.usm.my*

Received: 13 November 2003

ABSTRAK

Secara tradisional, kebanyakan orang membeli sesuatu produk berdasarkan prestasi dan kos produk tersebut, akan tetapi kebelakangan ini, keselesaan dan ciri estetika lebih disukai. Pengguna kini semakin kompleks dan mengkehendaki produk yang bukan sahaja dari segi prestasinya, tetapi juga penampilannya. Untuk meningkatkan penampilan, pendekatan platform produk dicadangkan sebagai satu pendekatan baru dalam rekabentuk untuk estetika. Dalam kajian ini, platform dikenalpasti berdasarkan perkongsian komponen di kalangan variasi produk. Kemudian garis panduan estetika digunakan pada platform. Indeks Estetika Keluarga Produk (PFAI) dibangunkan untuk mengukur prestasi produk. Penilaian adalah berdasarkan kesepunyaan komponen dan aspek estetika. Keputusan menunjukkan Indeks Estetika Keluarga Produk telah meningkat melalui rekabentuk semula beberapa komponen produk tersebut. Satu kajian kes mengenai keluarga kipas rumah telah dijalankan untuk membuktikan metodologi yang telah dibangunkan.

ABSTRACT

Traditionally, most people buy a product based on performance and cost, but recently appearances, comfort and aesthetic are preferred. Customers are now becoming more complex and require not only good product performance but also appearance. To enhance product appearance, product platform has been proposed as new approach to the design for aesthetics. In this work, a platform is identified based on component sharing among the product variants. Then the aesthetic rules are applied to the platform. A Product Family Aesthetic Index (PFAI) was developed to measure the product performance. The evaluation is based on component commonality and aesthetic aspect. The result indicates that the Product Family Aesthetic Index had increased through redesigning several components in the product. A case study of the fan family was conducted to verify the methodology.

Keywords: Product platform, design for aesthetics, commonality, redesign

INTRODUCTION

Traditionally, most people buy a product based on performance and cost, but recently appearances, comfort and aesthetic appreciation are preferred. Aesthetic can be defined as a simultaneous communication of meaning and beauty, which can be principally interpreted as shape, while at the same time colour, texture, material and other visual properties are also important (Tovey 1992). Design for aesthetics will be the focus of research and development in the

future due to their role in enhancing product acceptance. Design for aesthetics was to be related to other aspects including ergonomics, manufacturability and suitability in the product development at different levels of dominance. Design for aesthetic is currently more popular in automotive industry as shown in *Fig. 1* but there is a tendency of application in industrial design and engineering (Tovey 1997).



Fig. 1: Evolution of Volkswagen passenger car with aesthetic design from early edition till the latest version (Brenner 1999)

There are three product characteristics that have interaction with design for aesthetics which are shape, geometry and form. Three parameters that influence the aesthetic design of a product are shape, composition and physical attributes (Chen and Owen 1997). Shape is defined as the totality of local characteristics of the geometry, while composition expressed shape features arrangement. Similarly, the physical attributes such as colour, texture, lighting conditions or material properties also influence the aesthetic characteristics. Geometry has no further contribution but only support the aesthetic shape mapping the design process. Whereas form typically can express the aesthetic characteristics more. This interaction can be illustrated in *Fig. 2*.

Product platform can be formulated as a general optimization problem in which the advantages of designing a common base must be balanced against the constraints of the individual product variants and of the whole family. Gonzales-Zugasti and Otto (2000) define product platform as a set of shared functionality across multiple products from similar or different families. Platform architecture can further be described as a set of selection and configuration choices shared among products (Gonzales-Zugasti *et al.* 2000). This can be viewed through components or part similarity from physical attributes, shape and composition to the developed platform.

The advantages of product platform are that using proven modules that are known to operate effectively at their designated sub-tasks can minimize design risk. Other than that, re-use of previously designed modules can bring savings at least in parts cost of redeveloping those sub-systems (Martin and Ishii 2000). The concept of product platforms and aesthetic aspect has been successfully applied in automotive part design consumer and industrial product recently. For example, Sony used three platforms to support hundreds of different personal portable stereo products in its Walkman family. Volkswagen and their

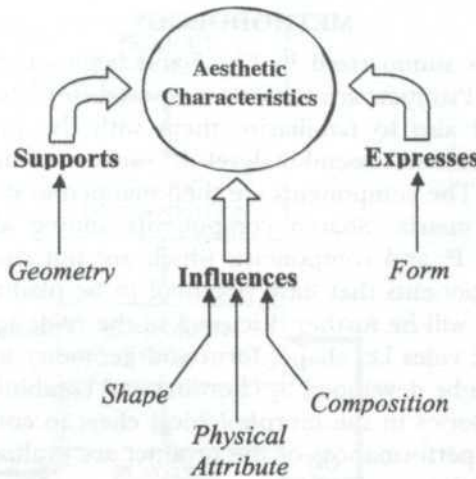


Fig. 2: Product characteristics and the interaction with the aesthetic characteristics

partners in producing new technology of passenger car also used product platform (Brenmer 1999).

The contribution of this work is the presentation of new methodology to increase part commonality and aesthetic value of the product based on product platform. This methodology can be beneficial to the manufacturers and industries that are involved in product design and development. The paper discusses the background of the research, the definition and advantages of design for aesthetic and product platform. It is then followed by related research on the topic. The approach taken is discussed in detail and to implement the approach, a case study was carried out.

RELATED WORK

The methodology and research on product platform development is not new and a number of products have been applied to this technology. Sudjianto and Otto (2001) had developed a product platform from multiple brand products using brand architecting rules. Gonzales-Zugasti *et al.* (2000) used models of several spacecraft to identify possible subsystem that could be made common to all or specific requirements of the missions. Similarly Ripin and Abdullah (2001) developed a methodology to develop modular Unmanned Aerial Vehicle (UAV) based on the multi-mission requirements optimization. One of the objectives of product commonality is to increase product variety and research in the area has shown successful applications (Martin and Ishii, 2000). Research on aesthetic product design is moving towards computer-based design for aesthetic and claimed as one of the areas that will be highlighted in the future (Wallace and Jakiela, 1993; Takala and Woodward, 1988; Hsiau and Chen, 1997 and Knoop *et al.* 1998). But none of the research has taken into consideration the aesthetic aspect together with product platform.

METHODOLOGY

The methodology is summarized in *Fig. 3* and begins with a list of product variants or models. Products are then decomposed to identify all components in the systems and also to familiarize them with the interactions between components. Component assembly level is used to illustrate the product assembly hierarchy. The components are then mapped in the matrix, named as component-variant matrix. Shared components among all the variants are labeled as platform P, and components which are not shared are labeled as accessories A. Components that have potential to be platformed is labeled by an asterisks (*) and will be further discussed in the re-design stage. The introduction of aesthetic rules i.e. shape, form and geometry to the platform and product variants can be developed by choosing and combining the appropriate platform and accessories in the morphological chart to complete the product system. Finally, the performances of the product are evaluated based on commonality and aesthetics.

Analytically, the number of designed models can be determined from the relationship between the number of design and the total number of components (i.e. platform and accessories). The number of models may be infinite for complex system or product which has high number of platform and accessories. Other factors such as performance, reliability, manufacturing and functionality should be considered also before the product can be produced. As shown in *Fig. 4*, a system or products which have n number of platform and accessories and by assuming that the number of design for each platform and accessories are the same, the number of models can be determined as follows;

$$\text{Number of model, } M_n = N_t^D \quad (1)$$

Where N_t is total number of components in the product and D is number of design options.

But in application, the number of design for each platform and accessory are different and depend on the creativity of the designer to initiate new and innovative design. The combination of platform and accessories to form a complete system or product are also different. Thus the number of models cannot be determined quantitatively. Besides that, the contribution of accessories and platform in increase model is different, where accessories are only for certain variants, while platform can affect the whole variant.

The performance of the product and variant can be determined from commonality and aesthetic point of view. Product efficacy, E_i of certain variant can be calculated from the ratio of number of components that are shared with other variants and total number of components from all of the variants as shown in Equation 2, where weightage of 1 and 0 are used to represent best and poor commonality.

$$\text{Efficacy, } E_i = \frac{N_s}{N_t} \quad (2)$$

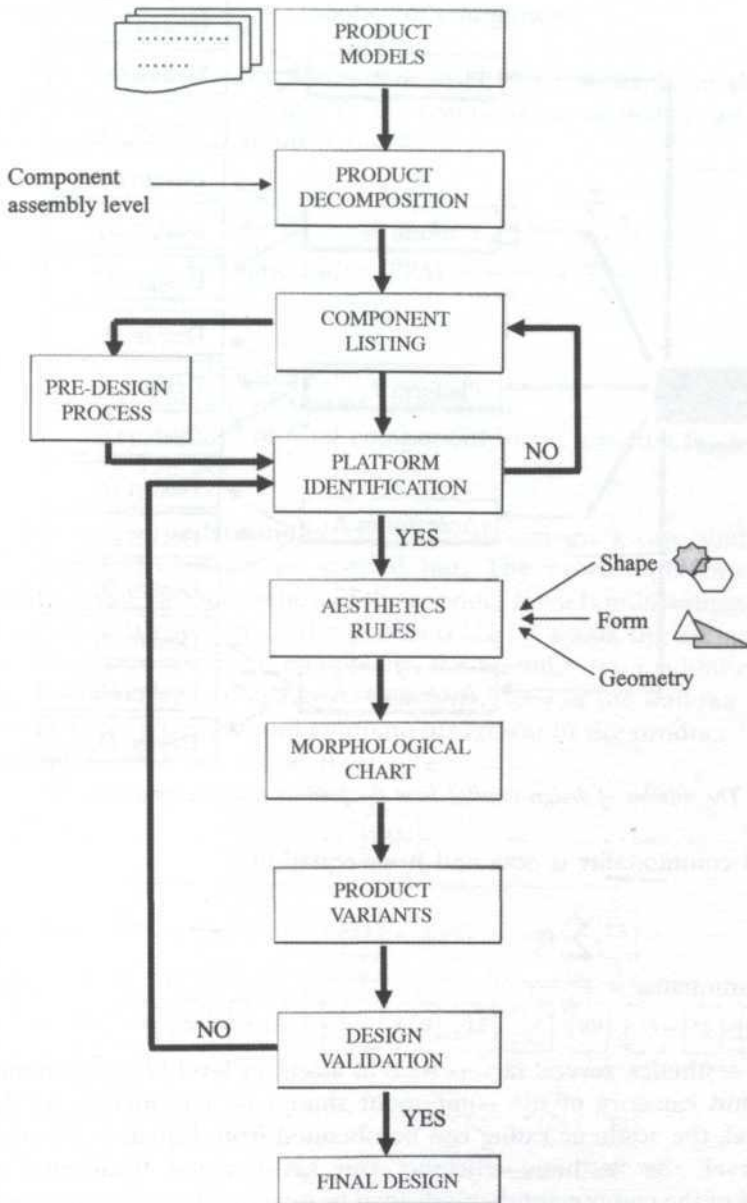


Fig. 3: Platform development process flow chart

$E_i = 1$ (best commonality), $E_i = 0$ (poor commonality)

Note that, $i = 1, 2, \dots, n$ (number of variant)

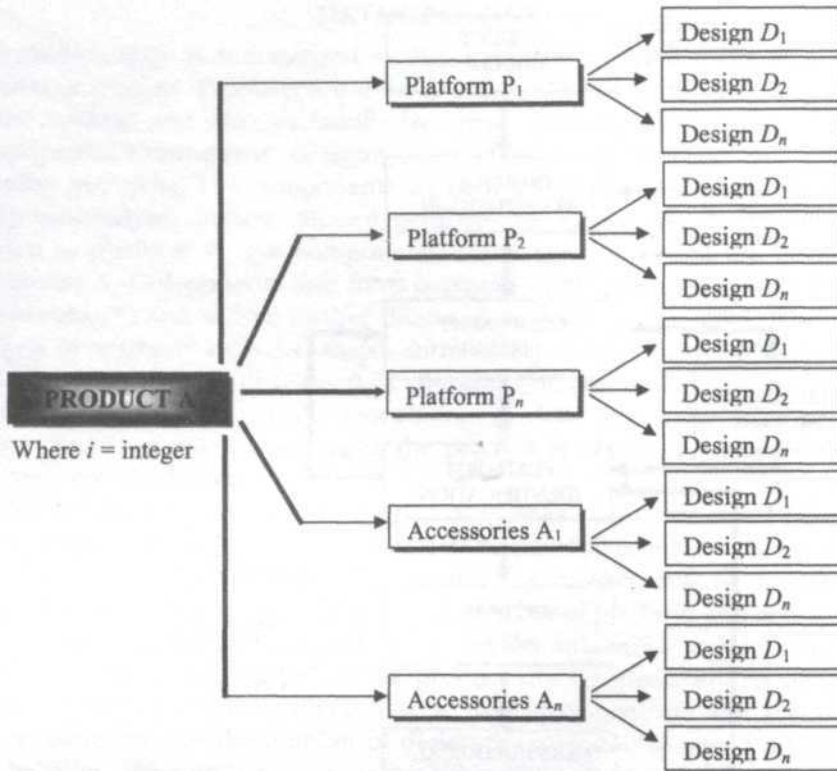


Fig. 4: The number of design resulted from the product platform approach

So the product commonality is obtained from equation 3.

$$\text{Degree of Commonality} = \frac{\sum_{i=1}^n E_i}{N_v} \quad (3)$$

In terms of aesthetics, several factors such as assembly level of components, attractiveness and category of the component should be considered. At the component level, the aesthetic rating can be obtained from Equation 4 and at the product level, the aesthetic efficiency can be obtained from total of aesthetic ratings of the component that is divided by total number of components in the variants as expressed in Equation 5.

$$\text{Aesthetic Rating, } C_R = A_j \times 100 \quad (4)$$

$$\text{Aesthetic Efficiency, } \xi_A = \frac{\sum_{j=1}^m A_j}{N_t} \quad (5)$$

Note that, $j = 1, 2, \dots, m$ (number of component)

The Product Family Aesthetic Index (PFAI) depends on the commonality and aesthetic characteristics of the components, so that it can be determined by summing up Equations 3 and 5.

$$\text{Product Family Aesthetic Index, PFAI} = \frac{\sum_{i=1}^n E_i}{N_v} + \frac{\sum_{j=1}^m A_j}{N_t} \quad (6)$$

Where N_v = Number of variant
 N_s = Number of shared component
 N_t = Number of total component in the product family
 E_i = Efficacy

For better understanding of the methodology, a case study of the home appliances fan family was carried out. The process platform identification begins by the decomposition of the product models to investigate and study the physical configuration of the products. Fig. 5 shows the components at each assembly level. To avoid complexity, the assembly level is limited to four only. Fig. 6 schematically illustrates an exploded view of the wall fan to visualize the product configuration and components consist in the product. The motor and oscillation knob are not in the figure.

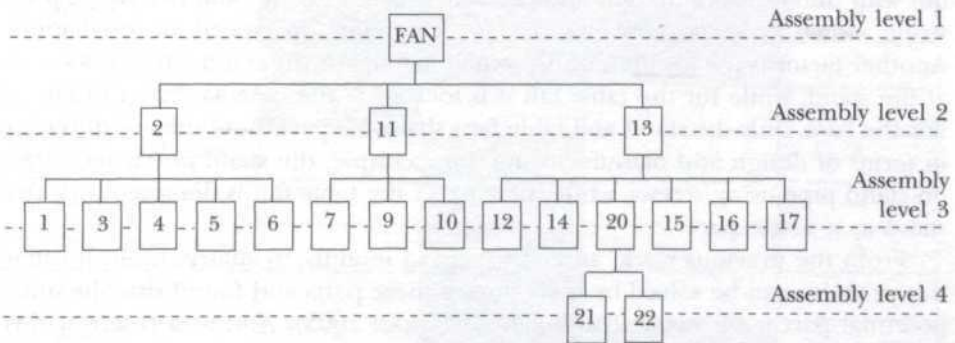


Fig. 5: Components assembly level

For the fan family, there are three variants, i.e. table, wall and stand fan. The wall fan consists of 14 components, 20 components for stand fan and 17 components for table fan as listed in Table 1. The final row indicated category of components either platform (P) or accessories (A). The shaded blocks depict the shared components among the variants. There are three components which cannot be specified either as platform or accessories represented by the asterisks (*) i.e. stand, base and switch panel which will be discussed later.

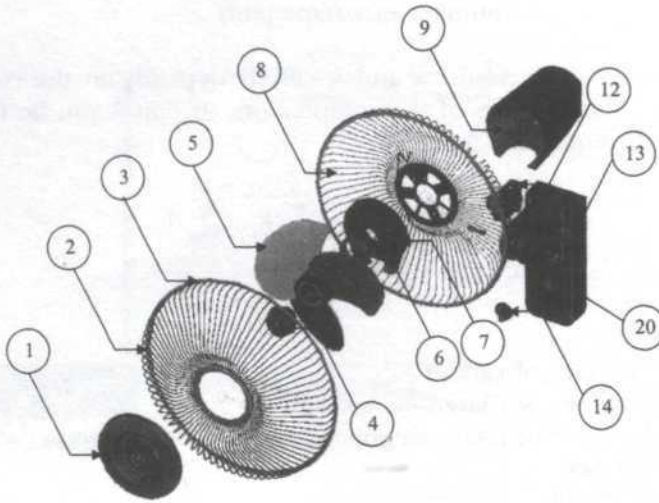


Fig. 6: Exploded view of wall fan

At the re-design stage, several factors and parameters should be taken into consideration such as components configuration, interaction and the constraint. For example, the stand and switch panel in some of the cases share the same functions but are physically different. The stand design for table and wall fan mounted on the base, while for stand fan it is designed as a single part as shown in Fig. 7. Similarly the switch panel design, for stand and table fan, are the same but with different orientation and the switch panel for the wall fan uses a pull-string switch type as a mechanism for changing the speed or oscillation. Another factor is the location of the switch panel. For the stand fan, it is located at the stand, while for the table fan it is located at the base as shown in Fig. 7. For the base, only the stand and table fans share the part. But both are different in terms of design and manufacturing, for example, the stand fan, is mounted on stand pipe using screws, while the base of the table fan is designed with the stand as a single part.

From the previous work, an analysis using modularity matrix indicates that this problem can be solved by re-designing these parts and found that the most potential part is the stand (Abdullah and Ripin 2003). And as a result of this method, two more platforms can be identified. The total number of platform becomes 13 and accessories are reduced to only 9 components. The stand and base are now designed separately and the location of the switch panel is now mounted on the stand for standardization as is shown in Fig. 8, to allow more space for component sharing.

The aesthetic rules can now be applied to the identified platforms. The components, either platforms or accessories have different degrees of attractiveness which can influence the overall appearance of the model. The spinner and guard lock nut which are covered by other components have a low degree of attractiveness compared to the grill or stand. A measure of effluence is introduced by giving

TABLE 1

Product-Components Matrix depicts the similar components shared by home appliance fan family variants. P, represents platform and A, represents accessories. Numbers in the bracket shows the total number of components in the product

Components Listing	Wall Fan (14)	Stand Fan (20)	Table Fan (17)	Category
1. Guard Mark				P
2. Front Guard				P
3. Guard Ring				P
4. Spinner				P
5. Fan Blade				P
6. Guard Lock Nut				P
7. Housing Cover				P
8. Rear Guard				P
9. Motor Housing				P
10. Oscillation Knob				A
11. Motor				P
12. Neck				P
13. Stand				*
14. Switch Panel				*
15. Pull String				A
16. Height Adjuster				A
17. Sliding Tube				A
18. Outer Pole Bowl				A
19. Stand Pipe				A
20. Base				*
21. Wheel				A
22. Base Cover				A

weightage of 1, 3 and 5 to represent low, medium and strong degree of attractiveness respectively. Then the morphological charts approach (Pahl and Beitz, 1996) can be used to pick and combine the design of components to create variants to proceed for production as shown in Fig. 9. The number of design depends on the designer's creativity and customer's demand.

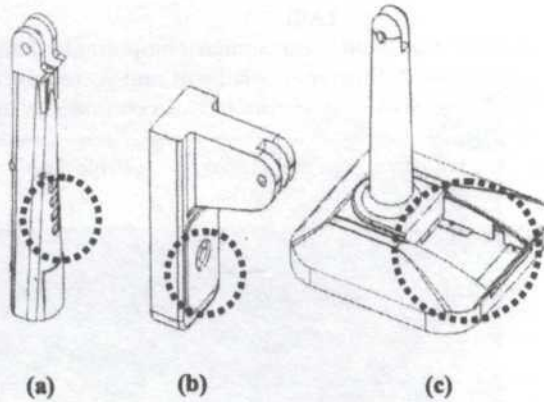


Fig. 7: Multi-design of stand for (a) stand, (b) wall and (c) table fan. Circle depicts the location of switch panel for respective variants

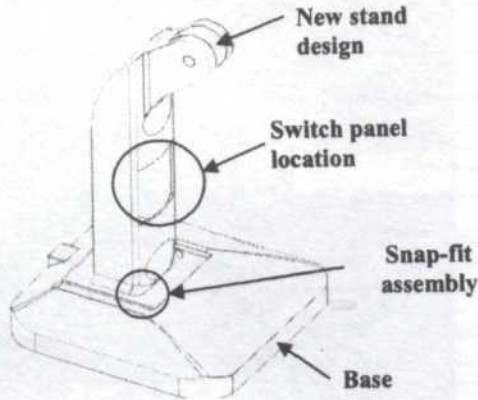


Fig. 8: New fan design of stand and base to enhance component sharing

The evaluation chart used to calculate the aesthetic rating of component and product level is shown in Appendix 1. A weightage is calculated by ratio of column_4 and column_5 and Aesthetic rating at the components level is get form ratio of column_6 and column_7 and at the product level can be get from total of components level aesthetic rating. The evaluation has been done before and after re-design and as a result there is an increase in degree of commonality aesthetic efficiency of the product. Low PFAI of about 11.5% is resulting from low aesthetic efficiency (4.5%). This is because most of the components in the product have a low degree of attractiveness. But the commonality of the product is quite high about 30% which indicates that there is wide possibility of upgrading the components and product appearance. The result is summarized in Table 2. After that, the result is compared to other approaches that developed by Kota *et al.* (2000) for the same case study and the result indicates similar patterns as shown in Table 3.

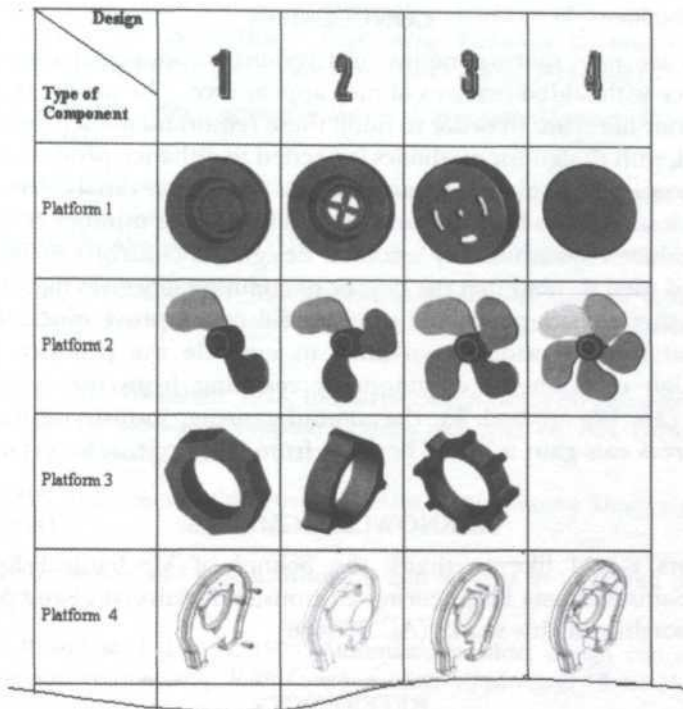


Fig. 9: A morphological chart of platform design

TABLE 2
Result from the methodology

	Before Re-design	After Re-design	Improvement
Efficacy	0.5	0.65	30.0%
Degree of Commonality	0.17	0.22	29.4%
Aesthetic Efficiency	44%	46%	4.5%
PFAI	0.61	0.68	11.5%

TABLE 3
Result for same case study by using Product Line Commonality Index (PCI) developed by Kota *et al.* (2000)

	Before Re-design	After Re-design	Improvement
Number of components, P	22	20	9%
MAX CCI, N	3	3	-
Sum (CCI)	43.028	42.139	2.1%
Sum (MinCCI)	8.943	7.833	14.2%
PCI	59.74%	65.76%	10.1%

CONCLUSION

Customers are now more complex and require products which are good in performance with added features of nice appearance. The products are recently having shorter life span. In order to fulfill these requirements, a product platform is proposed, with design for aesthetics is needed to enhance product appearance. A new approach that exploits product platform to increase variance by considering design for aesthetic has been presented. As a result, the number of variants that can be produced systematically under a designer's control can be increased. The method used showed that the degree of commonality gives higher weightage but the aesthetic efficiency of the product did not improve much. However, it showed that there is wide opportunity to upgrade the product appearance through high components commonality resulting from the re-design. This approach can be applied in the manufacturing industry effectively and manufacturers can gain a lot of benefits from this approach.

ACKNOWLEDGMENTS

The authors would like to thank the School of Mechanical Engineering, Universiti Sains Malaysia Engineering Campus and Universiti Sains Malaysia for their sponsorship of this work. (AC 073486)

REFERENCES

- ABDULLAH, A.B. and Z.M. RIPIN. 2003. Modularization To support product platform for redesign. In *Proceed. of 19th Int. Conf. on CAD/CAM, Robotics and Factories of the Future 2003*, I: 333-345.
- BRENNER, R. 1999. Cutting edge platform. *Financial Times: Automotive World*. p. 30-38.
- CHEN, K. and L. OWEN. 1997. From language and style description. *Design Studies* 18(3): 249-274.
- GONZALEZ-ZUGASTI, J. and K. OTTO. 2000. Modular platform-based product family design. In *2000 Design Engineering Technical Conference – Design automation Design*, ed. Renaud, J.E., Baltimore. MD. ASME: Paper no. DETC2000/DAC-14238.
- GONZALEZ-ZUGASTI, J., J. BAKER and K. OTTO. 2000. A method for architecting product platform with an application to interplanetary mission design. *Research in Engineering Design* 12: 61-72.
- HSIAU, S. W. and C. H. CHEN. 1997. A semantic and shape grammar-based approach for product design. *Design Studies* 18(3): 466-481.
- KNOOP, W. G, VAN BREEMEN J. J. ERNEST, I. HORVATH, VERGEEST, S. M. JORIS and B. PHAM. 1998. Towards computer supported design for aesthetics. In *Proceed. of 31st ISATA Conference*. 98M075.
- KOTA, S., K. SETHURAMAN and R. MILLER. 2000. A metric for evaluating design commonality in product families. *Journal of Mechanical Design* 122: 403-410.

- MARTIN M. and K. ISHII. 2000. Design for variety: Development of complexity indices and design charts. In *ASME Design Engineering Technical Conference – Design for Manufacturing*, Baltimore, MD. Paper No. DETC2000/DFM-14021.
- PAHL, G. and W. BEITZ. 1996. *Engineering Design: A Systematic Approach*. 2nd ed. New York: Springer-Verlag.
- RIPIN, Z.M. and A.B. ABDULLAH. 2001. A design study on modular platform of unmanned aerial vehicle. In *National Conf. on Aerodynamic and Related Topics*, ed. Z.M. Ripin, M. Z. Abdullah, R. Ahmad and Z. Hussain. p. 190-199. Pulau Pinang, Malaysia.
- SUDJIANTO, A. and K. OTTO. 2001. Modularization to support multiple brand platforms. In *ASME Design Engineering Technical Conference – Design for Manufacturing*. Pittsburgh PA.
- TARALA, T. and C. D. WOODWARD. 1988, Industrial design based on geometric intentions, In *Theoretical Foundations of Computer Graphics and CAD*, ed. B.A. Earnshaw, p. 953-963. NATO Asi Series, **F40**.
- TOVEY, M. 1992. Intuitive and Objective Processes in Automotive Design. *Design Studies* **13(1)**: 23-41.
- TOVEY, M. 1997. Styling and design: Intuition and analysis in industrial design. *Design Studies* **18(1)**: 5-32.
- WALLACE, D. R and M. J. JAKIELA. 1993. Automated product design concept: Unifying aesthetic and engineering. *IEEE Computer Graph Applications* **13**: 66-75.

APPENDIX 1

Evaluation chart of the case study before re-design

Components Number and Listing	Category	Degree of Attractiveness C_4	Component Assembly Level C_5	Weightage =	Number of Variant C_7	Aesthetic Rating, A_j
				$\frac{C-4}{C_5}$		$= \frac{C-6}{C_7}$
1. Guard Mark	P	5	3	1.67	3	0.556
2. Front Guard	P	5	2	2.50	3	0.833
3. Guard Ring	P	3	3	1.00	3	0.333
4. Spinner	P	3	3	1.00	3	0.333
5. Fan Blade	P	5	3	1.67	3	0.556
6. Guard Lock Nut	P	3	4	0.75	3	0.250
7. Housing Cover	P	3	4	0.75	3	0.250
8. Rear Guard	P	5	3	1.67	3	0.556
9. Motor Housing	P	5	2	2.50	3	0.833
10. Oscillation Knob	A	3	3	1.00	2	0.500
11. Motor	P	1	3	0.33	3	0.111
12. Neck	P	3	3	1.00	3	0.333
13. Stand	*	5	2	2.50	3	0.833
14. Switch Panel	*	5	3	1.67	3	0.556
15. Pull String	A	1	4	0.25	1	0.250
16. Height Adjuster	A	1	3	0.33	1	0.333
17. Sliding Tube	A	1	3	0.33	1	0.333
18. Outer Pole Bowl	A	1	3	0.33	1	0.333
19. Stand Pipe	A	1	3	0.33	1	0.333
20. Base	*	5	3	1.67	2	0.833
21. Wheel	A	1	4	0.25	1	0.250
22. Base Cover	A	1	4	0.25	1	0.250

Number of total components, N_t = 22
 Number of shared components, N_s = 11
 Number of variants, N_v = 3

Efficacy, E_e = 0.5
 Degree of Commonality = 0.17
 Aesthetic Efficiency = 44%
 Product Family Aesthetic Index = 0.61

TOTAL A_j = 9.75

Superconductivity in Layerd Cuprate $(\text{Ru}_{1-x}\text{Nb}_x)\text{Sr}_2\text{GdCu}_2\text{O}_8$

R. Abd-Shukor*, C. A. Kek & W. K. Yeoh

School of Applied Physics
Universiti Kebangsaan Malaysia
43600 Bangi, Selangor, Malaysia

Received: 25 May 2004

ABSTRAK

Satu siri bahan kuprat berlapis $(\text{Ru}_{1-x}\text{Nb}_x)\text{Sr}_2\text{GdCu}_2\text{O}_8$ (Ru1212) dengan $0 \leq x \leq 1$ telah disintesis melalui kaedah tindakbalas keadaan pepejal. Analisis pembelauan sinar-X sampel bentuk serbuk menunjukkan bahawa pengaliran oksigen adalah penting bagi sampel dengan fasa Ru1212 dan kesuperkonduktoran sistem ini. Corak pembelauan bagi sampel dengan komposisi nominal $(\text{Ru}_{1-x}\text{Nb}_x)\text{Sr}_2\text{GdCu}_2\text{O}_8$ boleh diindeks sebagai struktur tetragonal dengan kumpulan ruang P4/mmm. Bahan kurang dop menunjukkan suhu genting (T_c) tertinggi dengan $T_{c\text{ mula}}$ 65 K dan $T_{c\text{ sifar}}$ 55 K. Kajian ini menunjukkan bahawa pendopan dengan Nb menurunkan kekonduksian keadaan biasa dan menekan kesuperkonduksian sistem.

ABSTRACT

A series of layered cuprate $(\text{Ru}_{1-x}\text{Nb}_x)\text{Sr}_2\text{GdCu}_2\text{O}_8$ (Ru1212) for $0 \leq x \leq 1$ has been synthesized by the solid state reaction method. Powder X-ray diffraction analysis indicates that oxygen flow is important in the formation of the Ru1212 phase and superconductivity in the system. Samples with nominal composition $(\text{Ru}_{1-x}\text{Nb}_x)\text{Sr}_2\text{GdCu}_2\text{O}_8$ can be indexed as a tetragonal structure with space group P4/mmm. The undoped compound exhibits the highest superconducting transition with $T_{c\text{ onset}}$ of 65 K and $T_{c\text{ zero}}$ of 55 K. Our results also show that doping with Nb decreases the normal state conductivity and suppresses superconductivity in the system.

Keywords: Electrical resistance, Ru-based superconductor, transition temperature

PACS No.: 74.25.Fy, 74.62.Bf, 74.72.Jt

INTRODUCTION

The remarkable coexistence of ferromagnetism and superconductivity in $\text{RuSr}_2\text{GdCu}_2\text{O}_8$ (Ru1212) has been of enormous interest in the past few years (Wang *et al.* 2003; Tallon *et al.* 2000; Felner *et al.* 1999; Bernhard *et al.* 1999; Matveev *et al.* 2004). Ferromagnetism in this material was considered to be due to the RuO_2 sublattice with $4d^3$ high spin state and the superconductivity originates from CuO_2 layers, similar to that observed in the superconducting layered cuprate $\text{RuSr}_2(\text{Gd,Ce})_2\text{Cu}_2\text{O}_8$ (Ru1222). These materials are the first cuprate superconductors with magnetic ordering transition $T_m > T_c$. Usually these with two order parameters mutually destroy each other but this nonuniform

* Corresponding author
Email: ras@pkrisc.cc.ukm.my

ferromagnet might be ordered in the form of a spiral structure or a domain-like structure such as the Chevrel compound HoMo_6S_8 (Chu *et al.* 2000). Neutron scattering studies have shown that the Ru-spins order antiferromagnetically with Ru moments forming the G-type AFM structure (Lynn *et al.* 2000). An interesting comparison between the pairing state of the Cu oxide and Ru oxide based superconductors has also been reported recently (Sugahara *et al.* 2004).

The nonsuperconductive $\text{MBa}_2\text{LaCu}_2\text{O}_8$, $\text{M}=\text{Nb}$ (Vybornov *et al.* 1995) has been successfully synthesized from the parent material of $\text{YBa}_2\text{Cu}_3\text{O}_{7.8}$ by replacing the Cu-O chain with a single octahedral plane (MO_2) between the apices pyramidal CuO_2 planes and Y with La respectively. Results from recent band structure calculations for $\text{LaBa}_2\text{NbCu}_2\text{O}_8$ and $\text{BaLa}_2\text{Cu}_2\text{TiO}_8$, predict that a pair of nearly degenerate and half-filled s-antibonding subbands in these materials might become superconductor if they could be properly doped or prepared under appropriate conditions (Mattheis 1992). The ruthenium based layered cuprate was first reported by Bauerfeind *et al.* (1995) with $T_c = 42$ K and $T_m = 133$ K for Ru1212 , and $T_c = 45$ K and $T_m = 180$ K for Ru1222 .

In this paper we report the effect of niobium substitution in the RuO_2 sublattice to elucidate the nature of superconductivity in the Ru1212 material. Niobium was chosen due to the d^0 configuration (fully ionized transition-metal) and is believed to lead to change in conducting property. This assertion becomes evident when Z. Sun *et al.* (2001) successfully demonstrated superconductivity in $(\text{Ru}_{1-x}\text{Ta}_x)\text{Sr}_2\text{GdCu}_2\text{O}_8$.

MATERIALS AND METHODS

Samples with nominal compositions $(\text{Ru}_{1-x}\text{Nb}_x)\text{Sr}_2\text{GdCu}_2\text{O}_8$ for $x = 0$ to $x = 1$ were prepared by the solid state reaction method from starting oxides of RuO_2 (99.999 %), Nb_2O_5 (99.99 %), SrCO_3 (99.9+ %), Gd_2O_3 (99.999 %) and CuO (99.999 %). The mixed powder was thoroughly ground and calcined in air at 980°C for 48 hours with intermediate grindings. A calcination step is performed to decompose the carbonates. Then, the resulting powders were ground and pressed into pellets. The first annealing step at 1010°C was performed in flowing nitrogen for 10 hours. Then, the samples were reground and pelletised. The pellets were then annealed at 1050°C for 24 hours in flowing oxygen. Finally, the samples were slowly cooled at the rate of $1^\circ\text{C}/\text{min}$ to 300°C in flowing oxygen to avoid freezing of disorder. Both prereaction and sintering were performed in alumina crucibles.

The powder X-ray diffraction method using a Siemens D 5000 diffractometer with CuK_α source has been used to identify the resultant phase. The volume fractions are estimated by comparing the highest intensity peak for each phase. The d.c. electrical resistance-temperature measurement was carried out by the four point probe technique with silver paste contacts in a CTI Closed Cycle Refrigerator down to about 8 K.

RESULTS AND DISCUSSION

In order to properly evaluate the purity of 1212 phase of $(\text{Ru}_{1-x}\text{Nb}_x)\text{Sr}_2\text{GdCu}_2\text{O}_8$ system, powder XRD measurements were performed after each heat treatment. The powder X-ray diffraction patterns after sintering in air of $(\text{Ru}_{1-x}\text{Nb}_x)\text{Sr}_2\text{GdCu}_2\text{O}_8$ samples with $x = 0.00, 0.05, 0.08, 0.10$ and $x = 0.15, 0.20, 0.45, 0.50$ are shown in Fig. 1(a) and 1(b) respectively. The results show that the 1212 phase is the dominant phase. These results reflect that the 1212 phase can be stabilized with partial substitution of Nb ions into the Ru site. However, $\text{Sr}(\text{Ru},\text{Nb})\text{O}_3$ marked with (#) phase (Lorenz *et al.* 2001) is found as secondary phase at about $2\theta = 31.8^\circ$ together with small amounts of $(\text{Ru},\text{Nb})\text{Sr}_2\text{GdO}_6$ (+) and CuO (*) in the doped samples. The 1212 phase gradually decreases while the secondary phase of $\text{Sr}(\text{Ru},\text{Nb})\text{O}_3$ is increased as the Nb content is increased. This finding suggests that the M1212, M = Ru and Nb are very sensitive to the reaction temperature and the reaction temperature between $960^\circ\text{C} - 980^\circ\text{C}$ might be optimum for the Ru-system to form a pure 1212 phase but it is too low for the formation of Nb1212.

In Fig. 2, the powder X-ray diffraction patterns after the heat treatment in reducing atmosphere clearly implies the absence of any phase with 1212 structure. However, the main phase is likely to appear as unreacted CuO and a cubic perovskite of the form $(\text{Ru},\text{Nb})\text{Sr}_2\text{GdO}_6$. This step is important to

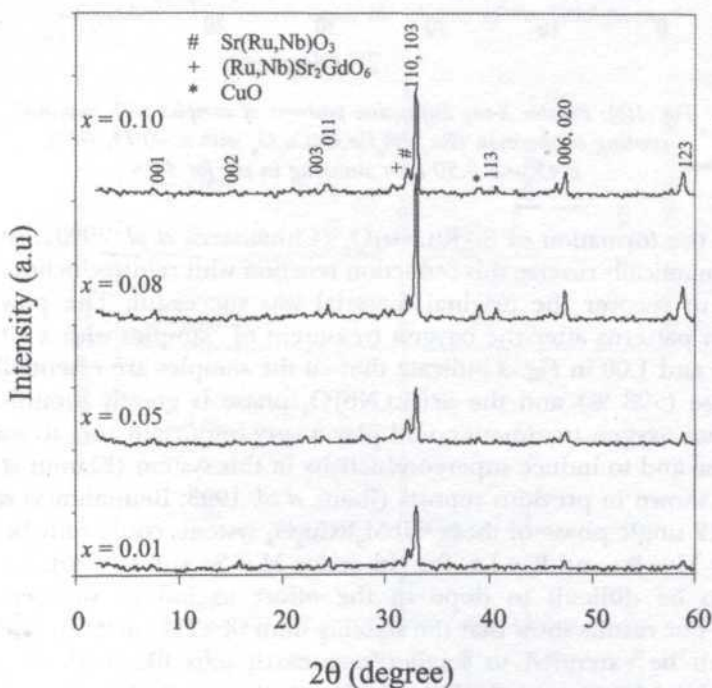


Fig. 1(a): Powder X-ray diffraction patterns of samples with nominal starting composition $(\text{Ru}_{1-x}\text{Nb}_x)\text{Sr}_2\text{GdCu}_2\text{O}_8$ with $x = 0.01, 0.05, 0.08$ and 0.10 after sintering in air for 48 h

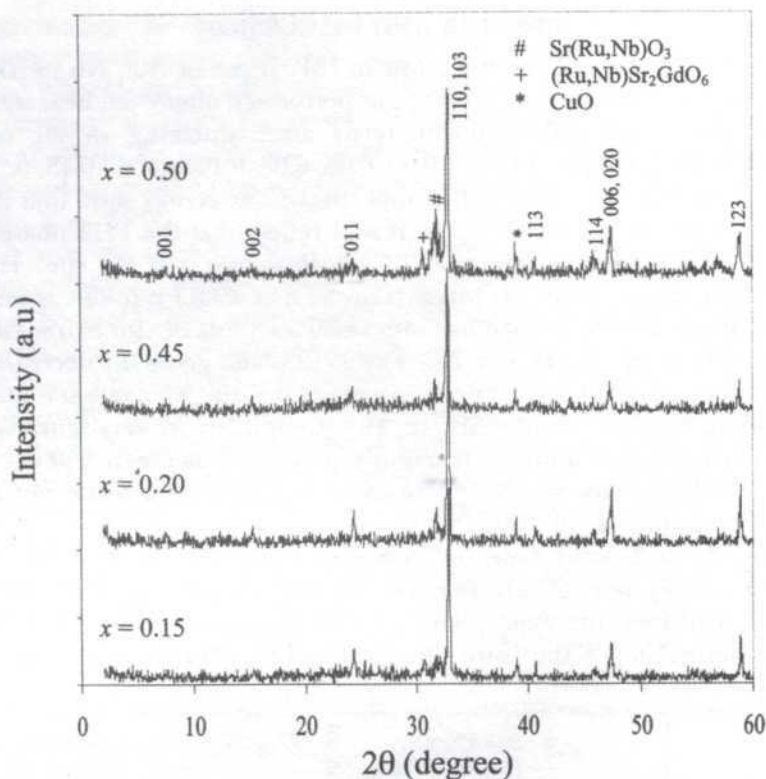


Fig. 1(b): Powder X-ray diffraction patterns of samples with nominal starting composition $(\text{Ru}_{1-x}\text{Nb}_x)\text{Sr}_2\text{GdCu}_2\text{O}_8$ with $x = 0.15, 0.20, 0.45$ and 0.50 after sintering in air for 48 h

minimize the formation of $\text{Sr}(\text{Ru},\text{Nb})\text{O}_3$ (Chmaissem *et al.* 2000). Attempts to thermodynamically reverse this reduction reaction with reintroduction of oxygen in order to recover the original material was successful. The powder X-ray diffraction patterns after the oxygen treatment of samples with $x = 0.08, 0.20, 0.40, 0.60$ and 1.00 in Fig. 3 indicate that all the samples are essentially a single 1212 phase (>98 %) and the $\text{Sr}(\text{Ru},\text{Nb})\text{O}_3$ phase is greatly diminished. This implies that oxygen treatment could play a very important role to stabilize the 1212 phase and to induce superconductivity in this system (Klamut *et al.* 2001).

It was shown in previous reports (Jhans *et al.* 1993; Bennahmias *et al.* 1992) that a 1212 single phase of these $\text{NbM}_2\text{RCu}_2\text{O}_8$ systems could only be stabilized for either $M = \text{Ba}$ and $R = \text{La}, \text{Pr}, \text{Nd}$ or for $M = \text{Sr}$ and $R = \text{Nd}, \text{Eu}$ and have proven to be difficult to dope in the effort to induce superconductivity. However, our results show that the stability limit of 1212 phase in $\text{NbSr}_2\text{RCu}_2\text{O}_8$ system can be extended to smaller rare earth ions like Gd^{3+} (0.94 Å) and superconductivity can only be induced by substituting Ru ions into the Nb ions sites.

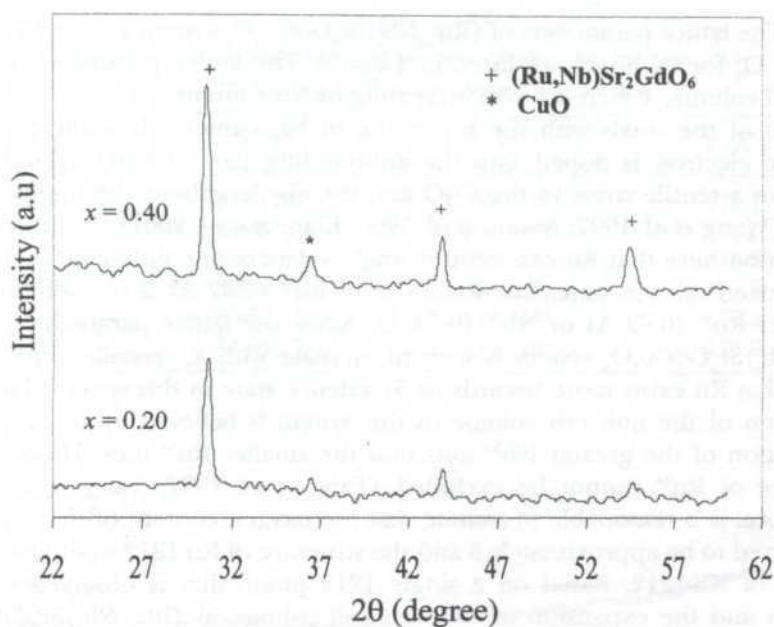


Fig. 2: Powder X-ray diffraction patterns of samples with nominal starting composition $(\text{Ru}_{1-x}\text{Nb}_x)\text{Sr}_2\text{GdCu}_2\text{O}_8$ after heat treatment in reduction atmosphere which clearly imply the absence of the 1212 phase

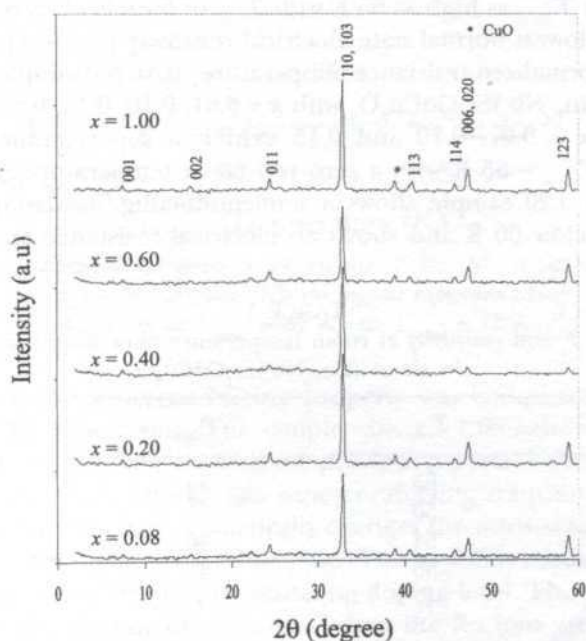


Fig. 3: Powder X-ray diffraction patterns of samples with nominal starting composition $(\text{Ru}_{1-x}\text{Nb}_x)\text{Sr}_2\text{GdCu}_2\text{O}_8$ with $x = 0.08, 0.20, 0.40, 0.60$ and 1.00 after annealing in flowing oxygen for 24 h

The lattice parameters of $(\text{Ru}_{1-x}\text{Nb}_x)\text{Sr}_2\text{GdCu}_2\text{O}_8$ system after annealing in flowing O_2 for 24 hours are listed in Table 2. The lattice parameters a , c and unit cell volume, V increase with increasing of Nb content. This is shown by the increase of the a -axis with the increasing of Nb content. It suggests that an effective electron is doped into the antibonding part of CuO orbital which results in a tensile stress in the CuO and thereby lengthens the in-plane CuO bonds (Wang *et al.* 1997; Awana *et al.* 1996; Klamut *et al.* 2001). It is interesting to mention here that Ru can exist in single valence state either in 4+ or in 5+ or in mixed valence state. The ionic size of Ru^{5+} (0.57 Å) is smaller than that of either Ru^{4+} (0.62 Å) or Nb^{5+} (0.64 Å). Since the lattice parameter c of the $(\text{Ru}_{1-x}\text{Nb}_x)\text{Sr}_2\text{GdCu}_2\text{O}_8$ system is seen to increase with x , crystallographically it seems that Ru exists more towards its 5+ valence state in this system. Thus, the expansion of the unit cell volume of this system is believed to be due to the substitution of the greater Nb^{5+} ions into the smaller Ru^{5+} ions. However, the presence of Ru^{4+} cannot be excluded (Tang *et al.* 1997; Tang *et al.* 1996). Therefore, it is reasonable to assume that the oxygen content of the cuprate is considered to be approximately 8 and the structure of Ru-1212 would be similar to that of Nb-1212. Based on a single 1212 phase that is observed in XRD patterns and the expansion of the unit cell volume in $(\text{Ru}_{1-x}\text{Nb}_x)\text{Sr}_2\text{GdCu}_2\text{O}_8$ system, we conclude that the Nb ions are readily incorporated into the structure.

The electrical resistivity *vs.* temperature measurement for the $(\text{Ru}_{1-x}\text{Nb}_x)\text{Sr}_2\text{GdCu}_2\text{O}_8$ sample with $x = 0.00$ is shown in Fig. 4. The undoped sample exhibits metallic normal state until 100 K where a semiconducting upturn occurred and a $T_{\text{c-onset}}$ as high as 65 K with $T_{\text{c-zero}}$ of 55 K is observed. This sample also shows the lowest normal state electrical resistivity (Table 1). Fig. 5 and Fig. 6 display the normalized resistance-temperature curve for samples with nominal composition $(\text{Ru}_{1-x}\text{Nb}_x)\text{Sr}_2\text{GdCu}_2\text{O}_8$ with $x = 0.01, 0.10, 0.15, 0.20$ and 1.00. The samples with $x = 0.01, 0.10$ and 0.15 exhibit a superconducting transition temperature, $T_{\text{c-onset}} \sim 55$ K with a zero resistance temperature, $T_{\text{c-zero}} \sim 40$ K. In Fig. 6, the $x = 0.20$ sample shows a semiconducting/insulating transition in normal state below 60 K and shows an electrical resistance anomaly at 50 K.

TABLE 1
 T_c and resistivity at room temperature after sintering
in air of $(\text{Ru}_{1-x}\text{Nb}_x)\text{Sr}_2\text{GdCu}_2\text{O}_8$

x	$T_{\text{c-onset}}$	$T_{\text{c-zero}}$	ρ (mΩ-cm)
0.00	65	55	10.0
0.01	56	41	12.0
0.10	54	40	12.7
0.15	55	41	12.8
0.20	47	-	13.0
0.40	-	-	14.8
0.60	-	-	22.8
1.00	-	-	278

TABLE 2
Lattice parameters and unit cell volume of $(\text{Ru}_{1-x}\text{Nb}_x)\text{Sr}_2\text{GdCu}_2\text{O}_8$
after annealing in flowing oxygen for 24 h

x	a (Å)	c (Å)	V (Å ³)
0.00	3.841 (2)	11.532 (15)	170.1
0.08	3.845 (2)	11.554 (13)	170.8
0.20	3.849 (3)	11.558 (15)	171.2
0.40	3.854 (2)	11.566 (12)	171.8
0.60	3.856 (3)	11.591 (17)	172.3
1.00	3.866 (3)	11.633 (18)	173.9

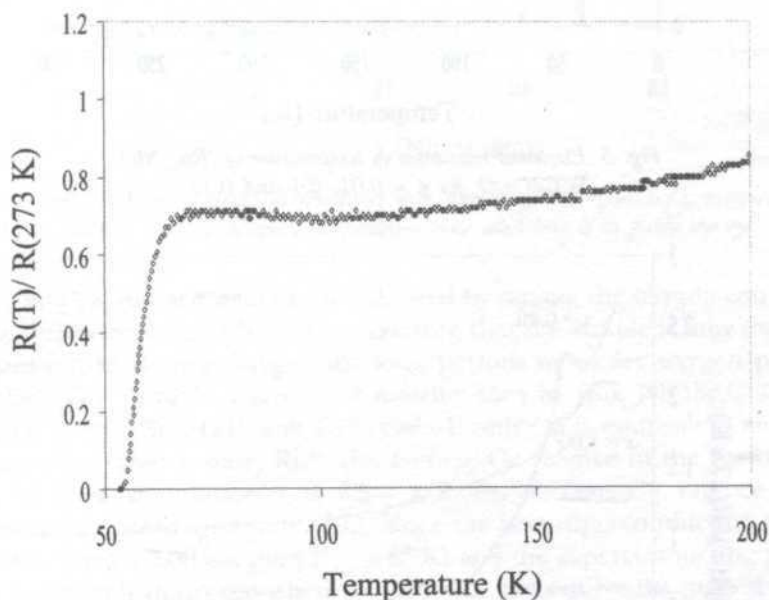


Fig. 4: Electrical resistance vs temperature of $(\text{Ru}_{1-x}\text{Nb}_x)\text{Sr}_2\text{GdCu}_2\text{O}_8$
for $x = 0.00$ which exhibits the highest superconducting
transition at $T_{\text{c-onset}} = 65 \text{ K}$ with $T_{\text{c-zero}} = 55 \text{ K}$

This means that the superconducting property was completely destroyed at about 20 % of Nb substitution. The sample with $x = 1.00$ exhibits an insulator-like behavior in good agreement with the previous reports (Vybornov *et al.* 1995 and Greaves *et al.* 1989) without any superconducting transition.

The presence of Nb ions dramatically changes the normal state behavior of the samples from metallic to semimetallic. This is followed by a narrow gap semiconducting-like behavior with increasing doping level. The sample exhibits a large gap semiconducting-like behavior when the Ru ions are fully replaced by Nb ions. The resistivity as a function of x (Nb content) at room temperature corresponds well with their normal state behaviors as shown in Fig. 7. The room

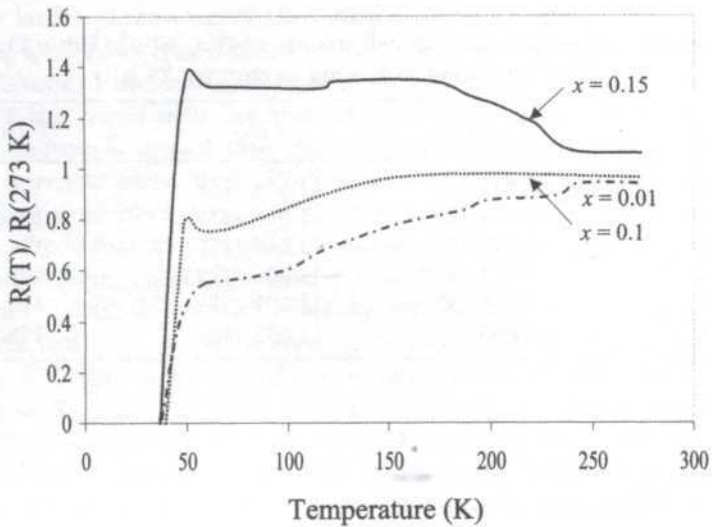


Fig. 5: Electrical resistance vs temperature of $(Ru_{1-x}Nb_x)Sr_2GdCu_2O_8$ for $x = 0.01, 0.1$ and 0.15

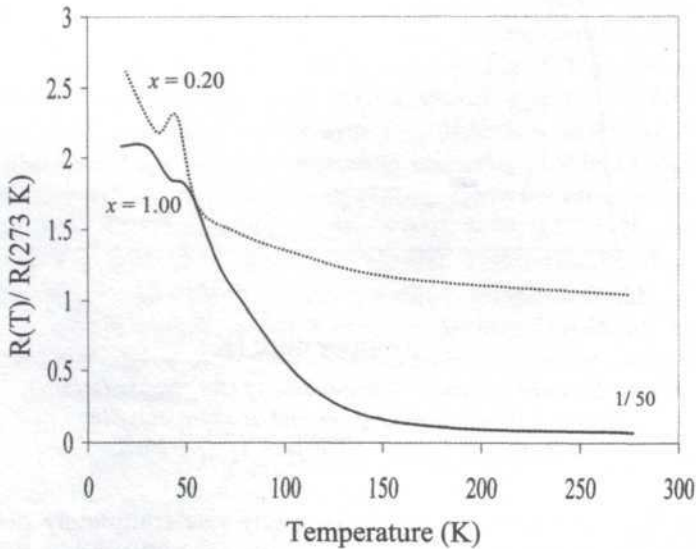


Fig. 6: Electrical resistance vs temperature of $(Ru_{1-x}Nb_x)Sr_2GdCu_2O_8$ for $x = 0.20$ and 1.00

temperature resistivities for all the samples are in the range of $10^1 - 10^2$ m Ω -cm. The sample with $x = 1.00$ shows the highest resistivity, $\rho \sim 278$ m Ω -cm.

For the cuprates with 1212-type structure, the average Cu valence is an important factor that influences superconductivity. Experimental results showed that the optimum value of Cu valence for maximum T_c is between 2.15+ and

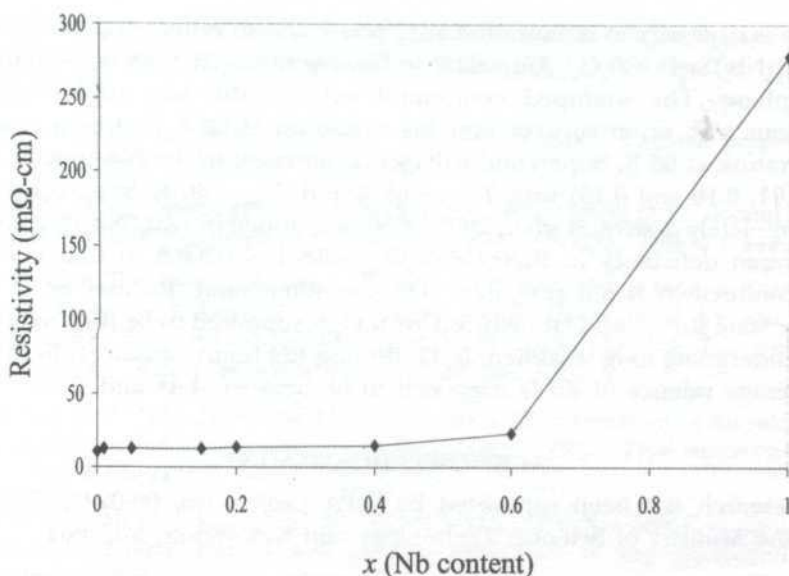


Fig. 7: Plots of electrical resistivity vs x for $(\text{Ru}_{1-x}\text{Nb}_x)\text{Sr}_2\text{GdCu}_2\text{O}_8$ samples with $0 \leq x \leq 1$ at room temperature. The solid line is to guide the eye

2.30+. The Cu valence state can be adjusted by varying the oxygen content and/or the cation ratio $\text{Ru}^{4+} : \text{Nb}^{5+}$. To make sure that the sample is fully oxygenated, a treatment in flowing oxygen for long periods or under oxygen pressure is essential. The possible valences of metallic ions in $(\text{Ru}_{1-x}\text{Nb}_x)\text{Sr}_2\text{GdCu}_2\text{O}_8$ are $\text{Ru}^{4+}/\text{Ru}^{5+}$, Nb^{5+} , Sr^{2+} , Gd^{3+} and $\text{Cu}^{2+}/\text{Cu}^{3+}$. If only Cu is multivalent and that Ru is in a single valence state, Ru^{4+} , the average Cu valence in the Ru-1212 phase with an ideal stoichiometry is $2.5 - x/2$. An average Cu valence of $2.5 +$ represents an overdoped hole state. Since the best superconducting properties occurs in the $x = 0.00$ sample ($T_{c\text{-max}} = 65$ K) and the superconducting properties were completely destroyed when $x = 0.20$, our present results suggest that if Ru is in the 4+ state, this means the oxygen deficiency might be the reason for optimization of Cu valence, thus inducing superconductivity in this system. The optimum Cu valence may be achieved through the hole filling by an aliovalent cation substitution in Ru-system (Klamut *et al.* 2001). However, the samples were heated in flowing oxygen for 24 hours, so that they are assumed to be fully oxygenated. If there is no oxygen deficiency, we expect Ru to be in the mixed valence state, $\text{Ru}^{4+/5+}$ with average value between 4.4+ and 4.6+ to obtain optimum Cu valence. This is in agreement with the results on Ru valence in Ru-1212 system (Butera *et al.* 2001; Liu *et al.* 2001).

CONCLUSIONS

In conclusion, the influence of partial substitution of Nb for Ru, period of sintering and atmosphere of annealing as well as the cooling rate on the purity of 1212 phase for $(\text{Ru}_{1-x}\text{Nb}_x)\text{Sr}_2\text{GdCu}_2\text{O}_8$ were studied. Annealing in flowing

oxygen is necessary to stabilize the 1212 phase and to induce superconductivity in $(\text{Ru}_{1-x}\text{Nb}_x)\text{Sr}_2\text{GdCu}_2\text{O}_8$. Annealing in flowing nitrogen does not stabilize the 1212 phase. The undoped compound exhibits the best superconducting behaviour with onset superconducting transition at 65 K and zero resistance temperature at 55 K. Superconductivity is suppressed in the Nb-doped samples ($x = 0.01, 0.10$ and 0.15) with $T_{\text{onset}} \sim 55$ K and $T_{\text{zero}} \sim 40$ K. Superconductivity was completely destroyed when 20 % of Nb was doped in $(\text{Ru}_{1-x}\text{Nb}_x)\text{Sr}_2\text{GdCu}_2\text{O}_8$.

Oxygen deficiency in $\text{RuSr}_2\text{GdCu}_2\text{O}_{8-\delta}$ with $\delta = 0.2-0.3$ so that it exhibits superconductivity is not probable. On the other hand, Ru may be in mixed valence state $\text{Ru}^{4+/5+}$ and $(\text{Ru},\text{Nb})\text{Sr}_2\text{GdCu}_2\text{O}_8$ is supposed to be fully oxygenated after undergoing long treatment in O_2 flowing (24 hours or more). In this case, the average valence of Ru is suggested to be between 4.4+ and 4.6+.

ACKNOWLEDGEMENTS

This research has been supported by IRPA project no. 09-02-02-0072EA199 from the Ministry of Science, Technology and Innovation, Malaysia.

REFERENCES

- AWANA, V.P.S., L. MENON and S.K. MALIK. 1996. Effect of substituting Ce at the Ca site on the high-temperature superconductor $\text{Bi}_2\text{Sr}_2\text{CaCu}_2\text{O}_{8+d}$. *Phys. Rev. B* **53**: 2245-2248.
- BAUERNEFELD, L., W. WIDDER and H.F. BRAUN. 1995. Ruthenium-based layered cuprates $\text{RuSr}_2\text{LnCu}_2\text{O}_8$ and $\text{RuSr}_2(\text{Ln}_{1-x}\text{Ce}_{1-x})\text{Cu}_2\text{O}_{10}$ ($\text{Ln} = \text{Sm}, \text{Eu}$ and Gd). *Physica C* **254**: 151-158.
- BENNAHMAS, M., J.C. O'BRIEN, H.B. RADOUSKY, J.T. GOODWIN, P. KLAVINS, J.M. LINK, C.A. SMITH and R.N. SHELTON. 1992. Magnetic, structural, and Raman characterization of $R\text{Ba}_2\text{Cu}_2\text{NbO}_8$ ($R = \text{Pr}, \text{La},$ or Nd). *Phys. Rev. B* **46**: 11986-11992.
- BERNHARD, C., J.L. TALLON, CH. NIEDERMAYER, TH. BLASIUS, A. GOLNIK, E. BRÜCHER, R.K. KREMER, D.R. NOAKES, C.E. STRONACH and E.J. ANSALDO. 1999. Coexistence of ferrimagnetism and superconductivity in the hybrid ruthenate-cuprate compound $\text{RuSr}_2\text{GdCu}_2\text{O}_8$ studied by the muon spin rotation and dc magnetization. *Phys. Rev. B* **59**: 14099-14107.
- BUTERA, A., A. FAINSTEIN, E. WINKLER and J.L. TALLON. 2001. Ferrimagnetic correlations and mixed Ru valence in the magnetic superconductor $\text{RuSr}_2(\text{Eu},\text{Gd})\text{Cu}_2\text{O}_8$. *Phys. Rev. B* **63**: 054442(1-4).
- CHMAISSEM, O., J.S. JORGENSEN, H. SHAKED, P. DOLLAR and J.L. TALLON. 2000. Crystal and magnetic structure of ferrimagnetic superconducting $\text{RuSr}_2\text{GdCu}_2\text{O}_8$. *Phys. Rev. B* **61**: 6401-6407.
- CHU, C.W., Y.Y. XUE, S. TSUI, J. CMAIDALKA, A.K. HEILMAN, B. LORENZ and R.L. MENG. 2000. A possible crypto-superconducting structure in a superconducting ferrimagnet. *Physica C* **335**: 231-238.
- FELNER, I., U. ASAF, S. REICH and Y. TSABBA. 1999. Magnetic properties of $\text{RSr}_2\text{RuCu}_2\text{O}_{8+d}$ ($R = \text{Eu}$ and Gd). *Physica C* **311**: 163-171.

- GREAVES, C. and P.R. SLATER. 1989. Nb and Ta substitutions in $\text{YBa}_2\text{Cu}_3\text{O}_{7-x}$ and related phases: structural characterization of $\text{La}_{1.1}\text{Ba}_{1.9}\text{Cu}_{2.1}\text{M}_{0.9}\text{O}_8$ (M= Nb, Ta). *Physica C* **161**: 245-251.
- JHANS, H., S.K. MALIK and R. VIJAYARAGHAVAN. 1993. Synthesis and magnetic properties of the $\text{R}_{1+x}\text{Sr}_{2-x}\text{Nb}_{1-x}\text{O}_{8-y}$. *Physica C* **215**: 181-190.
- KLAMUT, P.W., B. DABROWSKI, J. MAIS and M. MAXWELL. 2001. Effect of Ce doping on the superconducting and magnetic properties of $\text{RuSr}_2\text{GdCu}_2\text{O}_8$. *Physica C* **350**: 24-28.
- KLAMUT, P.W., B. DABROWSKI, S.M. MINI, M. MAXWELL, S. KOLESNIK, J. MAIS, A. SHENGELAYA and R. KHASANOV, I. SAVIC, H. KELLER, T. GRABER, J. GEBHARDT, P.J. VICCARO and Y. XIAO. 2001. Magnetic properties of $\text{RuSr}_2\text{RECu}_2\text{O}_8$ (RE=Gd, Eu) and $\text{Ru}_{1-x}\text{Sr}_2\text{GdCu}_{2+x}\text{O}_{8-y}$ superconductors. *Physica C* **364-365**: 313-319.
- LIU, R.S., L.Y. JANG, H.H. HUNG and J.L. TALLON. 2001. Determination of Ru valence X-Ray absorption near-edge structure in $\text{RuSr}_2(\text{Gd,Ce})_2\text{Cu}_2\text{O}_8$ -Type superconductor. *Phys. Rev. B* **63**: 212507(1-5).
- LORENZ, B., R.L. MENG, J. CMAIDALKA, Y.S. WANG, J. LENZI, Y.Y. XUE and C.W. CHU. 2001. Synthesis, characterization and physical properties of the superconducting ferromagnet $\text{RuSr}_2\text{GdCu}_2\text{O}_8$. *Physica C* **363**: 251-259.
- LYNN, J.W., B. KEIMER, C. ULRICH, C. BERNHARD and J.L. TALLON. 2000. Evidence for a Bulk Meissner State in a Ferromagnetic Superconductor $\text{RuSr}_2\text{GdCu}_2\text{O}_8$ from dc Magnetization. *Phys. Rev. B* **61**: R14960-R14963.
- MATTHEISS, L.F. 1992. Electronic structure of $\text{LaBa}_2\text{Cu}_2\text{NbO}_8$ and related candidates for High- T_c superconductivity. *Phys. Rev. B* **45**: 2442-2446.
- MATVEEV, A.T., E. SADER, V. DUPPEL, A. KULAKOV, A. MALJUK, C.T. LIN and H.U. HABERMEIER. 2004. Decomposition of $\text{RuSr}_2\text{GdCu}_2\text{O}_8$ phase under high-temperature treatment. *Physica C* **403**: 231-239.
- SUGAHARA, M. and Jr. N.N. BOGOLUBOV. 2004. Unified model of superconductivity of singlet-pair Cu oxide superconductor and triplet-pair Ru oxide superconductor, *International J. of Mod. Phys. B* **18**: 71-86.
- SUN, Z., S.Y. LI, Y.M. XIONG and X.H. CHEN. 2001. Preparation, Structure, and Superconductivity of Ru1222 and Ta-Doped Ru1212 . *Physica C* **349**: 289-294.
- TALLON, J.L., J.W. LORAM, G.V.M. WILLIAMS and C. BERNHARD. 2000. Heat capacity and transport studies of the ferromagnetic superconductor $\text{RuSr}_2\text{GdCu}_2\text{O}_8$. *Phys. Rev. B* **61**: R6471-R6474.
- TANG, K.B., Y.T. QIAN, L. YANG, Y.D. ZHAO and Y.H. ZHANG. 1997. Crystal structure of a new series of 1212 type cuprate $\text{RuSr}_2\text{LnCu}_2\text{O}_x$. *Physica C* **282 - 287**: 947-948.
- TANG, K.B., Y.T. QIAN, Y.D. ZHAO, L. YANG, Z.Y. CHEN and Y.H. ZHANG. 1996. Synthesis and characterization of a new layered superconducting cuprate: $\text{RuSr}_2(\text{Gd,Ce})_2\text{Cu}_2\text{O}_{10}$. *Physica C* **259**: 168-172.
- VYBORNOV, M., W. PERTHOLD, H. MICHOR, T. HOLUBAR, G. HILSCHER, P. ROGL, P. FISCHER and M. DIVIS. 1995. Synthesis and characterization of compounds $\text{Sr}_2\text{RMCu}_2\text{O}_{8-d}$ (R=Pr, Nd, Sm, Eu, Gd; M=Nb, Ta). *Phys. Rev. B* **52**: 1389-1404.

- WANG, C., C. DONG, G. CHE, Z.Y. QIAO, H. CHEN and Z.H. ZHAO. 1997. Relationship between the lattice parameter and superconductivity in the 2-1-4 Series N-Type Cuprates. *Phys. Rev. B* **55**: 3935-3942.
- WANG, D.Z., H.I. HA, J.I. OH, J. MOSER, J.G. WEN, M.J. NAUGHTON and Z.F. REN. 2003. Synthesis and Properties of Superconductor $\text{RuSr}_2\text{GdCu}_2\text{O}_8$. *Physica C* **384**: 137-142.

Preparation of Manuscript

General

The manuscript, including footnotes, tables, and captions for illustrations, should be typewritten double spaced on paper 210 x 297 mm in size, with margins of 40 mm on all sides. Three clear copies are required. Typing should be on one side of the paper only. Each page of the manuscript should be numbered, beginning with the title page.

Title page

The title of the paper, name of author and full address of the institution where the work was carried out should appear on this page. A short title not exceeding 60 characters should be provided for the running headline.

Abstract

Abstracts in Bahasa Melayu and English of not more than 200 words each are required for full articles and communications. No abbreviation should appear in the abstract. Manuscripts from outside of Malaysian may be submitted with an English abstract only.

Keywords

Up to a maximum of ten keywords are required and they should be placed directly below the abstract.

Footnotes

Footnotes to material in the text should not be used unless they are unavoidable. Where used in the text, footnotes should be designated by superscript Arabic numerals in serial order throughout the manuscript. Each footnote should be placed at the bottom of the manuscript page where reference to it is made.

Equations

These must be clearly typed, triple-spaced and should be identified by numbers in square brackets placed flush with the right margin. In numbering, no distinction is made between mathematical and chemical equations. routine structural formulae can be typeset and need not be submitted as figures for direct reproduction but they must be clearly depicted.

Tables

Tables should be numbered with Arabic numerals, have a brief title, and be referred to in the text. Columns headings and descriptive matter in tables should be brief. Vertical rules should not be used. Footnotes in tables should be designated by symbols or superscripts small italic letters. Descriptive materials not designated by a footnote may be placed under a table as a *note*.

Illustrations & Photographs

Illustration including diagrams and graphs are to be referred to in the text as 'figures' and photographs as 'plates' and numbered consecutively in Arabic numerals. All photographs (glossy black and white prints) should be supplied with appropriate scales.

Illustrations should be of print quality; outputs from dotmatrix printers are not acceptable, Illustrations

should be on separate sheets, about twice the size of the finished size in print. All letters, numbers and legends must be included on the illustration with the author's name, short title of the paper, and figure number written on the verso. A list of captions should be provided on a separate sheet.

Unit of Measure

Metric units must be used for all measurements.

Citations and References

Items in the reference list should be referred to in the text by inserting, within parentheses, the year of publication after the author's name. If there are more than two authors, the first author should be cited followed by 'et al.'. The names of all authors, however, will appear in the reference list.

In the case of citing an author who has published more than one paper in the same year, the papers should be distinguished by addition of a small letter, e.g. Choa (1979a); Choa (1979b); Choa (1979c).

In the reference list, the names should be arranged alphabetically according to the name of the first author. Serials are to be abbreviated as in the *World List of Scientific Periodicals*.

The abbreviation for *Pertanika Journal of Science and Technology* is *Pertanika J. Sci. Technol.*

The following reference style is to be observed:

Monograph

Aleff, G. and J. Herzberger. 1983. *Introduction to Interval Computations*. New York: Academic Press.

Chapter in Edited Book

Muzzarell, R.A.A. 1980. Chitin. In *Polymers in Nature*, ed. E.A. MacGregor and C.T. Greenwood, p. 417-449. New York: John Wiley.

Serials

Kamaruzaman Ampon. 1991. The effect of attachment of hydrophobic imidoesters on the catalytic activity of trypsin. *Pertanika* 14(2): 18-185.

Proceedings

Mokhtaruddin, A.M. and L.M. Maene. 1981. Soil erosion under different crops and management practices. In *Agricultural Engineering in National Development*, ed. S.L. Choa, Mohd Zohdie Badaie, N.C. Saxena and Van Vi Tran, p. 245-249. Serdang, Malaysia: Universiti Pertanian Malaysia Press.

Unpublished Materials (e.g. theses, reports & documents)

Sakri, I. 1990. Proper construction set-up of Malaysian Fish Aggregating Devices (Unjam). Ph.D. Thesis, Universiti Pertanian Malaysia, Serdang, Selangor.